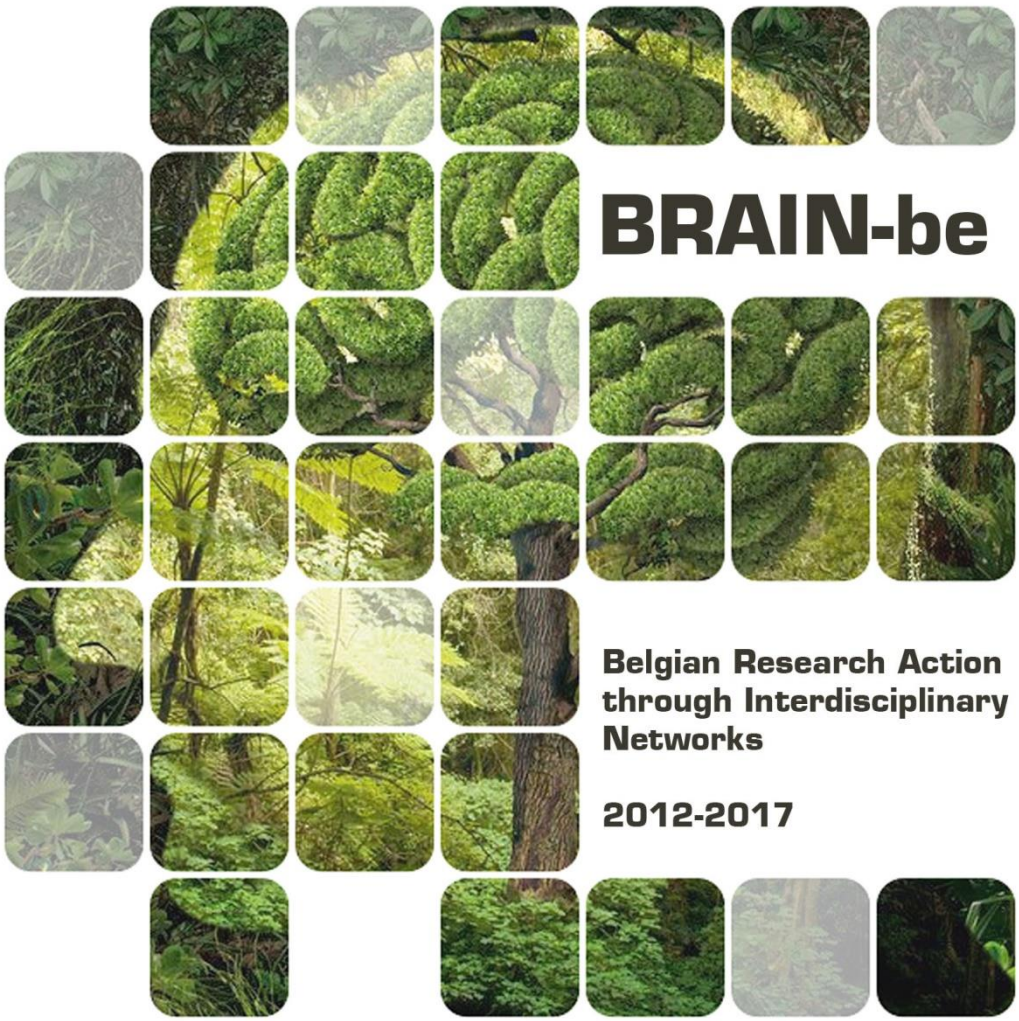

AEROCLOUD

How do aerosols and clouds affect the East Antarctic climate?

Nicole VAN LIPZIG (KU Leuven) – Hugo DE BACKER (RMI) – Michel VAN ROOZENDAEL (BIRA) – Niels SOUVERIJNS (KU Leuven) – Alexandra GOSSART (KU Leuven) – Alexander MANGOLD (RMI) – Quentin LAFFINEUR (RMI) – Caroline FAYT (BIRA) – Martina FRIEDRICH (BIRA) – Francois HENDRICK (BIRA) – Christian HERMANS (BIRA)

Axis 2: Geosystems, universe and climate

belspo .be

NETWORK PROJECT

AEROCLOUD

How do aerosols and clouds affect the East Antarctic climate?

Contract - BR/143/A2/AEROCLOUD

FINAL REPORT

PROMOTORS: Prof. Dr. Nicole van Lipzig (KU Leuven)
Dr. Hugo De Backer (RMI)Dr. Michel Van Roozendael (BIRA)

AUTHORS: Prof. Dr. Nicole van Lipzig (KU Leuven)
Dr. Hugo De Backer (RMI)
Dr. Michel Van Roozendael (BIRA)
Niels Souverijns (KU Leuven)
Alexandra Gossart (KU Leuven)
Dr. Alexander Mangold (RMI)
Dr. Quentin Laffineur (RMI)
Caroline Fayt (BIRA)
Dr. Martina Friedrich (BIRA)
Dr. Francois Hendrick (BIRA)
Dr. Christian Hermans (BIRA)

Published in 2019 by the Belgian Science Policy Office
Boulevard Simon Bolivar 30 bte 7
Simon Bolivarlaan 30 bus 7
B-1000 Brussels
Belgium
Tel: +32 (0)2 238 34 11
http://www.belspo.be
http://www.belspo.be/brain-be

Contact person: Maaike Vancauwenberghe
Tel: +32 (0)2 238 36 78

N. van Lipzig, H. De Backer, M. Van Roozendael, N. Souverijns, A. Gossart, A. Mangold, Q. Laffineur, C. Fayt, M. Friedrich, F. Hendrick, C. Hermans. ***How do aerosols and clouds affect the East Antarctic Climate?***. Final Report. Brussels : Belgian Science Policy Office 2019 – 99 p. (BRAIN-be - (Belgian Research Action through Interdisciplinary Networks)

TABLE OF CONTENTS

CONTENTS

TABLE OF CONTENTS 4
CONTENTS 4
ABSTRACT 7
CONTEXT 7
OBJECTIVES 8
CONCLUSIONS 8
KEYWORDS 10
1. INTRODUCTION 11
2. STATE OF THE ART AND OBJECTIVES 13
2.1 THE HYDROLOGICAL CYCLE OVER ANTARCTICA 13
2.1.1 Clouds 13
2.1.2 Precipitation 14
2.1.3 Blowing snow 15
2.2 AEROSOL OBSERVATIONS OVER ANTARCTICA 17
2.3 THE CLOUD INDIRECT CLIMATE EFFECT AND AEROSOL-CLOUD-PRECIPITATION INTERACTIONS 18
2.4 REGIONAL CLIMATE MODELLING 19
2.5 OBJECTIVES 21
3. METHODOLOGY 22
3.1 INSTRUMENTATION AT THE PRINCESS ELISABETH STATION 22
3.2 CHARACTERISATION OF CLOUD AND PRECIPITATION PROPERTIES AND THEIR EFFECT ON THE SURFACE ENERGY AND MASS BUDGETS 25
3.2.1 Derivation of cloud properties from multiple sensors 25
3.2.2 Assessment of the effect of clouds on the surface energy balance 26
3.2.3 Estimation of snowfall rate from the vertically-profiling precipitation radar 26
3.2.4 Evaluation of the CloudSat precipitation climatology 27
3.2.5 Assessment of the individual components of the surface mass balance 28
3.3 CHARACTERISATION OF ATMOSPHERIC AEROSOLS 29
3.3.1 Estimation of aerosol characteristics from boundary layer measurements 29
3.3.2 Retrieval of total column and vertically resolved aerosol properties with remote sensing instrumentation 30
3.3.3 Improved estimation of aerosol characteristics by Mie-Calculation and radiative transport modelling 31
3.3.4 Estimation of cloud condensation nuclei and of ice nuclei 31
3.3.5 Assessment of the atmospheric aerosol variability at Utsteinen: composition by season, meteorological regime and altitude level 31
3.4 EVALUATION AND IMPROVEMENT OF THE REGIONAL CLIMATE MODEL 32
3.4.1 Antarctic-wide climate model simulations with COSMO-CLM² 32
3.4.2 High-resolution simulations with COSMO-CLM² 33
3.5 ASSESSMENT OF THE INDIRECT AEROSOL EFFECT IN DRONNING MAUD LAND 33
3.5.1 Identification of the relationship between atmospheric composition, cloud and precipitation properties and air mass origin 33
3.5.2 Identification of the model sensitivity to cloud condensation nuclei and ice nuclei 34
4. SCIENTIFIC RESULTS AND RECOMMENDATIONS 35
4.1 CHARACTERISATION OF CLOUD AND PRECIPITATION PROPERTIES AND THEIR EFFECT ON THE SURFACE ENERGY AND MASS BUDGETS 35
4.1.1 Derivation of cloud properties from multiple sensors 35
4.1.2 Assessment of the effect of clouds on the surface energy balance 35
4.1.3 Estimation of snowfall rate from the vertically-profiling precipitation radar 36
4.1.4 Evaluation of the CloudSat precipitation climatology 37
4.1.5 Assessment of the individual components of the surface mass balance 41
4.2 CHARACTERISATION OF ATMOSPHERIC AEROSOLS 46
4.2.1 Estimation of aerosol characteristics from boundary layer measurements 46

4.2.2 Retrieval of total column and vertically resolved aerosol properties with remote sensing instrumentation 51
4.2.3 Improved estimation of aerosol characteristics by Mie-Calculation and radiative transport modelling 52
4.2.3.1 Elevated cloud layer 53
4.2.3.2 Blowing snow event 53
4.2.3.3 Aerosol entrainment from upper atmospheric layers to the surface 54
4.2.3.4 Elevated aerosol layer in clear-sky conditions 56
4.2.3.5 Summary and recommendations 58
4.2.4 Estimation of cloud condensation nuclei and of ice nuclei 58
4.2.5 Assessment of the atmospheric aerosol variability at Utsteinen: composition by season, meteorological regime and altitude level 60
4.3 EVALUATION AND IMPROVEMENT OF THE REGIONAL CLIMATE MODEL 61
4.3.1 Antarctic-wide climate model simulations with COSMO-CLM² 61
4.3.2 High-resolution simulations with COSMO-CLM² 69
4.4 ASSESSMENT OF THE INDIRECT AEROSOL EFFECT IN DRONNING MAUD LAND 71
4.4.1 Identification of the relationship between atmospheric composition, cloud and precipitation properties and air mass origin 71
4.4.2 Identification of the model sensitivity to cloud condensation nuclei and ice nuclei 73
5. DISSEMINATION AND VALORISATION 79
5.1 NETWORK MANAGEMENT 79
5.1.1 Internal 79
5.1.2 Follow-up committee 79
5.2 CONTRIBUTION TO OTHER PROJECTS 79
5.2.1. Contribution to the scientific community 79
5.2.2 Contribution to POLAR-CORDEX 79
5.3 INSTRUMENT MAINTENANCE AND CALIBRATION 80
5.4 MANAGEMENT OF THE PE DATABASE AND DATA DISSEMINATION 80
5.5 ORGANIZATION OF SYMPOSIA 81
5.5.1. EGU General assembly splinter meetings 81
5.5.2 Antarctic climate symposium 81
6. PUBLICATIONS 83
6.1 SCIENTIFIC PUBLICATION IN INTERNATIONAL JOURNALS 83
6.2 CONTRIBUTIONS TO CONFERENCE PROCEEDINGS & NATIONAL PUBLICATIONS 84
6.3 OUTREACH TO THE SCIENTIFIC COMMUNITY 84
6.4 OUTREACH ARTICLES FOR THE GENERAL PUBLIC 84
6.5 POSTERS & PRESENTATIONS 85
6.5.1 Oral Presentations 85
6.5.2 Posters 87
7. ACKNOWLEDGEMENTS 90
8. REFERENCES 91

Parts of this report are based on the published articles listed in section 6.

ABSTRACT

Context

The water cycle, cloud microphysics and cloud-aerosol-radiation interactions are key components of the Antarctic climate system; clouds and aerosols play a significant role in the surface energy budget thus affecting the surface temperatures. Turner et al. (2006) hypothesize that changes in cloud amount or particle size have played a role in the major warming of the Antarctic winter troposphere. In addition, clouds are an important part of the hydrological cycle serving as the agents linking water vapour transport into Antarctica with precipitation. Because precipitation is the only source term in the mass balance of the Antarctic ice sheet, it is one of the key factors affecting sea level.

The remoteness and harsh conditions, inhibiting the deployment of instrumentation, limit the understanding of Antarctic cloud and aerosol processes. However, this is now changing with robust ground-based remote sensing instruments becoming available that can both vertically and temporally resolve the aerosol, cloud, precipitation and meteorological state (Stevens and Feingold, 2009). The first station, employing a comprehensive set of in-situ and remote sensing observations of clouds and aerosols is the Belgian Antarctic station Princess Elisabeth (PE) in Dronning Maud Land, East Antarctica. This is the only site that deploys a precipitation radar, which opens the avenue to obtain insight in quantitative precipitation amounts separately from the other components of the local surface mass balance. Note that these other components are mainly redistribution of snow and sublimation.

The PE observatory opens the avenue to study the direct effect of clouds, precipitation and aerosols on the East Antarctic climate system. But it also enables a study on how aerosols affect the Antarctic climate indirectly: The “aerosol indirect effect” refers to the role of aerosols as cloud condensation and ice nuclei, thereby affecting clouds and precipitation. To study this effect, the one-moment schemes for representation of cloud microphysics, which are currently used in many Antarctic models, are unsuitable by design as these models do not relate the drop or ice particle size distribution directly to the aerosol distribution. Comprehensive double-moment cloud microphysics schemes do take into account aerosol types that activate at a given supersaturation (Seifert and Beheng, 2006), and in this way include the aerosol indirect effect. The regional climate model COSMO (COnsortium for Small-scale MOdelling) in its climate mode (COSMO model in Climate Mode, CCLM) does include such a double-moment scheme. In addition, it is a non-hydrostatic model with no scale approximations and applicable especially at the kilometre scale (in our case 2.8 km resolution) and it has been coupled to the Community Land Model. This coupled version is referred to as COSMO-CLM². It is the first time that such a high-resolution climate model with a double-moment cloud scheme is applied to a region in Antarctica.

Objectives

The objectives of the AEROCLOUD project are:

1) Build up an extensive database on cloud, precipitation and aerosol properties derived from measurements performed at the Belgian station Princess Elisabeth in Dronning Maud Land, East Antarctica. This extensive database is referred to as the AEROCLOUD database.
2) Evaluate and improve the COSMO-CLM² regional climate model for Antarctica.
3) Assess the role of aerosols and clouds in the East-Antarctic climate system, with focus on precipitation, surface energy balance and near-surface temperature, using the AEROCLOUD database and COSMO-CLM² integrations.
4) Improve the understanding of the relation between aerosols and clouds in East Antarctica, using the AEROCLOUD database and COSMO-CLM² integrations.
5) Valorise the results by scientific publications and workshops, easy access to an integrated database with all observations, open lectures to the general public and press contributions.

Conclusions

In the framework of the AEROCLOUD project, a unique extensive database on cloud, precipitation and aerosol properties from the Princess Elisabeth Station (East Antarctica) was established. This database covers a 10-year period and consists of raw data from ground-based in-situ and remote sensing instruments together with derived products for which algorithms have been developed in the course of this project. More specifically, algorithms have been developed for cloud detection from ceilometer, for snowdrift from ceilometer and for snowfall from radar. The data has been extensively used, not only within the project but also by national and international research partners. Currently, data are available on request (aerocloud.be) and will soon be made freely available on the world data center PANGEA.

Basic understanding of cloud, precipitation and aerosol properties has substantially evolved during the AEROCLOUD project. For the first time ever in Antarctica, snowfall has been measured independently from accumulation (the latter also including the effect of surface and snowdrift sublimation and redistribution of snow by the wind). It was found that strong deviations exist between snowfall and accumulation: On the one hand, the Princess Elisabeth site receives accumulation during synoptic events from upstream fallen precipitation whereas, on the other hand, snow that has fallen at the site is ablated during katabatic events. Generally, snow storms of longer duration and larger spatial extent have a higher chance of resulting in accumulation on a local scale. This work highlights that the local accumulation is strongly influenced by synoptic upstream conditions.

An aerosol climatology was established exhibiting high number of particles during summer when the polar vortex is less intense. High values for hygroscopicity suggest sea salt content and high reflectivity of the aerosols points towards a sulfate component. These sulfate-

containing aerosols are likely from biogenic dimethyl sulfide sources (marine plankton), which is further supported by the high abundance of particles smaller than 35 nm and by the backward trajectories pinpointing the southern ocean (40°-60°S) as a source area for these aerosols. The MAXDOAS observations indicate the presence of elevated aerosol layers probably associated with long-range transport. Generally there is little connection between the aerosols in higher atmosphere and the near-surface aerosol content.

A regional climate model (COSMO-CLM^2) was adjusted for Antarctic conditions and shows satisfactory performance compared to a newly compiled dataset of in-situ data of temperature, wind, relative humidity and accumulation, although coastal accumulation and coastal albedo are underestimated. The model is a valuable additional member for the POLAR-CORDEX ensemble, adding to the ensemble of regional climate models for the region. The newly compiled dataset was also used to evaluate Antarctic re-analyses, indicating that ERA-5 outperforms the other re-analyses for accumulation and temperature and MERRA-2 is better than the other re-analyses for wind.

Apart from the evaluation of the regional climate model, the ground-based AEROCLOUD instrumentation was used to validate satellite data. Satellites provide a continent-wide perspective, but have hardly been validated for the Antarctic region. It was found that the frequently used snowfall products from the Cloud Profiling Radar on board the CloudSat satellite accurately represent the snowfall climatology at the three sites were ground-based vertically-pointing radars are operating (biases < 15 %). However, the CloudSat product does not perform well for individual snowfall events. Moreover, the snowdrift product, derived from the Cloud-Aerosol LIdar with Orthogonal Polarization (CALIOP) on board of CALIPSO, which is essentially a clear-sky product, deviates strongly from snowdrift in all-sky conditions. About 90 % of blowing snow happens under cloudy conditions at Neumayer and Princess Elisabeth station.

The effect of aerosols on cloud and precipitation processes was illustrated for model case studies with COSMO-CLM^2 for the Princess Elisabeth region. The models turned out to be sensitive for the number of ice nuclei: When the air is pristine like in Antarctica where few ice nuclei are present, clouds can sustain liquid water layers which is not the case for higher number concentrations of ice nuclei. Such liquid-containing clouds were also detected from the AEROCLOUD observatory. Local precipitation is reduced due to the longer residence time of these liquid containing clouds and the cloud radiative forcing is increased due to increased longwave downwelling radiation. The number of ice nuclei appeared to be much more important than the number of cloud condensation nuclei.

These findings, which were published in 13 peer-reviewed publications, clearly demonstrate the value of sensor synergy, referring to necessity of combining different instruments at one site to obtain a complete picture of the processes ongoing. Although much progress has been made within AEROCLOUD, some gaps have been identified that need to be addressed in future. First of all, to improve derived products from the raw data, observations need to be performed on the snow particle mass (which was identified as the most uncertain parameter for the snowfall

retrieval), on the size range of aerosols below 90 nm (which was not detectable by current instruments, but is highly relevant for Antarctica) and on the elevated aerosol layers (a LIDAR would add much value compared to the MAXDOAS). Moreover, for studying the cloud-aerosol effect, observations of the number of ice nuclei are of key importance as indicated in the model case studies. Additionally, research on cloud aerosol interaction would benefit from increased attention to the Southern Ocean, where the majority of aerosols were found to be originating from. Lastly and most importantly, it is recommended to continue the operation of the cloud-precipitation-aerosol observatory at the Princess Elisabeth Station in order to extent these valuable time series, which can then act as a basis for various climatological research.

Keywords

Aerosols, clouds, blowing snow, atmospheric regional cycle, Belgian Antarctic station, regional climate modelling

1. INTRODUCTION

Antarctica is a large continent approximately 1.5 times the size of continental Europe (14,000,000 km²). It is characterised by extreme cold temperatures, due to its location at high latitudes near the South Pole, but also due to the height of the continent (up to 4,000 m above sea level (a.s.l.); Figure 1). Antarctica is usually subdivided in two parts, along the Greenwich meridian or the Transantarctic Mountains. East Antarctica is almost completely covered by ice of several kilometres thickness and is considered a plateau, while West Antarctica has a much lower horizontal and vertical extent and is located at lower altitude. The amount of ice located on the Antarctic continent is sufficient to raise global sea level by approximately 58.3 m if melted completely (Vaughan et al., 2013). In the past, it was assumed the Antarctic Ice Sheet (AIS) was close to equilibrium, i.e. the amount of deposited snow equals the amount of ice discharge, and the contribution of the AIS to global sea level was considered to be low (Vaughan et al., 1999). Air temperature rises over the last decades have however been exceptionally high over the ice sheet (2.4°C in West Antarctica since 1958), making it a vulnerable region for future climate change (Bromwich et al., 2013).

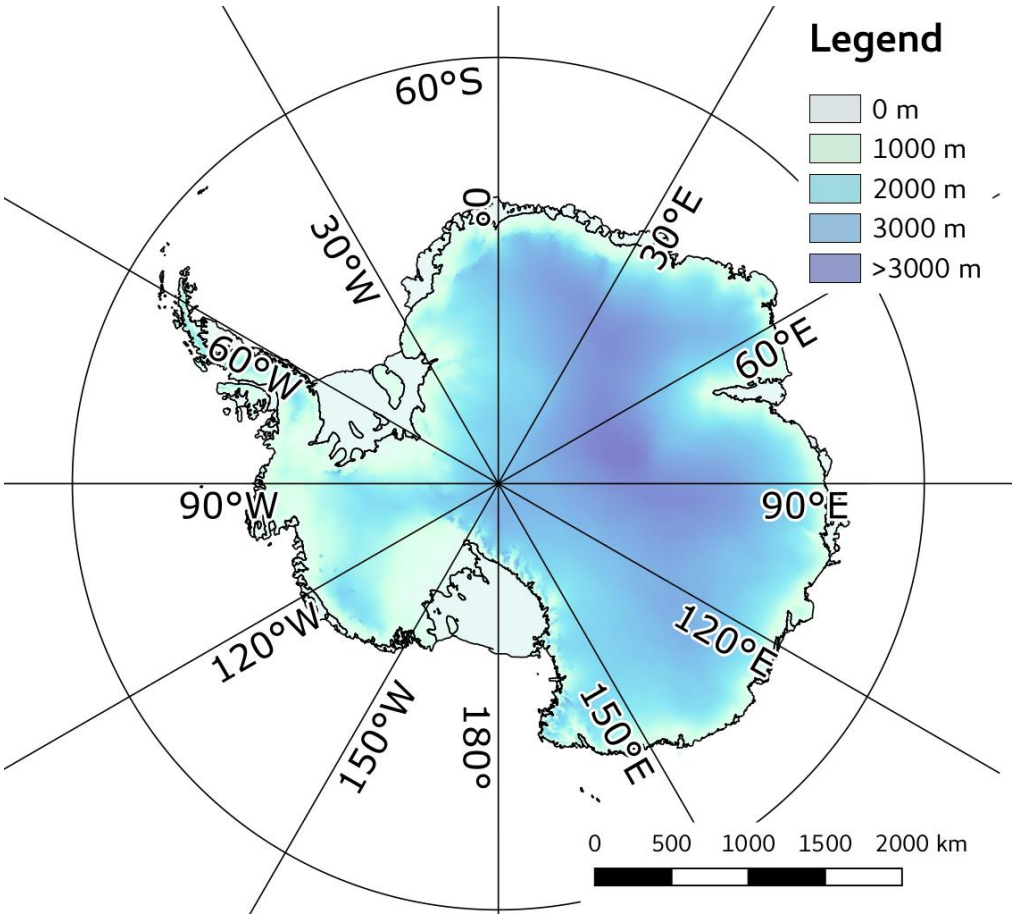

Figure 1: Location and altitude of the Antarctic Ice Sheet. Source: Landsat Image Mosaic of Antarctica (Lima) Project, .

Despite its importance in regulating sea level rise and the global climate, accurate observations of climatological variables is still lacking. In recent times, efforts have been made to expand the

amount of observations of basic meteorology such as temperature and wind speed, both near the surface and for the full atmospheric column. Furthermore, surface mass balance measurements have been performed at several locations. However, observations of other atmospheric parameters, such as clouds, precipitation and aerosols are still limited to a few locations over the continent. Nevertheless, the role of clouds in the climate system, their interaction with radiation, the coupling between aerosols and clouds and the atmospheric branch of the hydrological cycle are recognized as key elements in the climate system by several international consortia, such as the Joint Programming Initiative Connecting Climate Change Knowledge for Europe (JPI Climate). Although these research topics are high on the international research agenda, hardly anything is known about the interaction between clouds, precipitation and aerosols in the Antarctic. This is unfortunate, as the Antarctic ice sheet is expected to become a dominant contributor to sea level rise in the 21st century. Since precipitation is the only source of mass to the ice sheet, and precipitation and cloud processes are closely connected, an improved insight in these processes is essential.

AEROCLOUD's main objective is to improve the understanding and modelling of clouds, precipitation and their interaction with aerosols in Dronning Maud Land (DML; East Antarctica). This includes an improved insight in the so called "indirect aerosol effect", which refers to the role of aerosols to act as cloud condensation nuclei and ice nuclei, thereby affecting the characteristics of clouds. In the project, this was tackled from two perspectives.

On the one hand, observations from the meteorological cloud-precipitation-aerosol observatory that has been established during 2009-2012 at the Belgian Antarctic station Princess Elisabeth (PE) are used. The observatory has been installed in the framework of two projects, financed by the Belgian Science Policy (BELSPO). The observatory is unique in its set of robust ground-based in-situ and remote sensing instruments (see also section 3.1 and Figure 2 to 5). The data processing component provides improved algorithms, necessary to retrieve relevant cloud, precipitation and aerosol characteristics from the observed data.

On the other hand, a better understanding of the key atmospheric processes in the climate system of Antarctica is achieved using a regional climate model, COSMO-CLM². The use of models is beneficial as they provide spatial and temporal coherent information for long time periods for a certain region of interest. This allows to study processes and interactions in great depth and detail. However, a correct representation of the current climate is crucial in order to obtain confidence in the results of these models. By evaluating the COSMO-CLM² based on the limited number of observations that are available and by including parameterizations of aerosol and cloud microphysics, a reliable performance is obtained. Simulations at both the Antarctic-scale (horizontal resolution of 25 km) and the local scale (horizontal resolution of 2.5 km) delivers insights in the atmospheric processes and cloud-aerosol-precipitation interactions over the continent.

2. STATE OF THE ART AND OBJECTIVES

2.1 The hydrological cycle over Antarctica

2.1.1 Clouds

Clouds play an important role in the Antarctic climate and SMB. At first, they are capable of transporting high amounts of moisture over large distances, in which droplet formation or ice nucleation can form precipitation. Secondly, they have an important impact on the surface energy balance. Lastly, a correct representation of the cloud amount and phase is crucial in climate models for the simulation of precipitation timing and the surface energy balance representation.

The extreme environment and climate of the Antarctic Ice Sheet both lead to unique cloud properties and poses significant difficulties in cloud observations. In polar latitudes, low temperatures favour formation of thin ice clouds at all heights including near the surface during the entire year as compared to their occurrence globally only in the upper troposphere (Grenier et al., 2009; Bromwich et al.,2012). Thin ice clouds can have an important effect on the surface and top-of-atmosphere energy balance in the polar regions (Girard and Blanchet, 2001). Further, mixed-phase clouds containing supercooled liquid water at air temperatures as low as -38 to -40°C (below which homogeneous ice nucleation occurs) have been observed over the Antarctic ice sheet during short measurement campaigns (Lachlan-Cope, 2010). Lidar measurements at the near-coastal Antarctic stations also indicated frequent occurrence of liquid-containing clouds (Lachlan-Cope et al., 2016). Presence of liquid water has an important effect on cloud radiative properties by increasing cloud optical thickness and long-wave (LW) emissivity (e.g. Shupe and Intrieri, 2004). It is also an important player in precipitation formation favouring ice particle growth. Identifying ice and liquid-containing clouds is thus of high importance for understanding both precipitation processes and energy balance over the Antarctic ice sheet.

Observations of clouds and precipitation in Antarctica can be dated back to the first exploratory expeditions. The longest cloud and precipitation records in Antarctica (since 1950s) are available via visual observations of cloudiness, cloud types, precipitation and other weather phenomena at several year-round Antarctic stations (e.g. Turner and Pendlebury, 2004). Since the beginning of the satellite era in 1979, cloud occurrence and some properties have been derived from passive satellite observations; however, serious limitations were encountered over ice/snow surfaces (Town et al., 2007). The launch of active sensors (lidar and radar) on the A-train satellites marks another important step, especially for polar cloud observations, providing vertical profiles of cloud and precipitation microphysical and radiative properties (e.g. Grenier et al., 2009). CloudSat's radar measurements provided an opportunity to estimate the climatology of the Antarctic snowfall (Palerme et al., 2014). Despite tremendous progress in cloud observations from space, limitations in the characterisation of low-level clouds and precipitation persist: they can remain undetected by Cloud-Sat's radar (Maahn et al., 2014),

while CALIPSO's lidar is rapidly attenuated by cloud liquid water, leaving no information on atmospheric features occurring below the top of the liquid layer (Cesana et al., 2012). Cloud fraction and optical thickness have also been approximated using near-surface broadband LW radiation measurements (Kuipers Munneke et al., 2011). Recently available advanced ground-based remote-sensing and airborne measurement techniques provide valuable insights into cloud and precipitation microphysical properties (e.g. Lachlan-Cope,2010). These measurements, however, are usually limited to short periods requiring significant maintenance efforts, costs, and power/logistics demands. Ground-based remote-sensing instruments, operated during different periods at various locations over the Antarctic ice sheet, provided valuable statistics about cloud and precipitation properties. Information on cloud base height and phase has been obtained from lidar measurements at various Antarctic locations (e.g. Mahesh, 2005). Ceilometers have been mostly used for aviation reports at several Antarctic stations (e.g. Halley, Neumayer, Novolazarevskaya, South Pole, TerraNova). Measurements at the South Pole during the entire year of 1992 using ground-based infrared remote-sensing techniques provided information on cloud base heights and optical depths (Mahesh et al., 2001a, b). Bromwich et al. (2012) provided an extensive overview of existing Antarctic cloud data from various measurement techniques.

2.1.2 Precipitation

Precipitation rates over Antarctica are generally not measured directly. Most studies derive yearly precipitation amounts from ice cores and stake measurements, which are actually records of the local SMB. These records do not take into account the removal of precipitation due to (surface and blowing snow) sublimation, which can be considerable over the Antarctic, up to 20 % of the annual precipitation (Déry and Yau, 2002). Furthermore, they neglect disturbances by the transport and redistribution of snow by high wind speeds.

Local direct measurements of precipitation are currently limited to a few locations over Antarctica. On some locations, gauges are installed. However, Antarctic precipitation events are usually associated with high wind speeds, impeding the correct catchment of precipitation in the gauge. Furthermore, blowing snow associated with high wind speeds might enter the gauge, leading to erroneous measurements (Yang et al., 1999). Measurements using precipitation radars are not affected by these high wind speeds. These radars provide an estimate of the precipitation intensity by measuring the amplitude of the signal backscattered by hydrometeors. However, in order to derive precipitation rates from these backscatter values, information about the micro-structure of the snowflakes is necessary, such as their size, shape,... In the past, these microphysical characteristics were obtained in labour-intensive field campaigns, using petri dishes to capture individual snowflakes (e.g. Kajikawa, 1972). However, in recent decades disdrometers became available to obtain this information, having the advantage to capture large samples at high resolution (Brandes et al., 2007; Wood et al., 2013). Furthermore, robust multi-frequency radars have been developed in the last years, which are capable of deriving both an estimate of precipitation intensity and the microphysical properties of the snow particles, such as spheriodicity or the amount of riming and aggregation (Kneifel et al., 2015; 2016). Despite

the ability of radars to retrieve precipitation intensities, their application over the AIS remains limited. Furthermore, there is only a limited amount of information available about the microphysical characteristics of the snowflakes. As such, the estimate of precipitation rate by these single-frequency radars remains highly uncertain, limiting advancements in Antarctic ground-based precipitation retrieval.

The lack of spatial coverage of ground-based precipitation rate measurements can be tackled by using space-borne radars, such as aboard the CloudSat satellite. This satellite is used to retrieve vertical profiles of precipitation intensity which are converted to precipitation rates using a priori estimates of the microphysical characteristics of snow particles (Wood et al., 2013). However, the satellite has a limited swath width and only overpasses each location of the Antarctic within a range of 100 km on average once every 5 days. This low temporal resolution together with the uncertainty on the microphysical characteristics of the snow particles leads to very high uncertainties in the retrieved precipitation amounts.

Based on these measurements, a mean average precipitation rate of 171 mm year^{-1} is obtained over the AIS (north of 82°S; Palerme et al., 2014). Precipitation amounts are however highly variable. Coastal areas can receive precipitation amounts up to 500 mm year^{-1} and some locations over the Antarctic Peninsula attain for values close to 1000 mm year^{-1}. The inland of Antarctica is considered a cold desert, having low annual precipitation amounts ($<$ 20 mm year^{-1}) due to its remote location at high altitude and extreme cold temperatures.

Apart from a large spatial variability, there is also a high temporal variability in precipitation amounts (Gorodetskaya et al., 2013) which can be related to the characteristics of the precipitation regime over Antarctica. The annual precipitation amount is highly dominated by a few high-intensity events (Gorodetskaya et al., 2014). These events originate from low pressure systems moving around the AIS in the Antarctic Circumpolar Trough (Uotila et al., 2011). The strongest low pressure systems are capable of transporting moisture from mid-latitudes towards the AIS in a concentrated narrow and long band, denoted as an atmospheric river (Gorodetskaya et al., 2014). When atmospheric rivers make landfall at the AIS, very high precipitation rates are recorded. It is clear that due to the limited overpass frequency of CloudSat, these events can be missed, leading to large biases in precipitation numbers. Getting an estimate of the uncertainty of precipitation amounts obtained by the satellite are therefore highly desirable.

2.1.3 Blowing snow

Snow particles can be dislodged from the snow surface, picked up by the wind and lifted from the ground into the near-surface atmospheric layer. Drifting snow events are shallower than blowing snow events. Drifting snow typically stays below 2 m height whereas blowing snow can reach heights of several hundreds of meters. The transport involves a mix of suspension and saltation transport modes (Leonard et al., 2011), with a dominance of saltating particles (Bagnold et al., 1974) in the case of drifting snow, and suspended particles in blowing snow layers (Mellor et al., 1965).

Blowing snow impacts Antarctic ice sheet surface mass balance: wind-induced erosion or redeposition of transported snow particles from one location to another is crucial at the regional scale (Gallee et al., 2001, Dery et al., 2002, Lenaerts et al., 2012, Groot Zwaaftink et al., 2013) through the displacement and relocation of the snow particles (Dery et al., 2004). This phenomenon occurs approximatively on 70 % of the Antarctic continent during winter (Palm et al., 2011, 2017).

In addition to snow transport, the sublimation of blowing snow is an effective sink of AIS SMB (Kodama et al., 1985, Takahashi et al., 1992, Thiery et al., 2012, Dai et al., 2014). Particles suspended in the air offer a larger surface area to sublimation than those on the ground, resulting in more efficient sublimation (van den Broeke et al., 2004, Bintanja et al., 1995). The combination of blowing snow sublimation and transport is estimated to remove from 50 to 80 % (van den Broeke et al., 1997, Frezzotti et al., 2004, van den Broeke et al., 2008, Scarchili et al., 2010) of the accumulated snow on coastal areas.

Many studies have focused on a minimum wind speed as a threshold to dislodge snow particles, depending on the snow surface properties (Budd et al., 1966). Schmidt (1980, 1982) explained that cohesion between snow particles requires higher wind speeds or a higher impacting force of particles on the snowpack. In addition, the presence of liquid water in the snow and enhanced snow metamorphism with the higher atmospheric temperatures in the summer induce varying wind thresholds throughout the year (Bromwich et al., 1988, Li et al., 1997).

Currently, simulations of the AIS SMB are highly uncertain since both precipitation and blowing snow processes are poorly constrained and probably lead to inconsistencies between the atmospheric modelled precipitations and the measured snow accumulation value (Frezzotti et al., 2004, van de Berg et al., 2005, Scarchili et al., 2010, Groot Zwaaftink et al., 2013, Gorodetskaya et al., 2015).

A number of measurement campaigns have been organized in various regions of the AIS, using different types of devices: nets, mechanical traps and rocket traps, photoelectric and acoustic sensors, or piezoelectric devices (Leonard et al., 2011, Barral et al., 2014, Trouvilliez et al., 2014, Amory et al., 2015). However, custom-engineered sensors are rather expensive and scarce (Leonard et al., 2011), and both the remoteness of the continent and the harshness of the climate are limitations to widespread use of these devices.

Satellite remote sensing has recently been used to retrieve blowing snow observations on the entire AIS. In particular, the Cloud-Aerosol LIdar with Orthogonal Polarization (CALIOP) on board the Cloud Aerosol Lidar and Infrared Pathfinder Satellite Observations (CALIPSO) satellite has been used to design an algorithm that uses the CALIOP 20 Hz calibrated, attenuated backscatter profiles to derive blowing snow occurrence, layer height and optical depth (Palm et al., 2011). Furthermore, snow transport and sublimation rates over the full ice sheet were derived since 2006 (Palm et al., 2017). However, satellite blowing snow detection is hampered by the presence of (optically thick) clouds, which implies that the blowing snow retrieval is

limited to clear-sky or optically thin cloud (< 2-3) conditions. Additionally, the vertical resolution of CALIPSO limits the detection to blowing snow layers to a minimum 30 meter thickness (Palm et al., 2017). And lastly, despite its potential for blowing snow detection, the CALIPSO product has not yet been validated.

2.2 Aerosol observations over Antarctica

The Antarctic region is particularly interesting for atmospheric particle in situ studies. Antarctica is located far from anthropogenic activities and is one of the most pristine areas on Earth (Hamilton et al., 2014). It is therefore a favourable environment for studying natural aerosol particle background conditions and processes that prevailed in a preindustrial atmosphere. A more accurate knowledge on preindustrial aerosol processes, conditions and properties, including aerosol-cloud-interactions is important for a reduction of uncertainties of model estimates concerning radiative forcing (Carslaw et al., 2013; Hamilton et al., 2014). In addition, the Antarctic region is sensitive to climate change. A changing environment in the Antarctic region will lead to changing sources and pathways of atmospheric particles. Respective measurements are therefore important in order to detect and to understand these changes.

Aerosol particles can be emitted into the atmosphere either directly, e.g., by mechanical processes or combustion, or indirectly, via nucleation from the gas phase. Limited aerosol sources are present on the Antarctic continent like dust from mountain areas (Virkkula et al., 2009), bacteria (Gonzales-Toril et al., 2009) and melt water ponds leading to local new particle formation (Kyrö et al., 2013). The Antarctic baseline aerosol budget recently has been found to originate from air masses of the free troposphere or lower stratosphere region, descending over the central Antarctic continent (Fiebig et al., 2014).

Although Antarctica presents a harsh environment where access to in situ measurements is connected to heavy logistic support, various studies on atmospheric particles have been conducted at different Antarctic research stations during the last decades. A wide range of topics has been investigated, including new particle formation (NPF; Koponen et al., 2003; Asmi et al., 2010; Kyrö et al., 2013; Weller et al., 2015), seasonal cycles of number size distribution and mass concentration (Koponen et al., 2003; Fiebig et al., 2014; Kim et al., 2017), chemical composition (Wagenbach et al., 1988; Teinilä et al., 2000), hygroscopicity (Asmi et al., 2010, Kim et al., 2017; O'Shea et al., 2017) and optical properties of aerosol particles (Weller and Lampert, 2008; Fiebig et al., 2014).

In general, there is a yearly trend in particle number concentration, with maximum values in the austral summer. Fiebig et al. (2014) concluded that these cycles are common across the Antarctic plateau, with free tropospheric air masses contributing to air detected at the ground. The highest particle concentrations found in the austral summer are frequently reported to be due to NPF events. Particles formed during NPF events are likely related to sulphate and compounds containing ammonia that were found in the particulate phase in the submicron size range (Wagenbach et al., 1988; Teinilä et al., 2000; Schmale et al., 2013). Precursor gases for NPF can originate from the Southern Ocean (e.g., dimethylsulfid, DMS) and possibly also from

other sources, e.g., cyanobacteria in melt water ponds (Kyrö et al., 2013), microbiota from sea ice and the ocean influenced by sea ice (Dall'Osto et al., 2017).

Newly formed particles were sometimes found to grow to size ranges at which they became activated and could form cloud droplets (Koponen et al., 2003; Kyrö et al., 2013); Some studies have reported on Antarctic cloud condensation nuclei (CCN) properties, however, the locations they cover are limited to the Antarctic Peninsula (DeFelice et al., 1997; Kim et al., 2017) or the area of the Wedell Sea on the Brunt Ice Shelf (O'Shea et al., 2017). Both locations are part of West Antarctica and particularly the Antarctic Peninsula is mainly influenced by marine air masses that directly originate from the Southern Ocean. Further in situ measurements of atmospheric particles, NPF events and CCN properties are therefore needed for East Antarctica, in order to gain a better understanding of atmospheric aerosol processes and their potential climatic impact (see next section 2.3).

2.3 The cloud indirect climate effect and aerosol-cloud-precipitation interactions

Aerosols have an important influence on the global climate. They interact directly with radiation by scattering or absorbing shortwave and longwave radiation, mainly having a net cooling effect on the climate. Cloud active aerosols, i.e. cloud condensation nuclei (CCN) and ice nuclei (IN) also indirectly influence the climate by modifying cloud microphysical properties. This affects the surface energy balance by influencing both the shortwave and longwave surface radiative fluxes, directly and indirectly influencing the SMB. Clouds reflect part of the incoming solar radiation, lowering the amount reaching the surface, leading to cooler conditions. On the other hand, they reflect part of the outgoing longwave radiation emitted by the Earth back to its surface, leading to warming. Depending on their height and thickness, the impact on longwave and shortwave radiation differs (Dong et al., 2006). Furthermore, the cloud phase is an important parameter determining the net radiative effect at the surface (Matus and L'Ecuyer, 2017). Low-level liquid or mixed-phase clouds for example have a lower albedo and transmit more shortwave radiation, while also reflecting more longwave radiation back to the surface, having a profound warming effect compared to ice clouds (Bennartz et al., 2013).

Over polar regions, the relative effect of clouds on the net surface energy balance is more important than over other regions of the globe. Generally, clouds over snow surfaces have a net positive effect on the surface energy balance, both during day- and night-time (van den Broeke et al., 2006) since the amount of reflected shortwave radiation is smaller than the amount of backscattered longwave radiation, causing a net positive radiation balance at the surface, i.e. a warming. The amount of backscattered longwave radiation is even larger when liquid or mixed-phase clouds are present, significantly increasing melt and directly affecting the SMB (Van Tricht et al., 2016).

Despite their importance, research regarding Antarctic clouds has been hampered in the past by a lack of observations. However, there are several instruments and methods available to derive cloud (properties) over the AIS. Direct observations from ground-based or space-borne LIDARs are capable of retrieving properties of clouds (e.g. Grenier et al., 2009). Apart from ground-based and space-borne lidars, radiation measurements of simple AWSs are used to retrieve cloud properties (Kuipers Munneke et al., 2011). Based on measurements of shortwave and longwave radiation, an estimate of cloudiness and cloud optical thickness is obtained. Measurements at South Pole suggest that cloud cover frequency lies around 60 % (Town et al., 2007), whereas at more coastal sites, this value increases to 80-90 % (Lachlan-Cope, 2010). Similar increases in cloud cover fraction from the poles to the coast have been observed by satellite records (Scott et al., 2017). Over the Antarctic plateau, most of the clouds only consist of very small ice particles. However, based on ground-based, aircraft and satellite observations near the coast, mixed-phase clouds and clouds containing supercooled liquid have been observed frequently (which can occur when temperatures exceed -35°C) and have a significantly effect on the surface energy balance (e.g. Silber et al., 2019).

Cloud active aerosols, i.e. cloud condensation nuclei (CCN) and ice nuclei (IN) are capable of modifying cloud microphysical properties. Aerosol-cloud-precipitation interactions are considered one of the key uncertainties by the IPCC regarding the Earth's energy budget and anthropogenic climate forcing (Rosenfeld et al., 2014). This is attributed to a lack of understanding of the interactions between aerosols, clouds and precipitation, which have proven to be extremely difficult to untangle (Stevens and Feingold, 2009). Generally, higher amounts of CCN and IN increase the amount of nucleation surfaces, leading to a higher amount of small drops in a cloud, which coalescence slower into raindrops, increasing the lifetime of a cloud and decreasing the amount of precipitation, which in turn affects the radiative balance (Rosenfeld et al., 2008). However, depending on the cloud type, its location, the aerosol characteristics and vertical extent, high amounts of CCN and IN might lead to other feedbacks. Over polar regions, these interactions are currently not well known, due to a lack of observations and limited modelling studies. However, due to its importance in the radiative and surface mass balance, it is vital to further investigate these processes.

2.4 Regional climate modelling

Despite recent efforts and a great increase in the number of observational databases in the past years, the amount of long-term climate information remains sparse over large areas of the AIS. This impedes our understanding about the Antarctic climate and the interactions with the ice sheet, the SMB and sea level rise.

Climate models offer the possibility to fill this gap as their simulations are able to cover the full Antarctic region for long time periods. Up to the nineties, climate model information was derived from Global Climate Models (GCMs). The aim of these GCMs is to give an accurate representation of the climate on a global scale. However, improvements to model physics and parameterisations of the land-climate have mainly focused on mid-latitudinal and tropical

regions, as these areas offer the best observations to validate the model performance. Furthermore, most GCMs have a very coarse horizontal resolution. The state-of-the-art Fifth Climate Model Intercomparison Project (CMIP5) GCM ensemble used in the latest Intergovernmental Panel on Climate Change (IPCC) report has horizontal resolutions ranging from 100-200 km, which is very coarse in order to take the variability of the topography of the AIS, the representation of ice shelves, sea ice and ice-ocean interactions into account. Nevertheless, even up to now, these are the main models providing information about climate change scenarios for polar regions.

Regional Climate Models (RCMs) offer the possibility to tackle part of the problems of GCMs. RCMs are limited area models, which dynamically downscale coarse-resolution GCM fields. As such, a more detailed high-resolution simulation can be performed. Apart from the higher horizontal resolution and more detailed topography, it is possible to adapt the physics of the RCM for the specific climate over the region of interest. This is vital in order to correctly represent the climate over the region. RCMS are forced with atmospheric re-analyses, which are observations of the Earths atmosphere, land and ocean surface, assimilated in global climate model simulations in order to produce a spatially complete, multi-variate, 3-dimensional dataset of the Earth's atmosphere that is as close to reality as possible. To minimize the bias of the modeled atmosphere compared to observations, a wide variety of observational products is used, including satellite data, ground stations, sea buoys, radiosondes and airplane observations.

The first applications of RCMs over the Antarctic occurred at the end of the last century. The main goal of these studies was to perform an evaluation of basic meteorology for a short time period compared to a limited set of observations or the study of the impact of large-scale atmospheric features on the local climate (e.g. van Lipzig et al., 1999). Despite the large role of the AIS in the global climate system, the development of RCMs for the region has been limited. The regional atmospheric climate model (RACMO2) has been applied for several process- and evaluation-based studies over the Antarctic. The model has been updated throughout the last decades to accurately represent the Antarctic climate and SMB (van Wessem et al., 2018) and has been used to study the past (e.g. Lenaerts et al., 2018) and future of the AIS (e.g. Ligtenberg et al., 2013). Furthermore, the model has been used to study distinct processes influencing the SMB, such as blowing snow processes (Lenaerts and van den Broeke, 2012), sublimation (Lenaerts et al., 2010) and wind-albedo interactions (Lenaerts et al., 2017).

Apart from RACMO2, the Modèle Atmosphérique Régional (MAR) has been applied in several setups over the AIS. Studies of the boundary layer (Gallée et al., 2015) and the SMB (Agosta et al., 2012) have been performed. Furthermore, long-term historical simulations are available (Agosta et al., 2019). Both RACMO2 and MAR have been used to assess the future SMB and the response of the AIS under global warming (Pattyn et al., 2018; Shepherd et al., 2018). Apart from these two models, a limited set of other model setups are available over the Antarctic, such as the Antarctic Mesoscale Prediction System (AMPS; now Polar Weather Research and Forecasting model (POLAR-WRF)), which has mainly been used for meteorological applications,

such as near-surface meteorology and cloud microphysics (Listowski and Lachlan-Cope, 2017). A limited number of simulations have been performed using the Met Office Hadley Centre Regional Model 3 (HadRM3) and the high resolution limited area model (HIRHAM5) of the Danish Meteorological Institute.

In order to obtain reliable estimates of the future Antarctic climate and SMB including sea level rise, a large number of high-quality climate model simulations needs to be considered, following an ensemble approach (Giorgi and Gutowski, 2015; 2016). Providing this information at a regional level is the goal of the COordinated Regional climate Downscaling EXperiment (CORDEX; Giorgi and Gutowski, 2016). A set of regional domains has been defined for which RCM simulations are requested, downscaled from different GCMs. Within the new CMIP6 ensemble, a framework is planned to produce a set of baseline homogeneous high-resolution downscaled projections for these domains. For most of the regions in the world, a large set of historical and future scenario simulations is already available. Also for the Arctic, a set of simulations have been provided throughout the last years. For the Antarctic however, the amount of historical and scenario simulations is limited to three high-quality models, impeding adequate future scenario interpretations as the model ensemble is not large enough. It is therefore of key importance for the modelling groups and research centres to apply more RCMs over the Antarctic region in order to obtain a better historical and future representation of the SMB, precipitation amounts and other processes impacting these features.

2.5 Objectives

The objectives of AEROCLOUD are:

1) Build up an extensive database on cloud, precipitation and aerosol properties derived from measurements performed at the Belgian station Princess Elisabeth in Dronning Maud Land, East Antarctica. This extensive database is referred to as the AEROCLOUD database.
2) Evaluate and improve the COSMO-CLM² regional climate model for Antarctica.
3) Assess the role of aerosols and clouds in the East-Antarctic climate system, with focus on precipitation, surface energy balance and near-surface temperature, using the AEROCLOUD database and COSMO-CLM² integrations.
4) Improve the understanding of the relation between aerosols and clouds in East Antarctica, using the AEROCLOUD database and COSMO-CLM² integrations.
5) Valorise the results by scientific publications and workshops, easy access to an integrated database with all observations, open lectures to the general public and press contributions.

3. METHODOLOGY

3.1 Instrumentation at the Princess Elisabeth station

Observational evidence of the impact of aerosols, clouds and precipitation on the SMB of the AIS is currently lacking. In order to tackle these gaps in current research, atmospheric processes are studied at the Belgian Princess Elisabeth Antarctic station in Dronning Maud Land.

The station is located within the escarpment zone of the Antarctic plateau at 1,390 m a.s.l. on a rock outcrop (Utsteinen ridge, 71°57'S, 23°20'E; Figure). This location was chosen as it is situated just north of the Sør Rondane mountain ridge, damming high winds originating from the Antarctic plateau. During the first scientific campaign in 2009 and the two consecutive ones, instrumentation was installed to monitor the composition and chemistry of the atmosphere.

The aerosol in situ measurement instrumentation was installed in a specific shelter located 60 m south of the main station. It was most often exposed to uncontaminated air due to the fact that PE station was designed as a zero-emission station and that the daily activities were concentrated in the west-northwest sector while the main wind directions were from south to east. The aerosol in situ instruments comprised (i) a condensation particle counter (U-CPC, model 3776, TSI Inc., USA) for total particle number concentration, (ii) a Laser Aerosol Spectrometer (LAS, model 3340, TSI Inc., USA) for number size distribution of particles, (iii) an aethalometer (Magee Sci., AE-31, Slovenia) for measuring the aerosol absorption coefficient and deriving of the mass concentration of light-absorbing aerosol, (iv) a nephelometer (Ecotech Aurora 3000, Australia) for measuring the total aerosol scattering coefficient, and (v) a Tapered Element Oscillating Microbalance with Filter Dynamics Measurement System (TEOM-FDMS) for the total particle mass concentration. Using these measurements, valuable information regarding aerosol transport mechanisms, their origin and formation history are studied in this pristine region (Herenz et al., 2019). In Herenz et al. (2019) the set up of the instrumentation is also described in detail.

Figure 2: The aerosol in situ instrumentation in the shelter south of the main station; from left to right: TEOM-FDMS, aethalomter, nephelometer, LAS and U-CPC

Sun-photometer and MAX-DOAS (Multi-Axis Differential Optical Absorption Spectroscopy) remote sensing instrumentations for measuring total and vertically-resolved aerosol content and characteristics were also operated at the Princess Elisabeth Station (PES) in the framework of AEROCLOUD. A commercial EnviMeS MAX-DOAS spectrometer (see Figure 3) was installed at the station in late November 2015. By scanning the scattered sunlight in successive elevations close to the horizon and analysing the atmosphere absorption signal using the DOAS method, the MAX-DOAS technique enables the retrieval of aerosol extinction (and atmospheric gases concentration) in a few successive layers above the surface to approximately 2-3 km altitude. The EnviMeS instrument covers both the UV (295-450 nm) and visible (430 - 565 nm) wavelength regions and the telescope scans zenith and different elevation angles at a fixed viewing azimuth (38°N-NE; pointing direction between the Vesthaugen and Romnoesfjellet mountains).

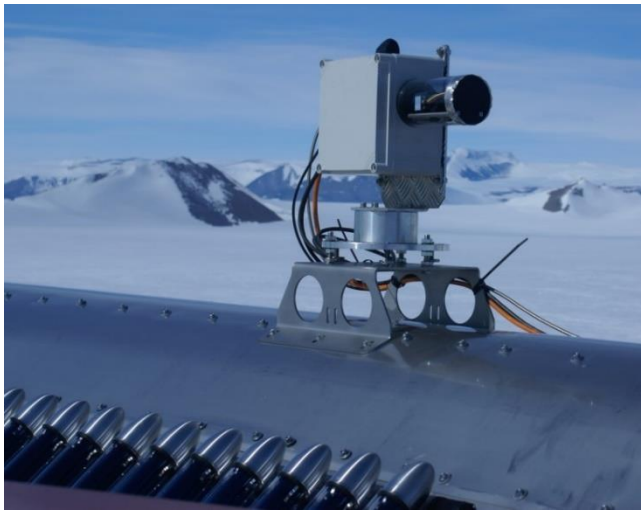

Figure 3: The EnviMeS MAX-DOAS instrument on the Northern roof of the PES.

The CIMEL CE 318 sunphotometer was installed at the station since 2009 (see Figure 4). CIMEL is a passive radiometer that measures direct sun and diffuse sky radiances (W/m-2) at 8 wavelengths (340 - 380 - 440 - 500 - 675 - 870 - 936 - 1020 nm). Total column aerosol optical depth (AOD) and the integrated precipitable water vapour (mm) are measured. Aerosol fine mode fraction, Angstrom exponent and single scattering albedo can also be derived. The instrument is yearly calibrated in Europe and travels forth and back in that purpose. CIMEl data are processed on-line and put on the AERONET portal (see https://aeronet.gsfc.nasa.gov/cgibin/type_one_station_opera_v2_new?site=Utsteinen&nachal=2&level=1&place_code=10).

Figure 4: the CIMEL sun-photometer instrument on the Northern roof of the PES.

Additionally, in 2009, an Automatic Weather Station (AWS) was installed 300 m east of the station (Figure 5). This instrument provides information regarding the atmospheric meteorological conditions near the station (temperature, wind speed and direction, humidity, pressure and radiative fluxes). It is also equipped with an acoustic height sensor, allowing to study changes in the total SMB. Based on these observations, a climatology of SMB and meteorological conditions has been provided, giving insight in the climate in the escarpment zone of the AIS (Gorodetskaya et al., 2011).

In 2010, the set of atmospheric measurements has been expanded by the installation of several instruments studying the hydrological cycle (Figure 5). A ceilometer was installed, which is a LIDAR instrument capable of detecting the height of the cloud base, including its phase. This instrument has been used to construct a climatology of cloud properties over the station (Gorodetskaya et al., 2015). At the same time, a Micro Rain Radar (MRR) was installed at the station. This instrument is an active vertically pointing radar capable of deriving vertical profiles of Doppler velocity, spectral width and precipitation intensity based on the return of the emitted

signal. Using the MRR measurements, a precipitation climatology was derived (Gorodetskaya et al., 2015) and an analysis of the vertical structure of precipitation was performed (Maahn et al., 2014). Furthermore, for the first time large precipitation events originating from atmospheric rivers were detected over Antarctica (Gorodetskaya et al., 2014). The installation of a webcam and a spotlight allowed to monitor the observatory year-round.

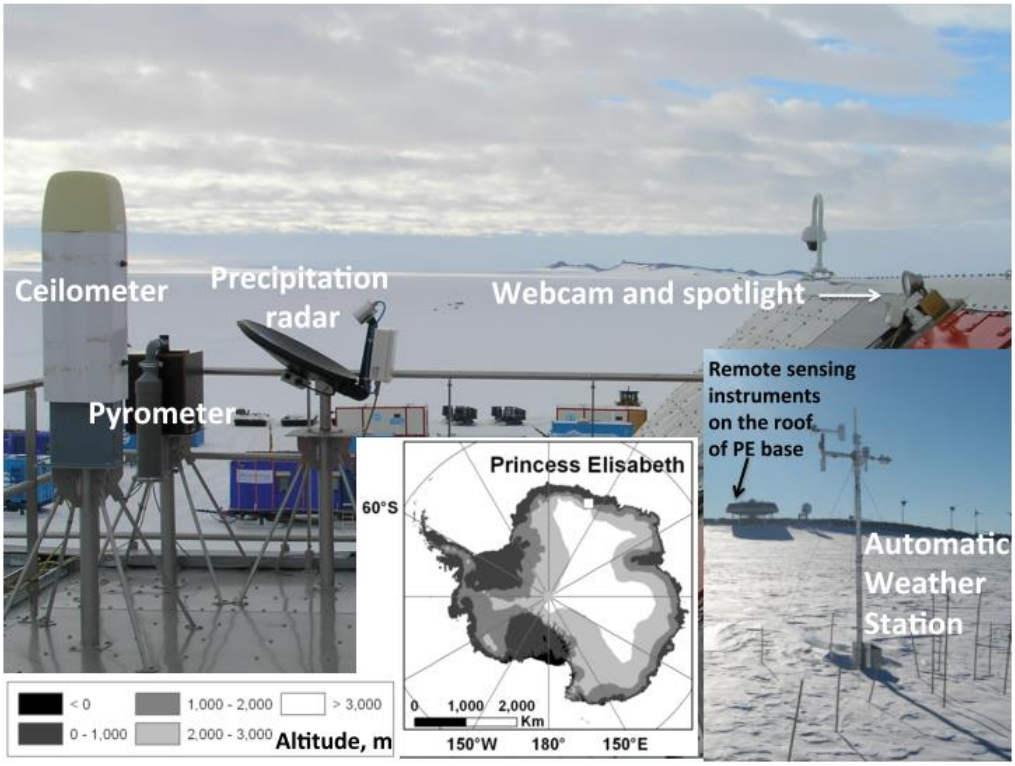

Figure 5: the cloud-precipitation-meteorological observatory at the Princess Elisabeth station in East Antarctica (Gorodetskaya et al., 2015)

3.2 Characterisation of cloud and precipitation properties and their effect on the surface energy and mass budgets

3.2.1 Derivation of cloud properties from multiple sensors

Cloud properties over the Princess Elisabeth station are analysed by the use of multiple instruments: a ceilometer, measuring cloud base height based on radar reflectivity and a pyrometer, measuring the temperature of the cloud base allowing to identify the phase of the cloud (liquid/ice). These instruments (and other cloud and precipitation instrumentation) are operated continuously and are maintained year-round. Based on their measurements, situations with clouds can be separated from clear-sky conditions and a subdivision between liquid and ice clouds is possible. This analysis has been executed for mainly summer measurements (winter measurements are scarce since instrumentation failure occurred during the period when there is no technical staff). This has led to a peer-reviewed publication (Gorodetskaya et al., 2015). Since 2013, measurements for winter period have also become available. Data transfer from the computers at PE to KU Leuven has been automated in order to have real time data

available and to enable rapid intervention in case of problems. Since the publication of the results, data analysis is executed each year to update the existing climatology.

3.2.2 Assessment of the effect of clouds on the surface energy balance

Radiative fluxes are retrieved from the Automatic Weather Station (AWS). These data records have been achieved for the whole observational period (2010-present). Apart from statistical results, the effect of different cloud types on the surface energy balance has been analysed based on several case studies. This work is presented in a peer-reviewed publication (Gorodetskaya et al., 2015).

3.2.3 Estimation of snowfall rate from the vertically-profiling precipitation radar

A vertically-profiling precipitation radar is deployed at PE since 2010 obtaining spectra for effective reflectivity (Ze), Doppler velocity and spectral width. The latest processing techniques are applied on this data. In order to obtain snowfall rates (SR) from the Ze measurements of the MRR, a relation between both quantities needs to be constructed (a so-called Ze-SR relation). For this, the Precipitation Imaging Package (PIP) is used (Figure 6). This instrument was installed in January 2016 and obtains information about snow particle microphysical characteristics. For every snow particle, several quantities are calculated such as diameter, area, axis ratio, grey level, among others. Apart from these classical optical measurements, PIP also calculates more advanced data products, such as the particle size distribution. Furthermore, a built-in tracker algorithm identifies the movement of snow particles throughout different image frames, allowing to calculate the terminal fall velocity of the particle. With this information, both Ze and SR are calculated from PIP measurements, allowing to construct a Ze-SR relation. An estimate of the Ze-SR relation for other locations over Antarctica is also found. A comparison between the Ze measurements of the MRR and calculated by the PIP shows good correspondence between both instruments for intense snow storms. As a last step, the uncertainty on the Ze-SR relation has been quantified for the first time. In order to identify the most important terms that attribute for uncertainty in SR estimates over Antarctica, a subdivision between different sources of uncertainty was made. With the Ze-SR relation obtained for PE, it is possible to convert all Ze spectra obtained by the MRR into SR. Furthermore, we are also able to calculate the uncertainty on SR. This work is published in the peer-reviewed international journal Atmospheric Research (Souverijns et al., 2017).

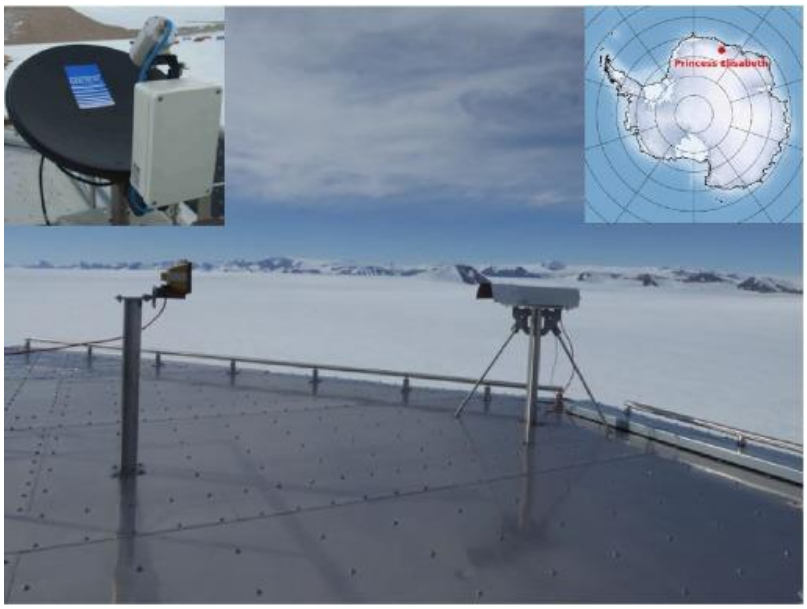

Figure 6: Precipitation Imaging Package deployed on the roof of the Princess Elisabeth station. The camera is located in the heated housing on the right of the image, while the halogen lamp is on the left. The upper left inset shows the MRR, while the upper right inset shows the location of the Princess Elisabeth station.

3.2.4 Evaluation of the CloudSat precipitation climatology

Apart from ground-based measurements, the Cloud Profiling Radar on board of the CloudSat satellite is the first to provide information about precipitation on a continental scale over the AIS. Launched in 2006, it overpasses each location on the AIS within 100 km with a temporal revisit time of seven days or less and has a strong latitudinal dependency. Palerme et al. (2014) constructed a continental precipitation climatology at a grid of 1° latitude by 2° longitude, including information about the phase and frequency of precipitation.

Using the ground-based precipitation radar at our station and two other stations (Dumont D'Urville and Mario Zucchelli station; Figure 7), the CloudSat precipitation climatology is evaluated. For this, first, the impact of the low overpass frequency of CloudSat and its effect on the uncertainty of the precipitation retrieval is calculated. Next, the precipitation amount obtained by CloudSat is compared to the retrievals of the MRR for overlapping periods of measurements. This work is published in the peer-reviewed international journal The Cryosphere (Souverijns et al., 2018b).

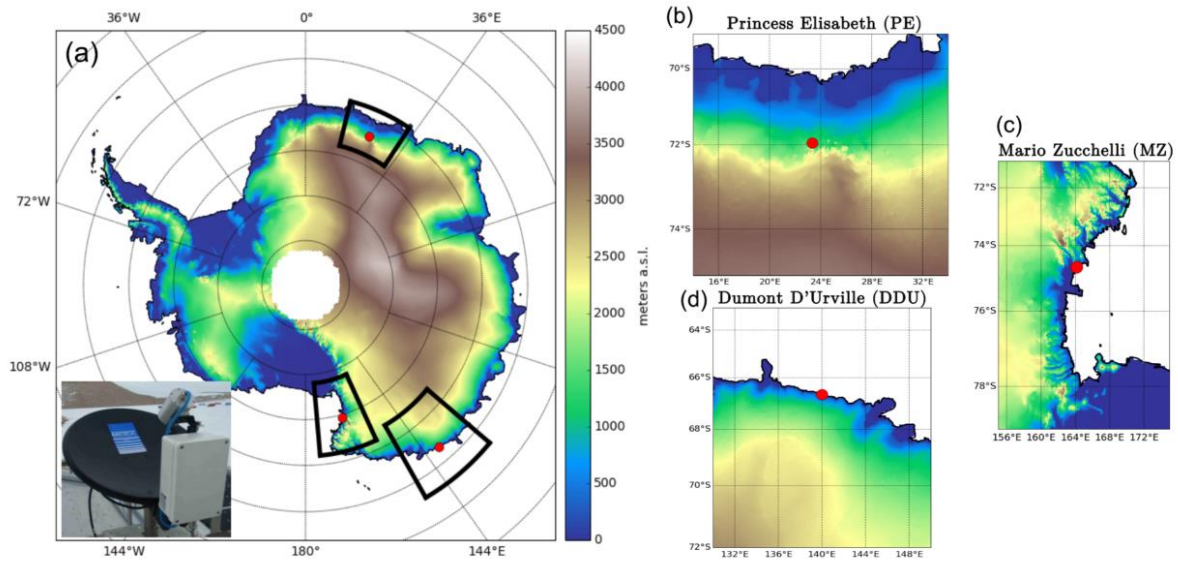

Figure 7: (a) Digital elevation map of the Antarctic ice sheet with three insets corresponding to the location of the Micro Rain Radars. The inset at the bottom left shows the Micro Rain Radar at the Princess Elisabeth station.

3.2.5 Assessment of the individual components of the surface mass balance

The local surface mass balance (SMB) at PE consists of four components: precipitation, erosion, surface sublimation and snowdrift sublimation. The latter two terms were quantified in Thiery et al. (2012), while the former two components were estimated by combining information from the MRR and the Automatic Weather Station (AWS), which is able to measure snow height changes. Using the unique collocated set of remote sensing instrumentation present at the PE station, the relation between snowfall and accumulation at the surface is investigated for the first time over Antarctica. Meteorological conditions during which precipitation, accumulation and ablation events occur are identified, indicating distinct atmospheric states that lead to SMB changes at the local scale. A paper on this work is published in the international peer-reviewed journal The Cryosphere (Souverijns et al., 2018).

The transportation of snow plays an important role in the local surface mass balance, as it can attain for both accumulation and ablation. In that aim, an algorithm was developed to routinely detect blowing snow, based on attenuated backscatter profiles from the ceilometer. This instrument measures the cloud base height (see task 1.1), but also yields information on boundary layer conditions and on the presence of suspended snow particles. The new algorithm uses a threshold-based method and calculates the concentration of particles in the vertical direction to assess the presence of blowing snow. At Neumayer Antarctic station, the detection algorithm was compared to visual observations, showing its ability to detect (heavy) blowing snow events. Collocated to AWS data, the key meteorological parameters during which blowing snow occurs were identified (wind speed, wind direction, relative humidity and stability of the boundary layer (temperature inversion)). A paper on the blowing snow detection algorithm is published in the peer-reviewed international journal The Cryosphere (Gossart et al., 2017).

The blowing snow retrievals from the ceilometer were then compared to satellite retrievals within a 1x1 degrees box around both stations (Figure 8). We looked at CALIPSO overpasses within the domain, and compared to ceilometer blowing snow frequencies and types at Princess Elisabeth and Neumayer station. Results display that most of the ceilometer detected blowing snow is missed since the vast majority of the events occur under cloudy circumstances at the two coastal locations. Since clouds impede satellite detection, they are missed by the satellite. In addition, the orography and the sharp blowing snow gradient around Princess Elisabeth station lead to false detection of blowing snow by the satellite. This analysis has been published in discussion in the peer-reviewed international journal The Cryosphere Discussions (Gossart et al., 2019).

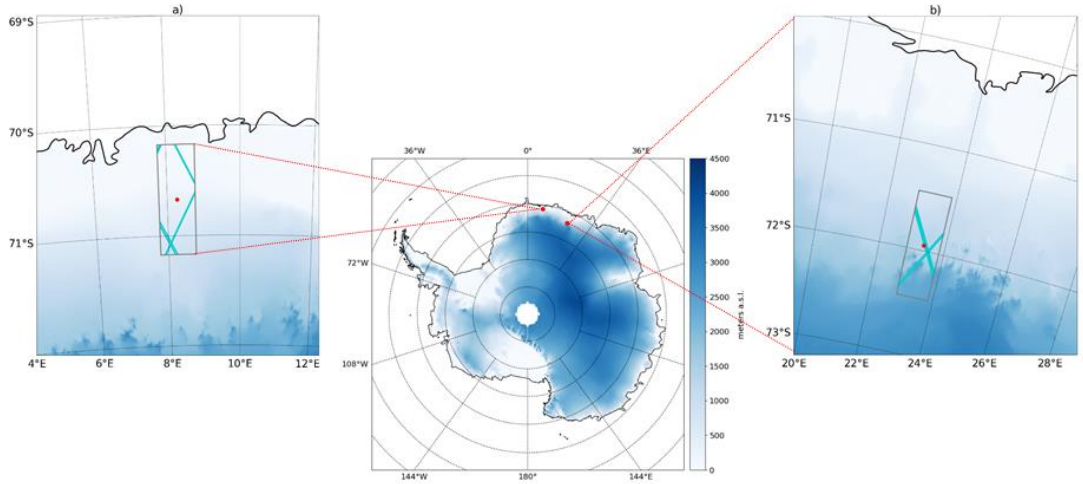

Figure 8: Comparison technique between the satellite overpasses in a 1°x1° box and the ceilometers at the Neumayer (a) and Princess Elisabeth station (b)

3.3 Characterisation of atmospheric aerosols

3.3.1 Estimation of aerosol characteristics from boundary layer measurements

Data from the aerosol observatory was combined to characterise the boundary-layer aerosol type, number, size and mass concentration. The aerosol could be classified as rather freshly produced or aged, long-range transported aerosol, if coarse sea salt or dust aerosol is present, if aerosol scattering dominated (indicative for sulphates, organics, coated particles), or if absorbing compounds were present (soot, organic carbon). The difference of the aerosol number between the Ultrafine Condensation Particle Counter (U-CPC) and the Laser Aerosol Spectrometer (LAS) gave the number of particles between 3 to 90 nm (nucleation/Aitken mode), indicating whether rather freshly produced aerosols were present. The dependency of aerosol absorption (aethalometer) and scattering (nephelometer) on wavelength put further constraints on aerosol type (e.g., flat spectral absorption of soot, stronger absorption of some organic compounds at shorter wavelengths). The Single Scattering Albedo (SSA; SSA = scattering / (scattering +absorption)) was directly determined by the simultaneous measurements of absorption and scattering. The SSA itself is a very good indicator if a distinct absorbing part is present. For all

instruments, final, validated and contamination-free (i.e. no traces of particles emitted by the station's activities) data are available from their respective start of observation and the data has been analysed statistically.

3.3.2 Retrieval of total column and vertically resolved aerosol properties with remote sensing instrumentation

MAX-DOAS extinction coefficient vertical profiles and corresponding AODs have been retrieved in both UV and visible ranges by applying the MMF profiling algorithm (Friedrich et al., 2019) on oxygen dimer (O_4) differential slant column densities (dSCDs) measured at 360 nm and 477 nm. MMF is based on the Optimal Estimation Method (OEM; Rodgers, 2000) and can operate in linear or logarithmic state vector space using VLIDORT (Spurr, 2006) version 2.7, the vectorized version of the LIDORT radiative transfer model (RTM) as forward model. A Round-Robin exercise carried out within the framework of the ESA FRM4DOAS project (Friess et al., 2019; see also http://frm4doas.aeronomie.be/) showed that MMF is performing better than the bePRO algorithm used during the first half of the project, due to the retrieval of concentration/extinction in a logarithmic space and the optimisation of the minimisation scheme (Levenberg-Marquardt instead of Gauss-Newton) and corresponding convergence criteria. Aerosol retrievals at PES were performed for the 2015/2016 and 2017/2018 seasons using the following settings:

- Temperature, pressure profiles from RMI radiosondes (2015/2016 and 2017/2018 seasonal averages)
- A-priori: exponentially decreasing with AOD = 0.05 and scaling height of 1km
- A priori covariance matrix S_a: 50% of the a priori profile on diagonal, Gaussian dependence for extra-diagonal terms with 250m correlation length
- Surface albedo: 0.8
- Henyey Greenstein phase function with asymmetry factor g = 0.7
- Single scattering albedo: 0.98 (typical values from RMI nephelometer)
- Altitude grid: 20 layers of 0.2km thickness from 1.39 km to 5.39 km asl.
- Quality control criteria based on degrees of freedom for signal (DOFS) and RMS of the difference between measured and calculated O_4 DSCDs have been applied.

It should be noted that MAX-DOAS measurements were not available during the 2016/2017 (PES station closed) and 2018/2019 (instrument blocked in zenith viewing mode) summer seasons.

As part of the AERONET network, the CIMEL sun-photometer provides daily aerosol optical, microphysical and radiative properties (AOD, size distribution, refractive index, single scattering albedo, asymmetry factor, phase functions) based on direct measurements of the solar radiation at different wavelengths. Detailed information about the AERONET retrieval can be found at https://aeronet.gsfc.nasa.gov/new_web/aerosols.html (see also Giles et al., 2019). In the time frame of AEROCLOUD, CIMEL measurements were only available during the 2017/2018 summer season.

3.3.3 Improved estimation of aerosol characteristics by Mie-Calculation and radiative transport modelling

The low aerosol content detected by the MAX-DOAS instrument over PES (see Sect. 4.2.2) has made difficult the retrieval of information on aerosol characteristics (particle size distribution) and type (marine versus continental) at clouds altitude levels. Therefore this task has been replaced by the identification of specific aerosol/cloud detection study cases by combining MAX-DOAS data with other aerosol surface measurements at PES (particle concentration from the RMI Condensation Particle Counter (CPC)), cloud information from the KULeuven ceilometer, temperature and pressure vertical profiles from RMI radiosondes, and temperature, wind speed and direction, and humidity from the AWS meteorological station. This new task aimed at getting a better insight on possible aerosol entrainment from the upper troposphere to the surface.

3.3.4 Estimation of cloud condensation nuclei and of ice nuclei

The number concentration of cloud condensation nuclei (N_{CCN}) was measured using a CCN counter (CCNc; Droplet Measurement Technologies, USA). The CCNc is a continuous-flow thermal-gradient diffusion chamber which is described in detail by Roberts and Nenes (2005). The CCNc was operated as recommended by Gysel and Stratmann (2013) for polydisperse CCN measurements. The CCNc was operated at five different supersaturations (ss; 01 %, 0.2 %, 0.3 %, 0.5%, 0.7 %). The instrument was provided by the Leibniz Institute for Tropospheric Research, TROPOS, Leipzig, Germany, during three austral summer seasons (2013/2014; 2014/2015 and 2015/2016). Prior to each of the three measurement periods, a calibration was done at the laboratory of TROPOS.

As the CCNc is only available during the summer seasons, empirical relations will be derived between measured aerosol physical properties and measured N_{ccn} in order to derive CCN concentrations for time periods when aerosol measurements were performed but there was no CCNc operational at PE. In order to estimate IN type and amount, which are not measured directly, we will use measure aerosol characteristics. The ice nucleation efficiency depends strongly on aerosol type, number and size. These data will be combined in order to assign ice nuclei concentrations as a function of supersaturation with respect to ice, based on the found aerosol properties and on literature data (e.g., Hoose and Möhler, 2012). This part of estimating CCN and IN numbers is still on-going when writing this report.

3.3.5 Assessment of the atmospheric aerosol variability at Utsteinen: composition by season, meteorological regime and altitude level

The complementary information on aerosol characteristics was integrated and combined with information on the meteorological conditions. An analysis has been performed of temporal variability (daily, monthly, seasonal properties) and of the dependency on meteorology. Time periods with potential new particle formation (increased nucleation/Aitken mode) received special attention. Furthermore, the vertical dependency of the aerosol extinction coefficient,

derived from the MAX-DOAS, was analysed together with the vertical exchange conditions using AWS and radio sounding data. The boundary-layer stability derived from the AWS (Thiery et al., 2012) indicated if exchange processes with the troposphere above were (i) suppressed (ii) possible or (iii) strengthened. Together, this allowed an estimation if the aerosol measured in the boundary layer was representative of the cloud level.

3.4 Evaluation and improvement of the regional climate model

3.4.1 Antarctic-wide climate model simulations with COSMO-CLM²

The COSMO-CLM climate model is a non-hydrostatic model that has mainly been used for climatic research over European regions. Its application to polar regions is limited. As such, several modifications to the original setup were necessary in order to achieve adequate performance over the Antarctic region:

- The COSMO-CLM model was coupled to the Community Land Model to improve the representation of the snow pack and snow metamorphism. This coupled version is referred to as COSMO-CLM². Adaptations to this land surface model to represent perennial snow cover were executed following the procedures described in Van Kampenhout et al. (2017).
- The roughness length of snow was adapted in order to match observed wind speeds.
- The near-surface climate over the AIS is typically characterised by an inversion, indicating a stable boundary layer limiting the amount of turbulence. The default turbulence scheme in COSMO-CLM² is not able to represent strong stable conditions as the minimum turbulent diffusion coefficients are relatively large, leading to a minimum amount of turbulence that is too high over the AIS. A sharp reduction of the minimum turbulent diffusion coefficients accounts for large improvements in surface temperature and boundary layer representation.
- Upper air relaxation using spectral nudging was applied to the top layers of the atmosphere adjusting the upper model levels to the large-scale driving model, ERA-Interim. This did not only reduce the bias at the highest model levels, but also improved temperature and wind speed representation at lower altitudes.
- In the default COSMO-CLM² setup, snowfall amounts over the AIS are generally overestimated. In order to get more insight in the drivers of precipitation over the AIS, the two-moment cloud microphysics parameterization scheme is implemented (Seifert and Beheng, 2006). This scheme parameterises all relevant homogeneous and heterogeneous nucleation processes including the activation of cloud and ice condensation nuclei (CCN and IN respectively).

Using this setup, an adequate representation of the Antarctic climate was achieved. A long-term (30-year) hindcast simulation was executed (1987-2016; excluding 4 years of spin-up time) on the Belgian Tier1 supercomputer (BrENIAC). Its performance was evaluated compared to several radiosounding, weather station and satellite measurements, obtaining an evaluation of upper-air and near surface temperature, wind speed and relative humidity. Furthermore, the performance of albedo, SMB and the surface radiative balance were assessed. As such, the COSMO-CLM² model also contributes to the CORDEX-Antarctica initiative as one of the few long-term hindcast

simulations over the region. A paper on the evaluation and performance of the long-term simulation over Antarctica was published in the peer-reviewed international journal Journal of Geophysical Research: Atmospheres (Souverijns et al., 2019).

We also evaluated four reanalysis products over the Antarctic Ice Sheet: European Center for Medium-Range Weather Forecasts's (ECMWF) ERA-5 and ERA-Interim, National Centers for Environmental Prediction (NCEP) Climate Forecast System Reanalysis (CFSR) and National Aeronautics and Space Administration (NASA) Modern-Era Retrospective analysis for Research and Applications, Version2 (MERRA-2). We investigate the near-surface temperature, wind speed, and relative humidity for the four re-analyses. We use the reanalysis output at timesteps 0 and 12 UTC. For SMB evaluation, 6-hourly precipitation and evaporation output is used.

3.4.2 High-resolution simulations with COSMO-CLM²

Using the Antarctic-wide simulation as a driving model at the boundaries, several simulations at high-resolution (2.8 kilometres) were performed centred over respectively the Princess Elisabeth station and the Roi Boudouin ice shelf. Both setups used an adapted version of the model presented in section 3.4.1.

Over the Princess Elisabeth station, COSMO-CLM² was expanded with an aerosol module (Possner et al., 2017). In combination with the detailed two-moment microphysical scheme of Seifert and Beheng (2006), this module is able to take into account detailed aerosol-cloud-precipitation interactions, processes such as aerosol activation, nucleation and the full aerosol cycle.

Over the Roi Baudouin ice shelf, a blowing snow routine was implemented in the COSMO-CLM^2 model in order to represent blowing snow sublimation and transport fluxes. This model was first tested in an offline simulation using only the land component, the Community Land Model, at two locations (D47 and D17 in Adélie Land) and proved good correspondence to field measurements (Amory et al., 2015). A paper over the blowing snow module is being prepared for submission.

3.5 Assessment of the indirect aerosol effect in Dronning Maud Land

3.5.1 Identification of the relationship between atmospheric composition, cloud and precipitation properties and air mass origin

The atmospheric circulation is a key factor affecting both cloud and precipitation systems but also the aerosol composition. An empirical study on the relation between aerosols and clouds can therefore only be done when taking into account large-scale airflow. Backward trajectories were calculated using the atmospheric trajectory model FLEXTRA (Stohl and Wotawa, 1995; Stohl et al., 2001), driven with meteorological input data from ECMWF, ERA-Interim. The calculations were done on a 0.75 ° x 0.75 °grid, on kinematic trajectories using 3D wind fields taking into account diabatic vertical motions.

To analyse the influence of the air mass origin on particle number and on N_{CCN}, two further models were applied. One is the NAME model (Jones et al., 2007), which was used to perform a residence time analysis and the other one is the Potential Source Contribution Function (PSCF), a more advanced type of residence time analysis that results in a probability field which represents the probability of a specific location to contribute to high measured receptor concentrations (Fleming et al., 2012). In our case, 75 % percentile values were taken. The NAME atmospheric dispersion model is a Langrangian particle-trajectory model, operated by the UK Meteorological Office. For the PSCF modelling, the NOAA Hysplit trajectory model (Stein et al., 2015) was used to calculate hourly resolved 10-day back trajectories based on 1° x 1° GDAS (Global Data Assimilation System) meteorological data.

3.5.2 Identification of the model sensitivity to cloud condensation nuclei and ice nuclei

In order to study the relation between aerosol content, cloud microphysics and precipitation, several test simulations were executed using aerosol concentrations measured at the PE station (Herenz et al., 2019). Ice nuclei concentrations are derived from literature. The effect of aerosol variability on clouds, precipitation amounts and the radiation balance has been studied for a short test case in summer.

		Aerosols (cm^{-3})		
		10	212	1300
Ice nuclei (L^{-1})	$2*10^{-3}$	X		X
	0.1		X	
	5	X		X

Table 1: Overview of the parameters set in the different simulations. Apart from these, also a simulation without the aerosol module was performed.

4. SCIENTIFIC RESULTS AND RECOMMENDATIONS

4.1 Characterisation of cloud and precipitation properties and their effect on the surface energy and mass budgets

4.1.1 Derivation of cloud properties from multiple sensors

Based on the measurement results of the ceilometer, a statistical analysis of the cloud properties over the Princess Elisabeth (PE) station could be executed. Using backscatter recordings, a distinction between cloudy and clear-sky conditions was made. Furthermore, backscatter values higher than 10^{-4} sr^{-1} m^{-1} indicate the presence of liquid water. These liquid-containing clouds are predominately found in the layers between 1 and 3 kilometres above the surface.

Furthermore, hourly cloud occurrence, snowfall occurrence and liquid-containing cloud occurrence frequencies were calculated for the period 2010-2013 (14 months of cloud measurements mainly in summer-beginning of winter). It was found that cloud occurrence shows a strong bimodal distribution with clear-sky conditions 51 % of the time and complete overcast conditions 35 % of the time (Figure 9). During the cloudy periods, liquid-containing clouds occur as much as 20 % of the time (Gorodetskaya et al., 2015). During 6 % of the time, the PE station experiences snowfall.

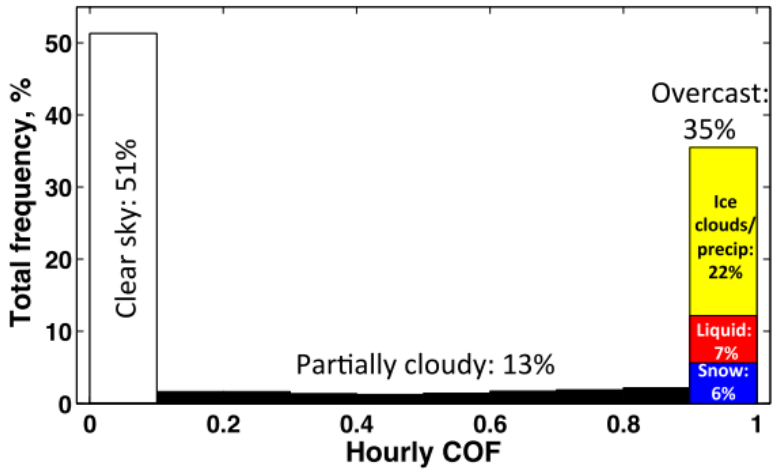

Figure 9: Total frequency relative to the measurement period (%) of hourly mean cloud occurrence frequency (COF; unitless fraction from 0 to 1) for all clouds and precipitation.

4.1.2 Assessment of the effect of clouds on the surface energy balance

The radiative importance of clouds over Antarctica is shown by investigating the surface energy balance for several case studies. Clouds have a net positive effect on the surface energy balance, increasing the amount of downward longwave radiation, while decreasing the amount of incoming shortwave radiation. It is shown that optically thin high-level ice clouds have a profound effect on the longwave radiation at the surface. During low-level cloudiness and precipitation, long wave incoming radiation increases up to values of 255 Wm^{-2} (February

2012), almost corresponding to the incoming shortwave radiation at clear-sky conditions at that time of the year. Liquid-containing clouds over Antarctica have a profound impact on the surface radiative fluxes. For the case study in February 2012, an increase in the surface incoming longwave flux from 160 Wm^{-2} during clear-sky conditions to 240 Wm^{-2} during liquid cloud presence was recorded. The occurrence of these clouds smoothens the daily cycle of temperatures, leading to warmer nights and colder days. Lastly, during precipitation periods, it is found that the net SW flux is characterised by a 2-fold reduction during the peak insolation hours.

4.1.3 Estimation of snowfall rate from the vertically-profiling precipitation radar

Using the PIP and a MRR, a Ze-SR relation ($Ze = A*SR^B$) over Antarctica was derived by performing bootstrapping simulations considering different uncertainty terms. The prefactor (A) was estimated to be 18 (with an uncertainty range [11-42]), while B equals 1.10 (with an uncertainty of [1.00-1.17]). This relation and its uncertainty can be applied to the MRR Ze measurements in order to obtain long-term records of snowfall rates using relatively compact low-power equipment, including an improvement of current uncertainty ranges (Figure 10 and Figure 11).

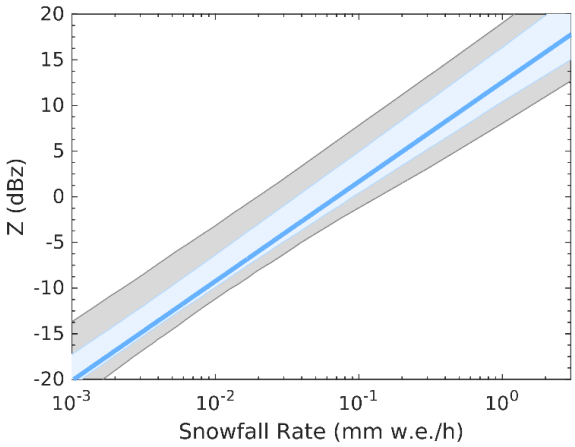

Figure 10: The 10-90 percentile uncertainty (blue shaded area) and the 1-99 percentile (grey shaded area) of the Ze-SR relation of all snow storms. The thick blue line denotes the ensemble average relation.

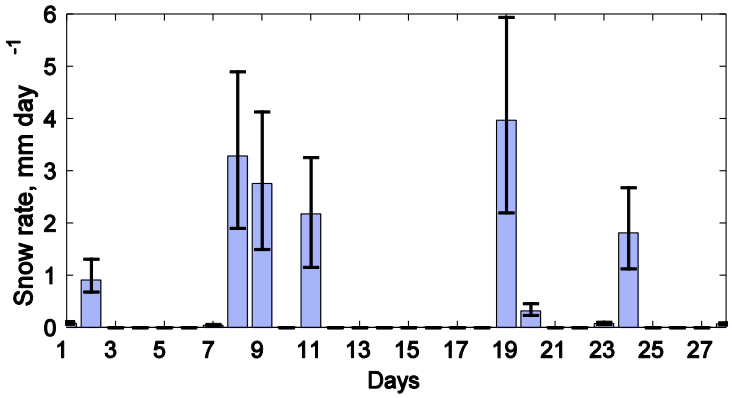

Figure 11: Snowfall rates and their uncertainty obtained by applying the Ze-SR relation and its uncertainty on Ze measurements of the MRR for the month February 2016.

Firstly, uncertainties on derived snowfall rates by the MRR based on the resulting Ze-SR relations are smaller than expected over PE (on average [-39% +40%]). The typical size of the snow particles and thereby the meteorological regime where the MRR is located, impacts the uncertainty. Snow particles over PE have a median size of around 0.7 mm. As the uncertainty of mass estimates is lowest for these diameters, relatively low uncertainties are found over PE. Larger or smaller particles (found at other locations on the continent) attain for higher uncertainties on Ze and SR, as the spread of mass estimates derived from literature is smallest for particle diameters around 1 mm.

Secondly, changes in the diameter of snow particles also influences the average value of the prefactor of the Ze-SR relation. Increases (decreases) in snow particle diameters lead to an increase (a decrease) in the value of this prefactor, while changes in the value of the exponent are limited. As snow particles have a low diameter over Antarctica, this explains the lower values of the prefactor compared to relations obtained by previous research from mid-latitudes.

Thirdly, this study demonstrates that the uncertainty of the Ze-SR relation is dominated by the uncertainty of the mass estimates of different snow particles. In contrast with previous research, this uncertainty term is larger than the uncertainty of the shape of the particle. In order to lower the uncertainty of the Ze-SR relation, it is therefore crucial to reduce the uncertainty of particle mass estimates within a particle class first. This should be a key point to be addressed in future research. Only then, particle shape detection might help lower the uncertainty of the Ze-SR relation further.

4.1.4 Evaluation of the CloudSat precipitation climatology

Apart from ground-based measurements of precipitation, the CloudSat satellite provides an overview of the precipitation climatology. Precipitation events over Antarctica (with a total precipitation amount exceeding 1 mm w.e. during the course of the event) generally span multiple hours (15 hours on average for the PE station; Souverijns et al., (2018b)). This is much shorter than the interval between two overpasses of CloudSat. This revisit time equals on average 2.5 days for the PE station, 4.7 days for the Dumont D'Urville (DDU) station and 2.1 days for the Mario Zucchelli (MZ) station in case the climatology is constructed based on a map

with a resolution of 1° latitude by 2° longitude. Therefore, the satellite often misses precipitation events. In addition, there is a strong variability in precipitation rates throughout individual events. One overpass every couple of days is therefore not representative to capture individual snow storm variability.

In order to get an estimate of the uncertainty induced by the low temporal sampling frequency of CloudSat, systematic sampling is applied on the MRR precipitation record (available on the minute time-scale). For the MZ station for example, the revisit time equals approximately 2.1 days. As such, subsamples are extracted from the MRR record with an interval of 2.1 days.

For all stations and as expected, an increase in the uncertainty of the total precipitation amount is observed when decreasing the temporal sampling frequency of data acquisition (Figure 12). In case less data is available, more uncertain estimates of the total precipitation amount are obtained. For the CloudSat temporal revisit time of Palerme et al. (2014) (2.5 days for the PE, 4.7 days for the DDU and 2.1 days for the MZ station) large uncertainties on the total precipitation amounts are obtained. The 10-90th percentile uncertainty equals [-31 % +10 %] for the PE station, [-37 % +45 %] for the DDU station and [-55 % +36 %] for the MZ station (Figure 12). This uncertainty is lower than current CMIP5 model variability (Palerme et al., 2016), showing the potential of CloudSat for evaluation purposes.

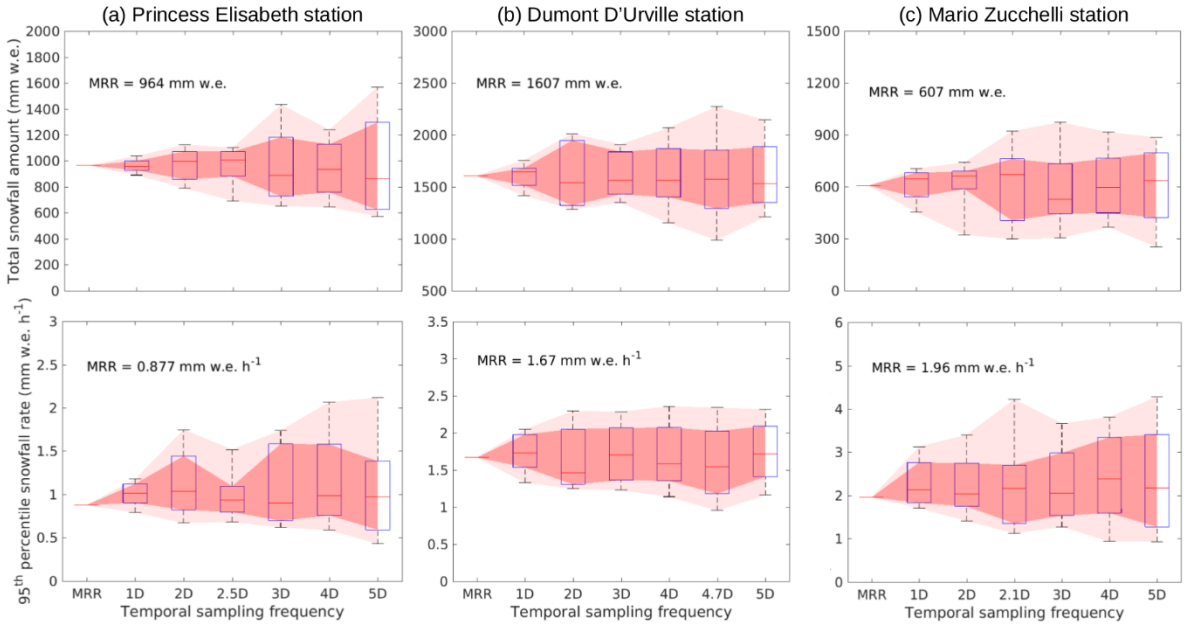

Figure 12: Boxplots showing the uncertainty when applying systematic sampling on the MRR precipitation record (10,000 bootstraps) using different temporal sampling frequencies (x-axis, D denotes days). Total precipitation amounts during collocated periods of MRR and CloudSat measurements (top) and the 95th percentile precipitation rate (bottom) are shown. The bottom and top edges of the boxplot indicate the 25-75th percentile (dark pink shading), while the whiskers denote the 10-90th percentile (light pink shading). The red line denotes the median.

Apart from considering the uncertainty on the total precipitation amount, also a median total precipitation amount is achieved from the bootstrapping simulations (Figure 12). Considering the CloudSat temporal resolution, on average the median total precipitation varies compared to

the full MRR precipitation record. For the PE station, an overestimation of 4 % was found, while at DDU and MZ station, a bias of respectively -2 % and +10 % is observed. These biases can be attributed to the skewed distribution of precipitation at the stations, showing the large influence of high precipitation numbers and needs to be considered when using the CloudSat climatology for model evaluation of surface precipitation rates over Antarctica.

Regarding extreme precipitation rates (95^{th} percentile), very high uncertainties are found for typical CloudSat temporal sampling frequencies (Figure 12) and equals [-21 % +72 %], [-38 % +52 %] and [-43 % +108 %] for respectively the PE, DDU and MZ station. Furthermore, also a high variability in the median 90^{th} percentile precipitation rate of all bootstrapping simulations compared to the value obtained for the full precipitation record is observed.

Long-term ground-based MRR precipitation measurements concurring with CloudSat retrievals are available for seven austral summer seasons at the PE station, attaining for 851 days. During this time period a total number of 839 mm w.e. of precipitation was registered by the MRR at 300 m a.g.l., approximately 0.99 mm w.e. day^{-1}. At the DDU station, concurrent precipitation rate estimates are available for 519 days (three austral summer seasons). A total precipitation amount of 1,113 mm w.e. was attained, leading to an average precipitation amount of 2.14 mm w.e. day^{-1}. Depending on the maximal distance between the CloudSat overpasses and the stations (i.e. the spatial resolution of the grid covering the AIS), a different number of CloudSat overpasses is available for the construction of the total precipitation amount for each grid cell. For the PE station, in case we only take CloudSat overpasses close to the station into account, i.e. for example a spatial resolution of 0.3° latitude by 0.6° longitude (overpasses within approximately 40 km of the station), only 77 overpasses are available for the calculation of the total precipitation amount in the grid box over the PE station, leading to a temporal revisit time of approximately 12 days (Figure 13). In case we increase the CloudSat spatial resolution to 2° latitude and 4° longitude (overpasses within approximately 250 km of the station), 726 samples are available, i.e. one sample every 1.3 days (yellow line in Figure 13).

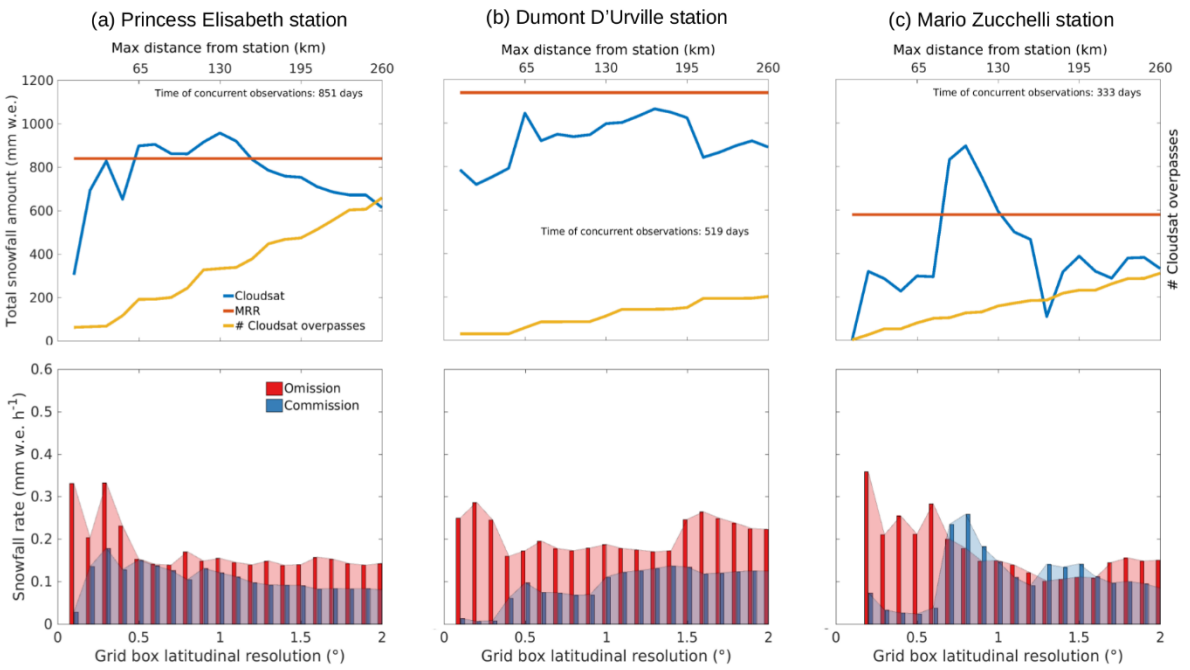

*Figure 13: (first row) Overview of the total precipitation amounts for the three stations as observed by CloudSat and the Micro Rain Radars during the periods of collocated measurements. (second row) Individual precipitation event error analysis. As Micro Rain Radar precipitation rates are considered truth, omission errors are defined as an underestimation, while commission errors are an overestimation of precipitation rates by CloudSat. The x-axis denotes different spatial resolutions of the CloudSat climatology (grid box longitudinal resolution = 2 * grid box latitudinal resolution).*

Apart from comparing the total precipitation amount detected by both the MRR and CloudSat, individual precipitation events detected by both instruments are investigated. Assuming the MRRs define the ground truth, for each precipitation event detected by both instruments, the average omission (misses by CloudSat) and commission errors (overestimations by CloudSat) are calculated (Figure 13). In order to facilitate the comparison, MRR precipitation rates are calculated by averaging precipitation rates over a time period. This time period depends on the spatial resolution of the grid and the wind speed at 300 m a.g.l.. For example, if the grid has a spatial resolution of 1° latitude by 2° longitude (i.e. with a maximal distance of 130 km between the edges of the grid box) and the wind speed equals 20 kmh^{-1} , the MRR record is averaged over 6.5 hours. The minimal MRR averaging period is one hour. Using this methodology, one has to assume that the precipitation systems are stationary in time and uniform in space, which is not valid over highly variable topography. This source of error needs to be considered when comparing both instruments.

For coarse spatial resolutions, CloudSat underestimates the total precipitation amount compared to the MRR records for each of the three stations (Figure 13). For these larger spatial scales, CloudSat overpasses are averaged over longer distances. As precipitation amounts are non-stationary, erroneous estimates can be obtained, leading to both omission and commission errors on both the individual event scale as the statistics (Figure 13). Furthermore, more CloudSat samples are available at higher latitudes (Palerme et al., 2014). As precipitation rates decrease with latitude (and altitude), which is valid for the PE and DDU station, an

underestimation of the precipitation amount (high omission errors) at all stations is observed at coarse spatial resolutions (Figure 13).

This indicates that fine spatial resolutions are preferred in order to obtain more reliable matches between individual events of CloudSat and the MRRs. However, for the finest spatial resolutions, also large omission errors are identified (Figure 13). Despite the higher accuracy of MRR measurements and CloudSat overpasses that are closer to the stations, the amount of overpasses is too low to capture enough high-intensity precipitation events (Figure 12). As the distribution of precipitation rates is skewed towards high intensities, these precipitation events are missed leading to an underestimation of the total precipitation amount, which is indeed observed for all stations (Figure 13).

For intermediate spatial resolutions, reasonable agreements between CloudSat and the MRRs are obtained (Figure 13). At the PE station, an almost perfect match between precipitation estimates is found for spatial resolutions between 0.5° latitude by 1° longitude and 1.2° latitude by 2.4° longitude (biases <10 %). For the DDU station, the underestimation of precipitation amounts by CloudSat is limited to 15 % between 0.5° latitude by 1° longitude - 1.5° latitude by 3° longitude. The wider range of accurate precipitation estimates for the DDU station can be attributed to their topographic location. The station is located at the coast of the AIS in a smoothly changing topographical area, minimising precipitation differences.

For intermediate spatial resolutions, lowest omission errors are observed for all three stations (Figure 13). However, here, commission errors are generally higher compared to coarse or fine spatial resolutions. The main difference between intermediate and coarse / fine spatial resolutions is that omission errors approximately equal commission errors. As such, the amount of precipitation that is missed by CloudSat approximately equals the amount of false positive precipitation detections. Consequently, when taking long-term averages of CloudSat precipitation rates, an accurate estimate of the total precipitation amount compared to the MRRs is obtained (Figure 13). One must understand that the accurate total precipitation amounts obtained by CloudSat can not be attributed to the fact that the satellite is recording correct individual precipitation quantities for each grid box, but to the fact that omission and commission errors cancel each other out. Consequently, it can be concluded that the gridded CloudSat product is not the right tool to investigate individual precipitation events / synoptic events at a single location.

Future work should aim to verify the results obtained above. At the moment CloudSat is only compared to observations at three stations. Its ability to derive snowfall amounts over Antarctica is of very high importance, as snowfall is the most important term in the surface mass balance, also regulating sea level.

4.1.5 Assessment of the individual components of the surface mass balance

The surface mass balance and its individual components have been analysed for the year 2012 (Figure 14). It is shown that snowfall (S), derived from MRR measurements, is the principal

positive term to the surface mass balance. Radar-derived snowfall rate summed over the year 2012 is 170 ± 20 mm w.e. yr^{-1}. During this time, surface sublimation (SUs) and drifting snow sublimation (Suds) removed together 16% of precipitation input at the site. Given the measured SH of 52 ± 3 mm w.e. $yr-1$, we obtain drifting snow erosion (ERds) rates of 30% of the precipitation input. This ERds value represents the total snow erosion by the wind over the year shows cumulative daily SMB components during 2012. Several extreme SH peaks can be attributed to intense snowfall events (e.g. beginning of May and July, end of September) with significant snow removal in-between the events (e.g. during May, July–September, October). A substantial fraction of this snow removal is due to SUs and SUds components, which are relatively small on a daily basis (thus closely following the S curve with much stronger changes), but persistent throughout the year. Removal by SUs also exhibits a seasonal cycle being larger during austral summer (November–February). Removal by the wind (ERds) shows a greater impact compared to sublimation terms with much higher temporal variability. The negative values of SH during January–April (relative to 1 January 2012) can be explained by both high SUs during summer months together with high ERds term, removing the snow accumulated during the previous year. Both S and ERds strongly contributed to the large SH peak in the beginning of February, followed by a significant snow removal by ERds and SUs. Later during the year, ERds also contributed to snow accumulation during some snowfall events (for instance, in early May and end of September), while some days with large S show negligible or even slightly negative SH changes (for example, beginning and end of August).

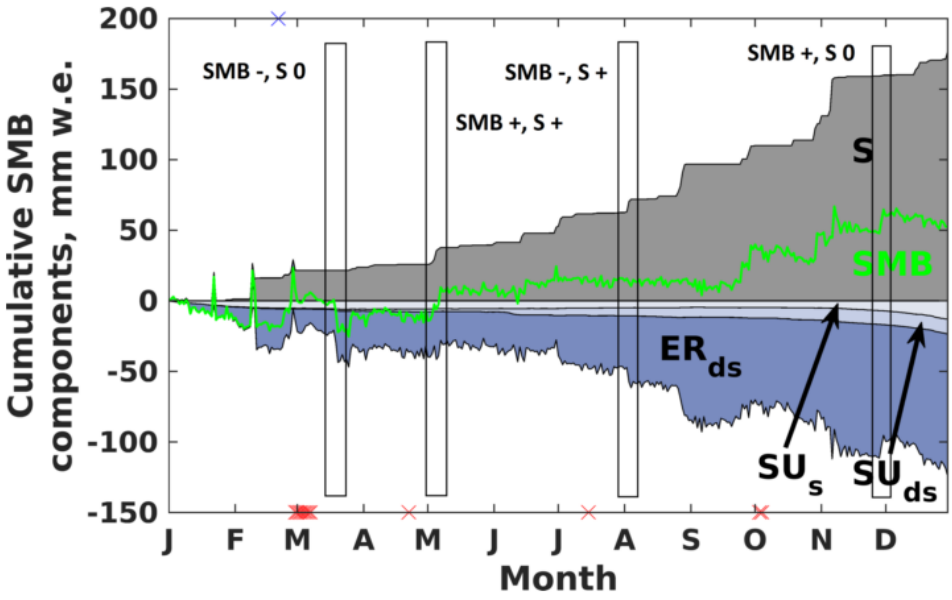

Figure 14: Cumulative daily surface mass balance components during 2012 at the Princess Elisabeth station: snowfall (S), surface sublimation (SUs), drifting snow sublimation (SUds), wind-induced accumulation and ablation (ERds) and accumulation and ablation deduced from measured snow height changes since 1 January 2012 (SMB; Souverjins et al., 2018). Red crosses at the bottom indicate days of missing MRR data, while blue crosses at the top denote missing AWS data. Letters on the x axis mark the first day of each month. Examples of the four types of events defined below are indicated with black rectangles.

Insight in the erosion component is gained by investigating the meteorological conditions during which these processes takes place. Four events are discriminated during the period 2010-2015 (see also Figure 14):

- Precipitation in combination with accumulation (SMB +, S +; N = 31)
- Precipitation in combination with ablation (SMB -, S +; N = 19)
- Accumulation without precipitation (SMB +, S 0; N = 72)
- Ablation without precipitation (SMB -, S 0; N = 87)

Precipitation events are usually characterised by high wind speeds at the surface, causing freshly fallen snow to be transported, which may cause both ablation and accumulation on a specific location. It was found that snow storms attributing for accumulation have a systematically larger horizontal extent compared to snow storms leading to ablation. In case a snow storm has a large spatial extent, precipitation occurs over larger areas. High wind speeds remove the freshly fallen snow at PE, but this is replaced by snow that precipitated upstream and is blown towards the station. In case the snow storm has a small spatial extent, less upstream snow is available for transport leading to a lower chance for snow that has been removed from PE to be replaced.

The displacement of snow can also take place without precipitation. These accumulation/ablation events usually take place within the first days after the precipitation event (85% after 24 hours and 90% after 48 hours), as freshly fallen snow has a low density and is easily picked up by the wind. Snow storms are usually accompanied by strong easterlies at PE. In case accumulation takes place in the days after the snow storm, the wind direction persists towards the eastward direction (Figure 15). Freshly fallen snow that precipitated upstream of PE is now picked up by these winds and transported towards the station, leading to accumulation up to days after the actual snow storm. In other cases however, after a snowfall event, winds turn towards the south. South of the station, a mountain range is present. From this mountain range, katabatic winds originate. These winds do not carry any snow particles having the potential to remove freshly fallen snow from the station.

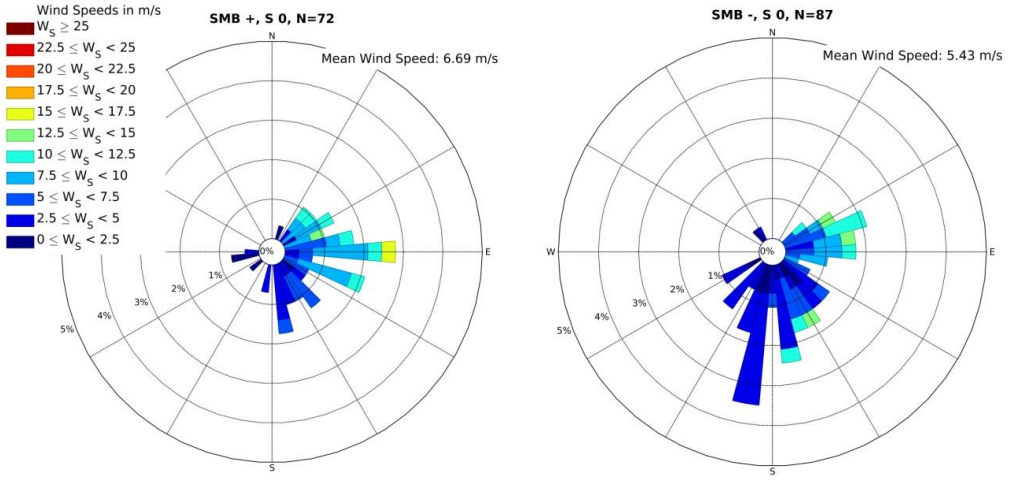

Figure 15: Wind speed and direction for the two events attaining for wind-induced accumulation (left) / ablation (right) without snowfall. N denotes the total number of events during our observation period.

Displacement of snow is an important part of the surface mass balance. The detection of this process is therefore very important. Using the ceilometer, an algorithm was developed to detect blowing snow events. At PE, (strong) blowing snow events resulting in layers extending higher than 15 meter occur around 10% of the time (Figure 16) and the vast majority occurs under synoptic conditions. This is also the case at Neumayer station. At both coastal stations, ceilometer detections of blowing snow were compared to satellite retrievals, and show that most of these events are missed by the satellite since the clouds impede the penetration of the satellite signal (Figure 17). This leads to under-estimations of blowing snow occurrences at coastal areas. In addition, using satellite retrievals at point locations or over complex terrain can lead to biases since CALIPSO can suffer from misinterpretations of the ground signal (Figure 18).

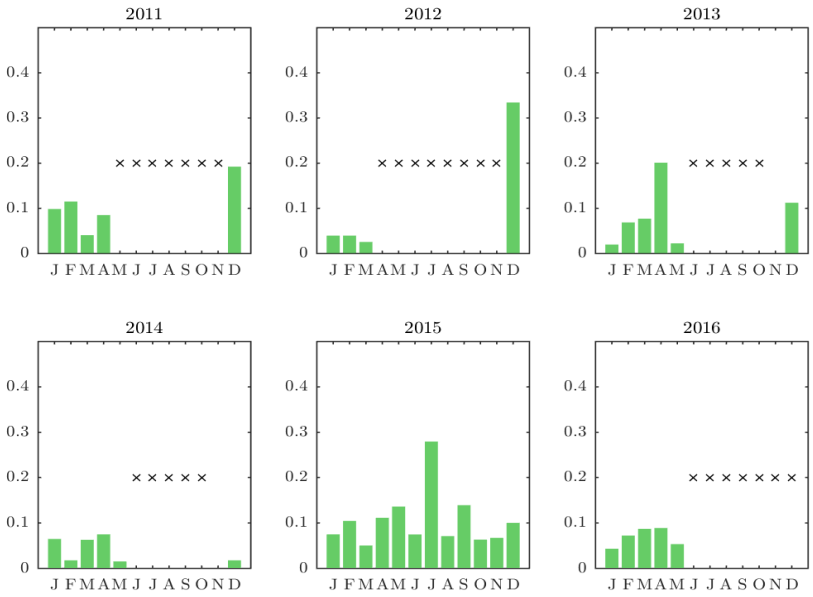

Figure 16: Snowdrift fractional occurrence as observed by the ceilometer. On average, snowdrift occurs 8% of the time. Crosses denotes no data was acquired by the ceilometer.

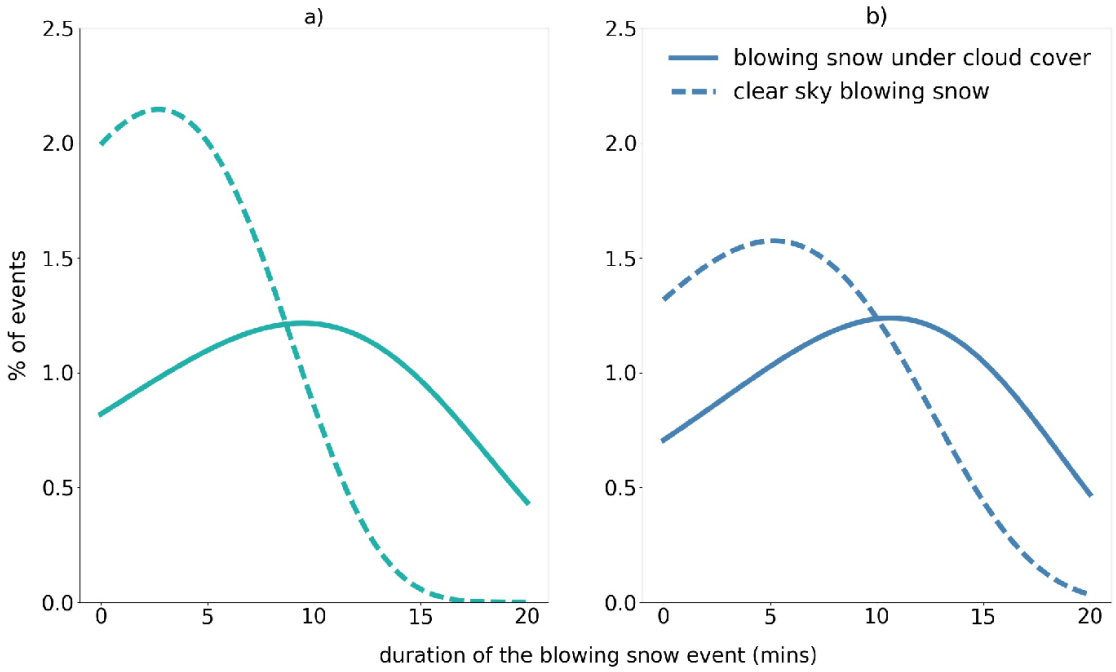

Figure 17: Probability density function for blowing snow under cloud cover (solid) or clear sky (dashed) conditions

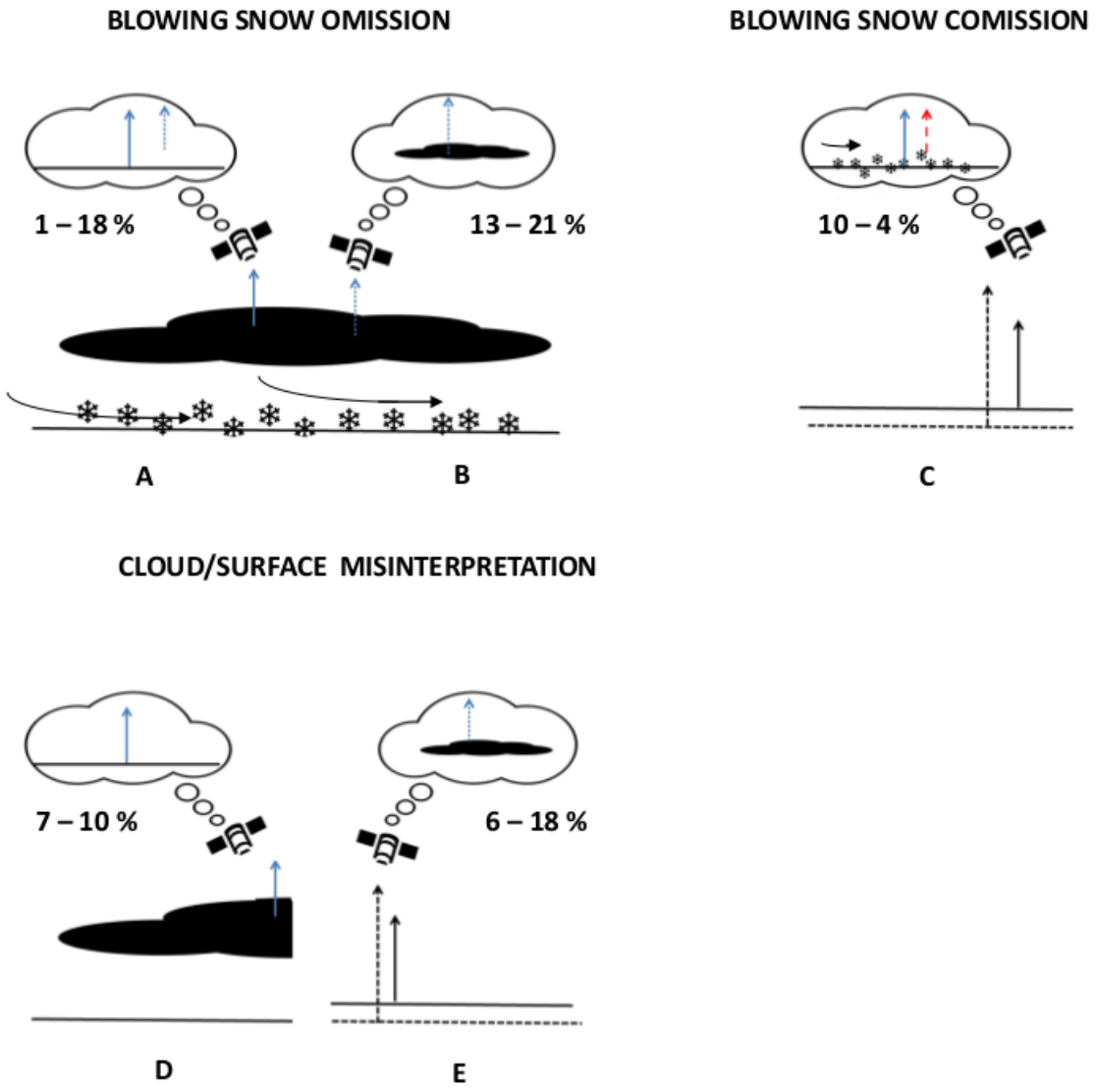

Figure 18: Possible type of blowing snow commission/omission and cloud/clear-sky mis-classification. Upper left image: the ceilometer-based BSD detects a blowing snow layer overlaid by clouds, while the satellite detects clear sky (A) or sees only the cloud (B) and effectively misses the blowing snow. Upper right: the satellite algorithm detects a blowing snow layer unseen by the ceilometer (possibly due to the pollution of the first bin above ground, misinterpretation of the ground return or of a low cloud or fog as blowing snow, C). Lower images: the satellite and ceilometer detect the same absence/presence of blowing snow but the satellite indicates clear sky while the ceilometer detects a cloud (D), or detects a cloud while the ceilomteter indicates clear sky (E). The percentages refer to Princess Elisabeth - Neumayer, respectively.

These conclusions were drawn from a limited set of observations at the Princess Elisabeth station (and Neumayer station). In order to confirm these findings, more data points need to be available. Also a continuation of the present observations is key in order to detect changes towards the future.

4.2 Characterisation of atmospheric aerosols

4.2.1 Estimation of aerosol characteristics from boundary layer measurements

Data of the aerosol in situ instruments have been analysed until either May 2016 or March 2018. After the data gap in May 2016, the restart of the instruments was only possible by

November 2017 (see also section 5.2). Some data after March 2018 became available only by late December 2018, too late for including these data into this report. In addition, some data are needed to correct other data, therefore, not all data could be analysed up to March 2018.

4.2.1.1 Particle number properties

Data of aerosol total number (N_{TOTAL}; in #/cm^3) have been analysed for all available periods since the installation of the U-CPC in February 2012. Figure 19 shows all available monthly means. N_{TOTAL} revealed a clear seasonal cycle (with inter-annual variation) with some hundreds of particles per cm^3 during austral summer, decreasing to some tens of particles per cm^3 in austral winter. Mostly in austral summer, N_{TOTAL} increased to some thousands of particles per cm^3 on a time scale of some hours to one day. This caused high standard deviations of the monthly means, visible also in the 10-% and 90-% percentiles in Figure 19. During austral summer, air masses of lower latitudes reach more easily into Antarctica, transporting thus more particles into Antarctica. The circumpolar circulation during austral winter hinders such transport. With return of sunlight in spring and weakening of the polar vortex and the circumpolar circulation, the values for N_{TOTAL} increased distinctly. Besides facilitated transport into Antarctica, also photooxidative processes in the free troposphere and subsequent descent to lower atmospheric layers might be responsible for that increase in N_{TOTAL}.

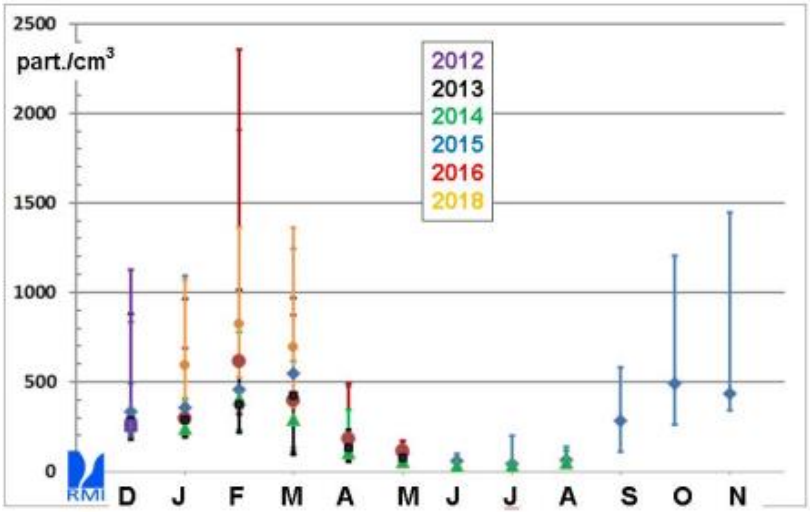

Figure 19: yearly cycles of monthly means of total particle number concentration (in particles per cm^3), the 10-% and 90-% percentiles are also given

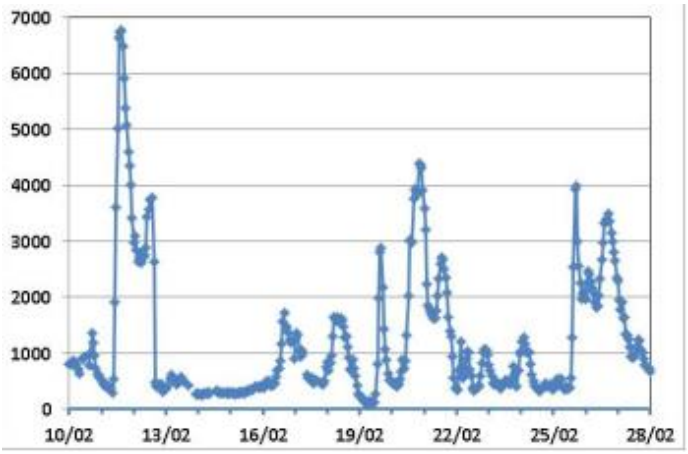

Figure 20: N_{TOTAL} (particles per cm^3) for a typical summer month (here February 2016), illustrating the strong variability of the total particle number concentration

Figure 20 shows an example summer months of hourly values for N_{TOTAL}. The strong variation and also the sudden and distinct increases of can be seen. Simultaneous measurements of size distribution revealed that during such events almost only particles smaller than 90 nm increased in number.

Results of the aerosol size distribution (90 to 7000 nm; measured in 99 log-channels) for all available months since February 2012 (Figure 21) revealed that the aerosol number density in this size range was between 20 to 50 particles per cm^3 during austral summer and decreasing distinctly during autumn and winter. The count median diameter was between 110 and 115 nm, indicating a narrow size distribution and a very weak contribution of particles larger than 500 nm. Figure 21 illustrates in addition that particles larger than 90 nm contributed on average around 10% to N_{TOTAL}, with even lower fractions during strong increases of N_{TOTAL}.

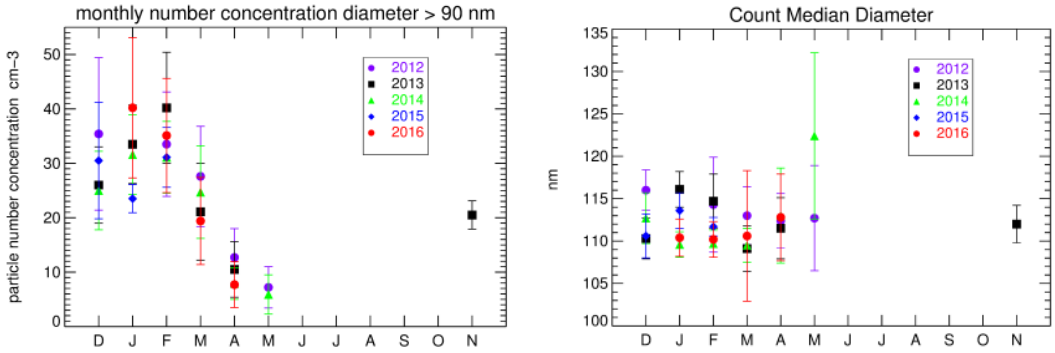

Figure 21: (left): yearly cycles of monthly means and standard deviation of the particle number concentration (in particles per cm^3) measured by the LAS, for sizes larger than 90 nm; (right): the count median diameter of the size distribution measured by the LAS

Figure 22 details the measured size distribution. Clearly, the particle concentration decreased distinctly with size. The dominant size fraction of particles larger than 100 nm was in the range up to 135 nm. Particles of sizes between 135 to 200 nm still showed concentrations around 1 per cm^3. Particles larger than 1 μm were in the order of 0.001 per cm^3. This size spectrum had also consequences for the concentration of CCN and IN (see respective section 4.2.4).

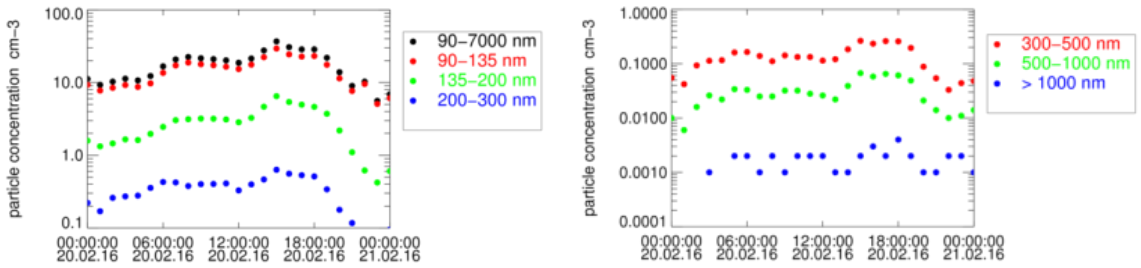

Figure 22: example of a typical size range distribution measured by the LAS

4.2.1.2 Aerosol optical properties

The monthly means of the mass concentration of light-absorbing particles for all available data since January 2011 show a clear seasonal cycle, with inter-annual variations and with values peaking during austral summer and hardly above zero in austral winter (Figure 23). However, with mass concentrations between 0 and 10 ng/m^3, the contribution of this kind of aerosol to the total aerosol mass concentrations (around 1 µg/m^3) was limited. Light-absorbing particles are mainly produced during incomplete combustion processes. These particles have to be long-range transported because no such natural sources are present in Antarctica. In addition, measured absorption values at 370 nm were consistently higher than at longer wavelengths (e.g., 660 nm), especially during austral summer. The aerosol absorption and its spectral dependency is usually given by an exponential relationship. In Figure 24, the exponent of the spectral dependency of the aerosol absorption coefficient (absorption Angstrom Exponent; AAE) is shown. Fresh soot would have more or less the same absorption strength at different wavelengths and thus an AAE around 1. AAE values > 1 measured at PE station indicate that the air masses transported to PE station contained also other light-absorbing compounds (e.g., from biomass burning, organics) which absorb stronger at shorter wavelengths. Both the influence of long-range transport and the fraction of such other light-absorbing compounds were more pronounced during austral summer months. Further, changes in the AAE value indicate also a change in the air mass composition, adding another piece of information on the air mass origin.

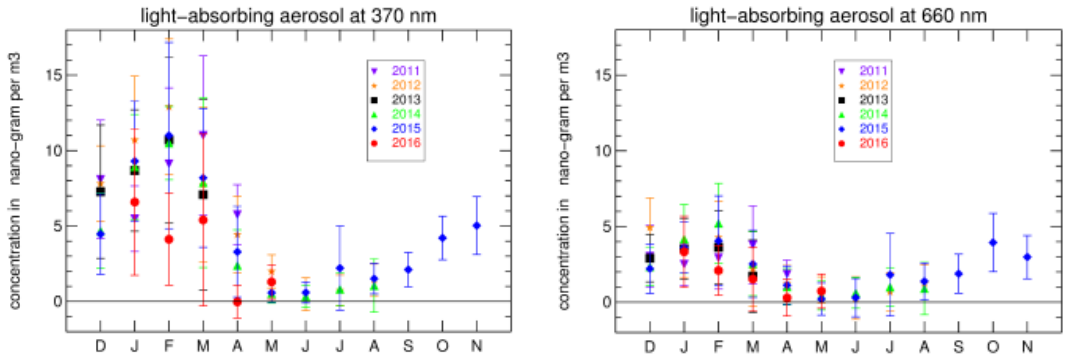

Figure 23: yearly cycles of monthly means of the mass concentration of light-absorbing aerosol, measured at 370 nm (left) and at 660 nm (right)

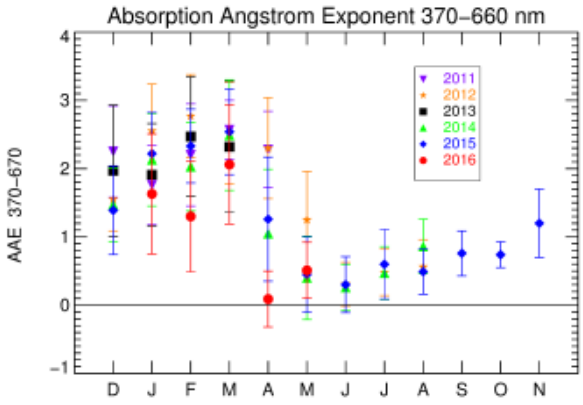

Figure 24: yearly cycles of monthly means of the Absorption Angstrøm Exponent (AAE)

Results of the nephelometer for the aerosol scattering coefficient have been analysed for all available data since February 2012. The multi-year monthly means of the total aerosol scattering coefficient is shown for the three wavelengths in Figure 25. The yearly cycle is less distinct than for particle number or aerosol absorption. This reflects that at low aerosol amounts and at the same time very small particle sizes, the scattering intensity is very weak. Therefore, the error margins for the scattering were relatively high.

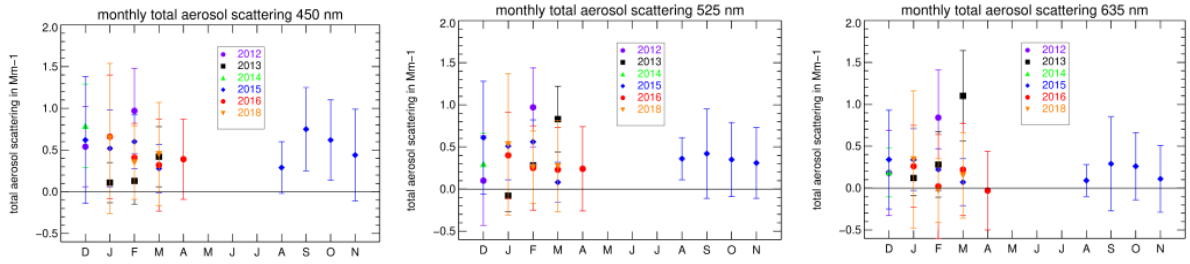

Figure 25: yearly cycles of monthly means of the total aerosol scattering coefficient measured at three wavelengths: 450 nm (left), 525 nm (middle) and 635 nm (right)

By combining the aerosol scattering and absorption coefficient into the Single Scattering Albedo (SSA; i.e. the fraction of scattering in relation to the sum of scattering and absorption), the radiative properties of the atmospheric aerosol can be characterised. Mean values of SSA were mostly around 0.98 to 0.99 (see Figure 26), however with high uncertainty (calculated via error propagation), given that the measurements were made at the detection limits of both the aethalometer and the nephelometer. Thus, the aerosol at PE is highly reflective (indicative of high amount of sulphate-containing particles, organics or coatings).

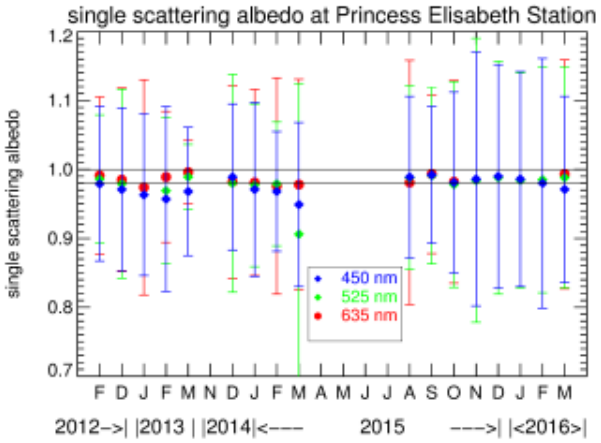

Figure 26: monthly means for the Single Scattering Albedo (SSA), derived from simultaneous measurements of the absorption and scattering coefficient

4.2.1.3 Recommendations

The particle number measurements showed that around 90 % of the particles at PE station are smaller than 90 nm. However, the size distribution could not be measured in that smaller size range due to the limits of optical particle detection. Size-resolved measurements in the size range smaller than 90 nm would be of great value in order to better understand the local aerosol processes. For such measurements, specific mobility particle sizing spectrometers, based on the detection of the electrical mobility of particles, would be necessary. Further, it is important to assure the continuation of the time series of aerosol in situ measurements. This is relevant in order to monitor the evolution of the respective aerosol properties with respect to a changing climate. Also, there is increasing interest by the scientific community in observations in East Antarctica and especially in Dronning Maud Land.

4.2.2 Retrieval of total column and vertically resolved aerosol properties with remote sensing instrumentation

AOD time-series measured by the CIMEL instrument at 360 and 470 nm during the 2017/2018 summer season together with coincident ($\pm$ 5 min) MAX-DOAS observations are presented in Figure 27 and Figure 28. As can be seen, both CIMEL and MAX-DOAS AOD values are most of the time smaller than 0.05. Except for some outliers, MAX-DOAS AODs are in good agreement with CIMEL measurements in the UV range, while MAX-DOAS tends to overestimate CIMEL data in the visible range. However, a better comparison statistics is needed to draw firm conclusions about the consistency between both data sets.

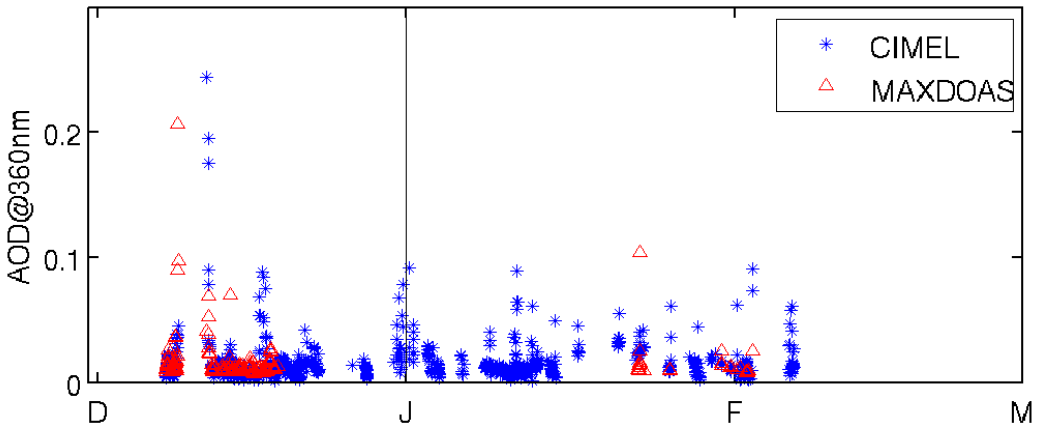

Figure 27: Time-series of CIMEL and MAX-DOAS AOD at 360 nm for the 2017-2018 Antarctic summer. It should be noted that the MAX-DOAS instrument was out of order between 18 December 2017 and 17 January 2018.

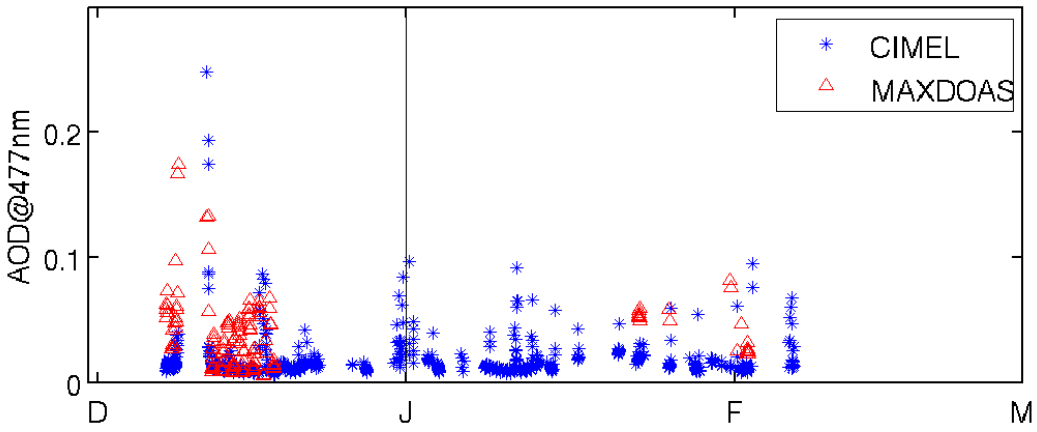

Figure 28: Same as Figure 27 but for 477 nm.

Due to technical issues for both CIMEL and MAX-DOAS instruments during the 2015/2016 and 2017/2018 summer seasons, only a limited number coincident measurements from these instruments are available. In case of future simultaneous operation of both instruments at PES, our recommendation is to carefully check and optimize them for working nominally in an adverse environment like Antarctica.

4.2.3 Improved estimation of aerosol characteristics by Mie-Calculation and radiative transport modelling

As discussed in Sect. 3.3.3, this task has been replaced by the identification of specific aerosol/cloud detection study cases combining MAX-DOAS measurements with ancillary observations at PES. After examining MAX-DOAS, ceilometer, CPC, radiosondes, meteorological station data sets, four different scenarios were identified and investigated:

- Elevated cloud layer
- Blowing snow event
- Aerosol entrainment from upper atmospheric layers to the surface
- Elevated aerosol layer in clear-sky conditions

These study cases are discussed in the sub-sections below.

4.2.3.1 Elevated cloud layer

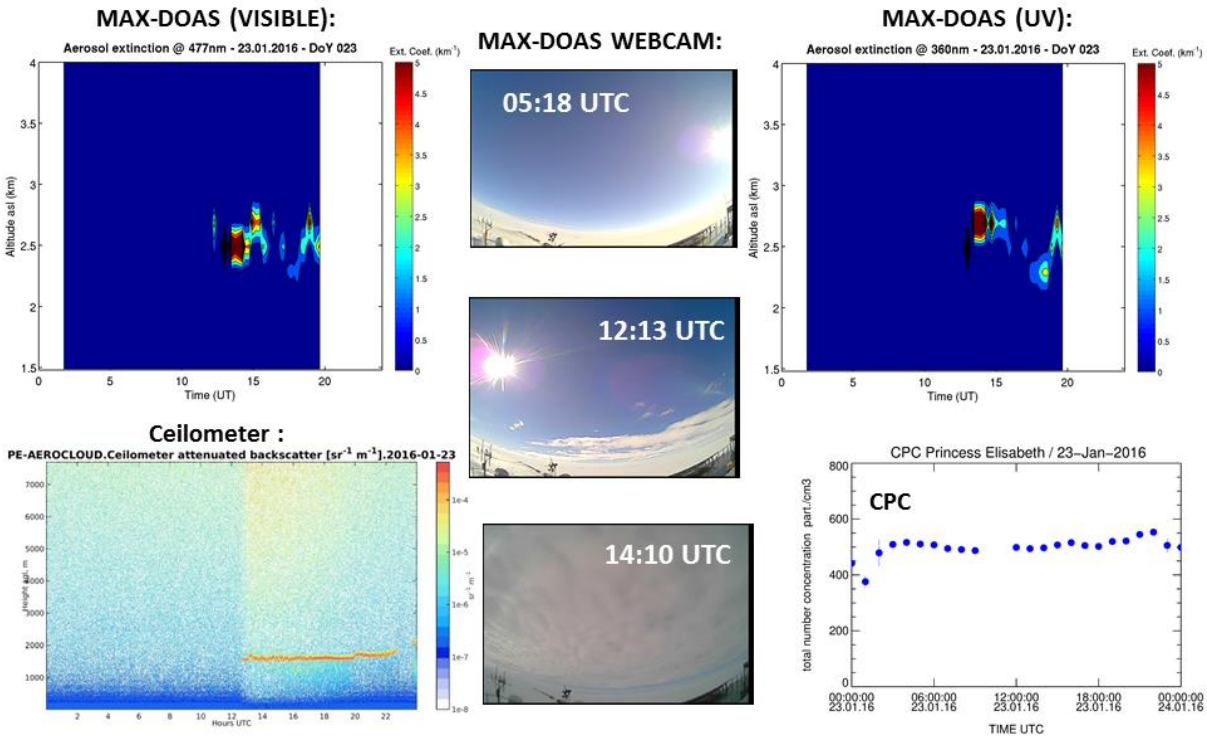

Figure 29: MAX-DOAS aerosol extinction profile diurnal variations retrieved at 360 and 477 nm by the MMF algorithm on 23/01/2016, together with corresponding ceilometer and CPC plots, and MAX-DOAS webcam images. Altitude (y-axis) in given in km asl and m agl in ceilometer and MAX-DOAS plots, respectively.

Figure 29 shows a typical day (23/01/2016) with clear-sky conditions during the morning, clouds progressively appearing from 12hUT and cloudy conditions during the afternoon (see MAX-DOAS webcam images). As can be seen, the cloud detection by the MAX-DOAS instrument corresponding to elevated (>5 km^{-1}) extinction coefficient values timely coincides with ceilometer observations. The altitude of the cloud layer retrieved from the MAX-DOAS measurements ($\sim$2.3-2.7km asl or 0.9km-1.3km agl and $\sim$2.5-2.8km or 1.1-1.4km for the visible and UV channels, respectively) is a few hundred meters lower than the cloud altitude range estimated from the ceilometer ($\sim$1.5-1.7km agl). These results indicate the good overall ability of the MAX-DOAS technique for the retrieval of elevated homogeneous cloud layers.

4.2.3.2 Blowing snow event

As described in Sect. 2.1.3, blowing snow events often occur in Antarctica. They corresponds to snow particles dislodged from the snow surface and lifted from the ground up to altitudes of several hundred meters. On 01/02/2016, blowing snow events were detected by the ceilometer around 4hUT and 18hUT and further confirmed by the increased particle concentrations measured at the surface by the CPC (800-1000 particle/cm^3; see Figure 30). The image from the webcam at 4h30Ut also showed a very low visibility at the station. During both events, increased aerosol extinction values ($\sim$0.3-0.5 km^{-1}) were also retrieved in the 0-600m altitude layer agl from the MAX-DOAS measurements.

It is worth noting that on that day, the temperature profile was very close to the frost point temperature profile, especially in the 2.7-3.5km altitude range asl (1.3-2.1 km agl) where both curves are superimposed. It means that 100% ice saturation conditions are met, with the likely presence of ice particles. As can be seen in Figure 30 an increased aerosol extinction coefficient (>0.7 km^{-1}) is also detected around 12hUT (radiosonde launch time) by the MAX-DOAS instrument in this altitude range, suggesting the presence of such particles.

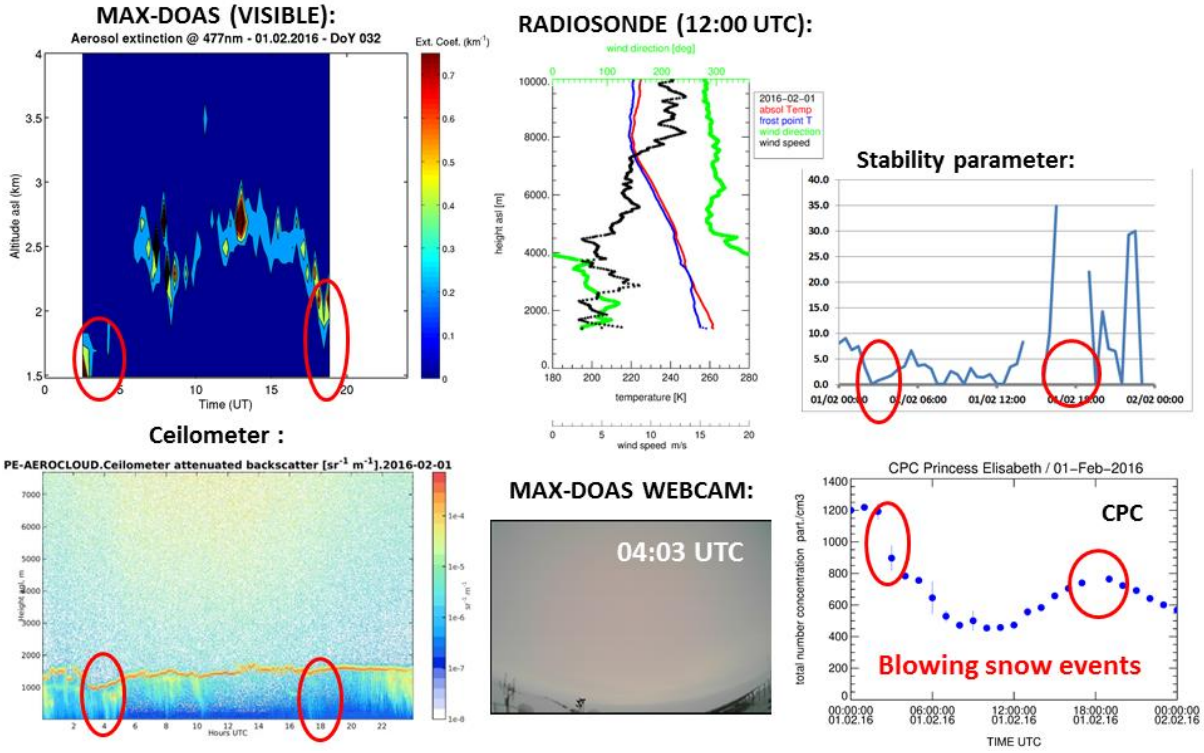

Figure 30: MAX-DOAS aerosol extinction profile diurnal variations retrieved at 477 nm by the MMF algorithm on 01/02/2016, together with corresponding ceilometer, radiosonde (temperature), CPC, and stability parameter plots, and MAX-DOAS webcam image during the second blowing snow event. Altitude (y-axis) in given in km and m asl in MAX-DOAS and radiosonde temperature plots, respectively, and m agl in ceilometer plot. Red circles indicate when blowing snow events occurred.

4.2.3.3 Aerosol entrainment from upper atmospheric layers to the surface

Since there is no local emissions of aerosols in Antarctica, the only possibility to detect aerosols at surface in clear-sky conditions is the entrainment from upper tropospheric layer to the ground of particles originating from long-range transport. Such an event possibly occurred on 21/02/2016 and is described here.

Starting from the day before (20/02/2016), the ceilometer data shows the presence of low clouds in the early morning and then a clearing up of the atmosphere (see Figure 31). This clearing up corresponds to a change in wind speed and wind direction in the course of the morning which causes a short period of atmospheric instability favorable for aerosol injection at the surface. Then, with lower wind speed and again stable atmospheric conditions observed after 12hUT, particles are not scavenged anymore and can accumulate, with an increase in particle concentration at surface as detected by the CPC. Regarding the MAX-DOAS measurements, high extinction coefficient values are retrieved close to the ground around 5hUT and then an elevated layer possibly due to remaining clouds (see webcam image) is observed

from 7hUT. It should be noted that no increase in the extinction coefficient corresponding to the increase in the particle concentration at surface is seen by the MAX-DOAS instrument.

On 21/02/2016, except some high clouds present at the beginning of the day, the ceilometer indicated clear-sky conditions. The CPC instrument measured during the first hours of the day a slow decrease of the particle number concentration at surface due to particle deposition. From 10hUT, less stable atmospheric conditions due to change in wind speed and direction are observed. During this period, which is favorable for aerosol injection from upper atmospheric layer, an increase in particle number concentration at surface with a maximum of about 3000 particles/cm^3 around 13h-14hUT is detected, together with elevated aerosol extinction coefficient values (~0.25 km^{-1}). These timely coincident observations of high particle number concentration and extinction coefficient at and close to the surface in clear sky conditions after a period of atmospheric instability strongly suggests an aerosols entrainment from the upper troposphere to the boundary layer. Later during the day (after 15hUT), the MAX-DOAS instrument detected an elevated layer with higher extinction coefficients values, which seems to correspond to the presence of thin high clouds (see webcam image).

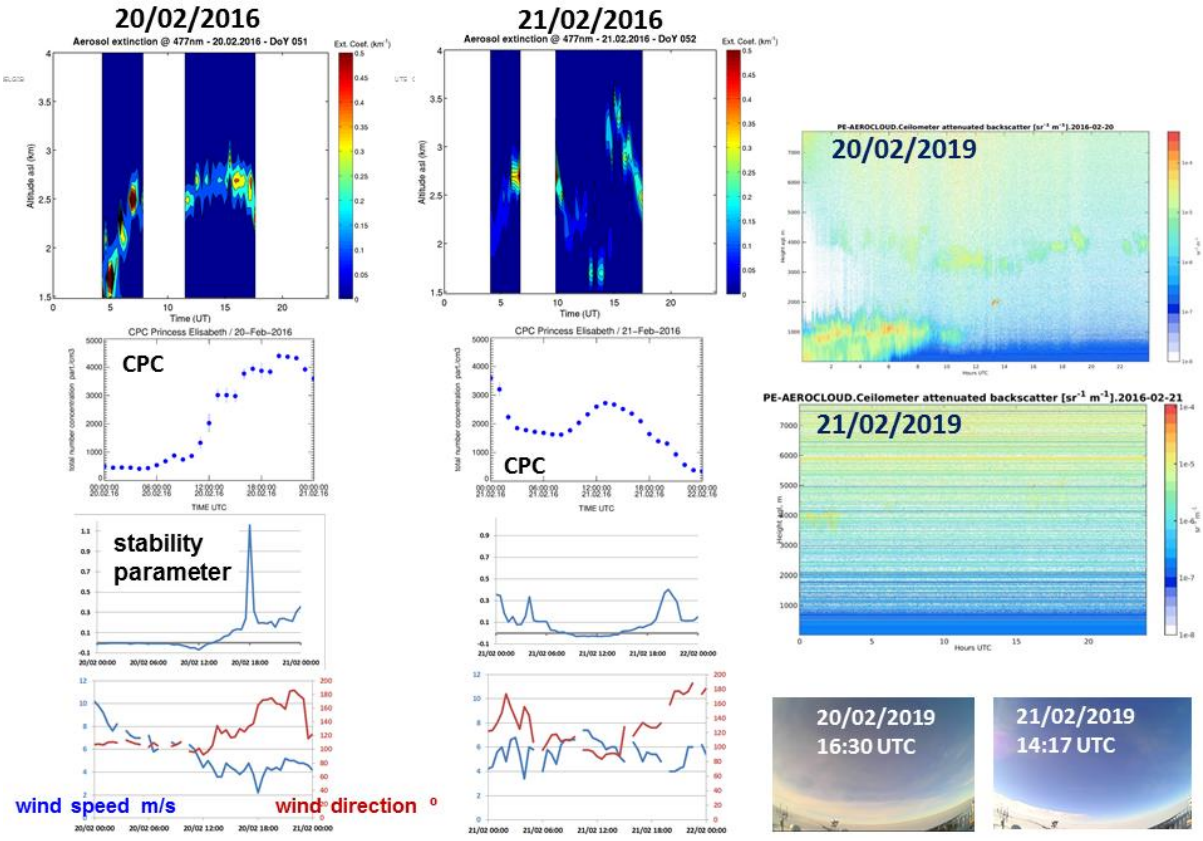

Figure 31: MAX-DOAS aerosol extinction profile diurnal variations retrieved at 477 nm by the MMF algorithm on 20 and 21/02/2016, together with corresponding ceilometer, radiosonde (temperature), wind speed and direction, CPC, and stability parameter plots, and MAX-DOAS webcam images. Altitude (y-axis) in given in km and m asl in MAX-DOAS and radiosonde temperature plots, respectively, and m agl in ceilometer plot.

4.2.3.4 Elevated aerosol layer in clear-sky conditions

The fourth and last study case investigated here corresponds to the detection of an elevated aerosol layer in clear-sky conditions by the MAX-DOAS instrument. Figure 32 illustrates such a scenario. On 06/01/2016, the ceilometer, radiosonde, MAX-DOAS webcam, CPC, and meteorological station data sets indicate the presence of stable atmospheric conditions, without clouds and with particle number concentration at surface at background level (~200 particle/cm3). Despite these conditions, significantly higher extinction values (up to 0.2 km-1) were retrieved in the 2.5-3.1 km asl altitude range (1.1-1.7 km agl) from MAX-DOAS measurements. Statistics were made on all the clear-sky morning and afternoon of the 2015/2016 and 2017/2018 seasons. Among the 20 selected clear-sky mornings, 12 showed an elevated aerosol layer and 6 did not show this feature. For the 18 afternoon cases, an elevated aerosol layer was observed in 16 of them. Figure 33 and Figure 34 show the mean aerosol extinction profile diurnal variations in both the UV (360 nm) and visible (477 nm) wavelength ranges corresponding to all those cases. In the visible region, the aerosol layer is located on average between ~0.9 and 1.6 km agl with extinction coefficient and corresponding total AOD in the 0.05-0.25 km-1 and 0.03 and 0.09 ranges, respectively. The corresponding values at 360 nm are 1.2-2 km, 0.05-0.12 km-1, and 0.005-0.06.

Since sensitivity tests on retrieval settings (a priori AOD and temperature profile) indicated that this observed elevated aerosol layer should not be related to MAX-DOAS retrieval artefacts, we can only speculate about its origin(s). A plausible explanation could be the presence of thin ice particles resulting from the activation of long-range transport aerosols. However, this possibility could only be further confirmed using a powerful multi-wavelength profiling LIDAR and such instrumentation is not available at PES.

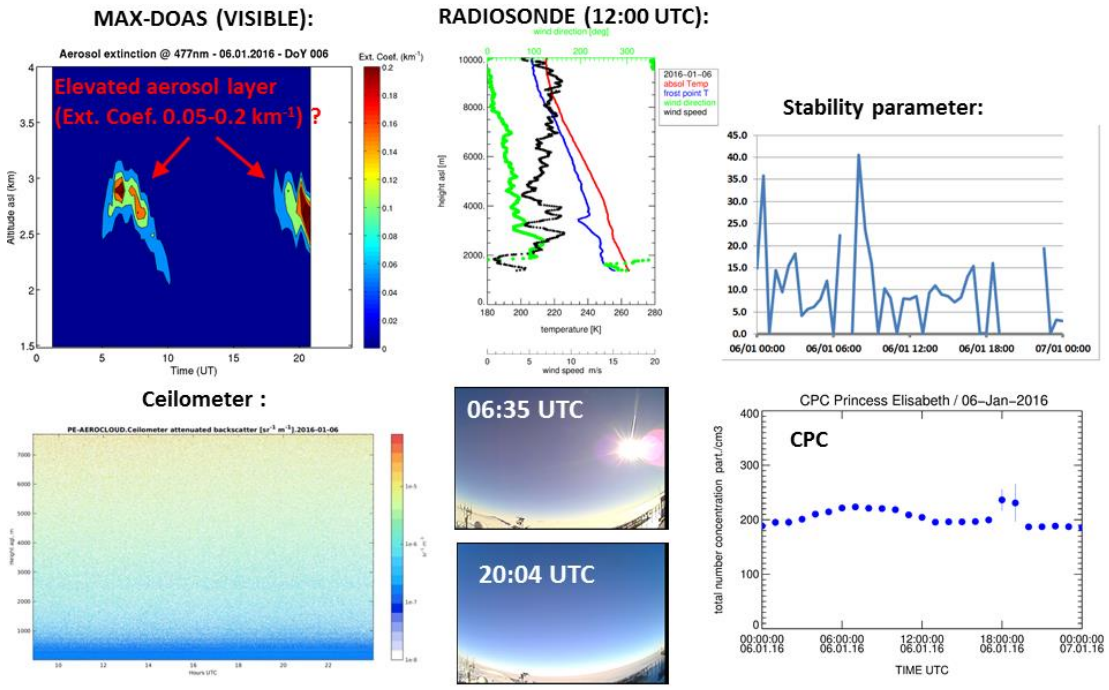

Figure 32: MAX-DOAS aerosol extinction profile diurnal variations retrieved at 477 nm by the MMF algorithm on 06/01/2016, together with corresponding ceilometer, radiosonde (temperature), and CPC plots, and MAX-DOAS webcam images. Altitude (y-axis) in given in km and m asl in MAX-DOAS and radiosonde temperature plots, respectively, and m agl in ceilometer plot.

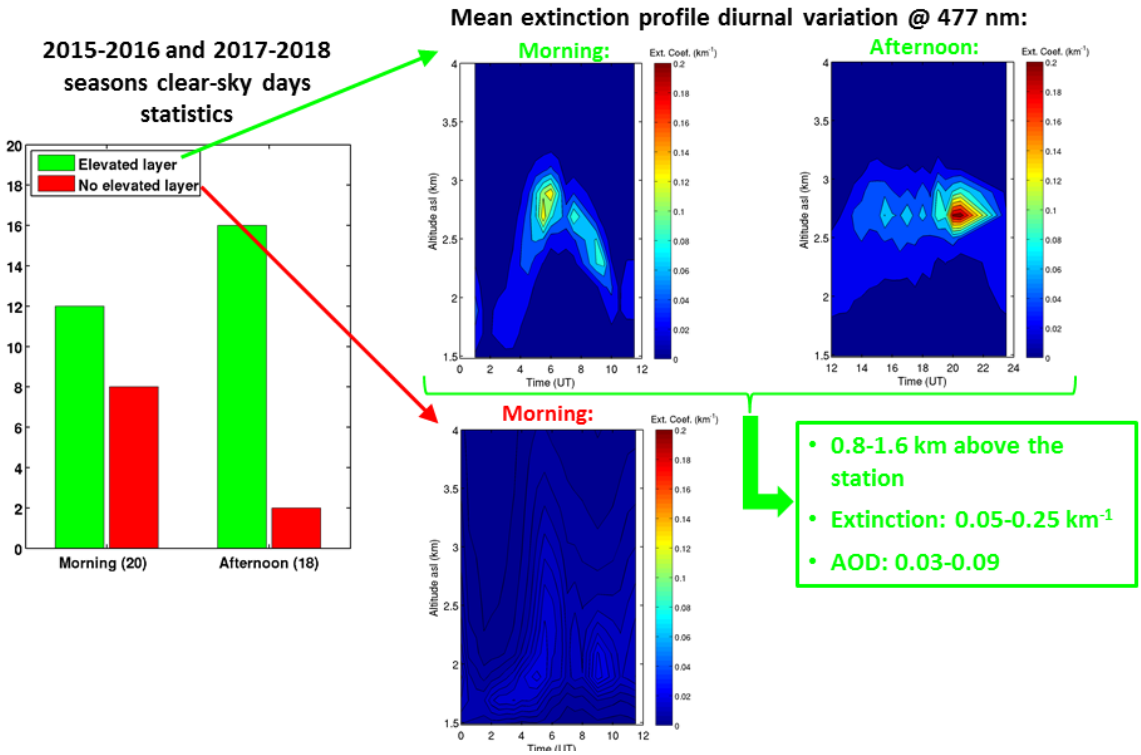

Figure 33: Clear-sky days statistics for the 2015/2016 and 2017/2018 seasons and corresponding mean aerosol extinction coefficient vertical profile diurnal variation (visible range). Mean afternoon profiles are not show given the low statistics (only 2 selected afternoon).

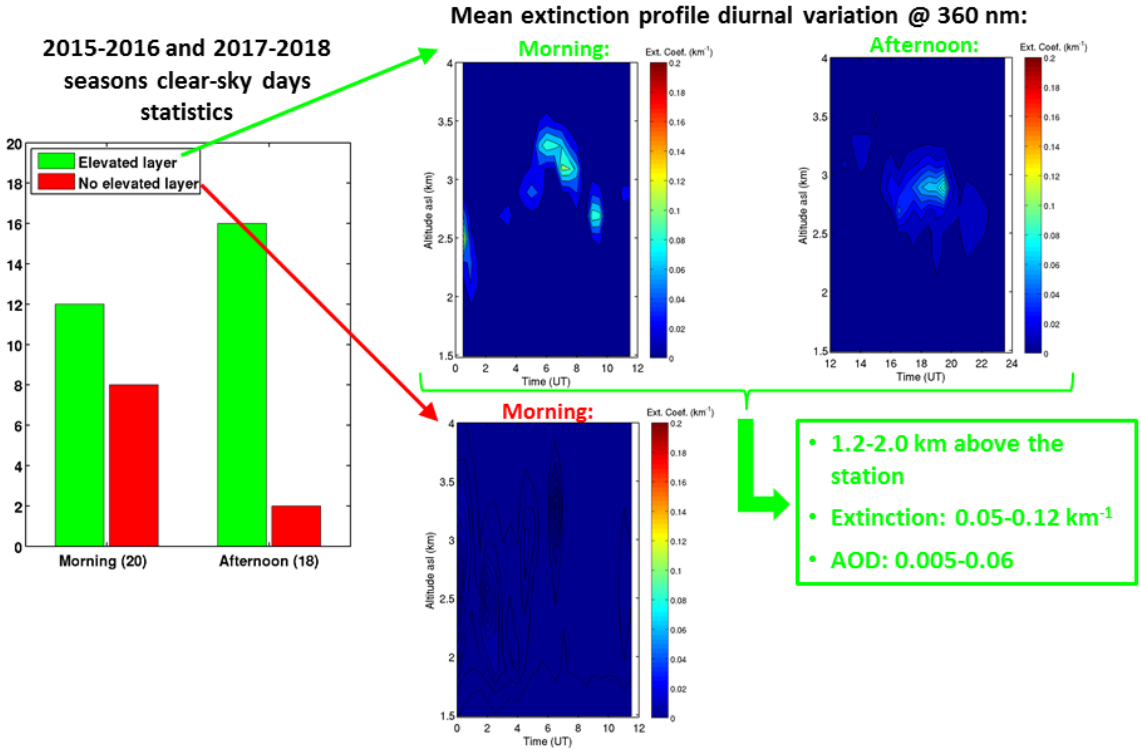

Figure 34: Same as Figure 33 but for the UV wavelength range.

4.2.3.5 Summary and recommendations

Due to the absence of local emission sources, the small particle number and size, and the contamination by clouds, the optical detection of aerosols in Antarctica is a very challenging task. Combining MAX-DOAS measurements at PES with co-located ancillary observations from ceilometer, CPC, and radiosonde instruments and from the AWS meteorological station, typical clouds and aerosols detection study cases have been identified and investigated. Our results showed the good overall ability of the MAX-DOAS technique for retrieving elevated cloud layers and blowing snow events. Regarding aerosols, only one day with aerosols entrainment from upper troposphere to boundary layer was possibly identified during the two seasons (2015/2016 and 2017/2018) where the MAX-DOAS instrument was in operation at PES. Elevated aerosol layers were also retrieved from MAX-DOAS measurements during 12 and 16 clear-sky mornings and afternoons, respectively, without any corresponding signals in the ceilometer and CPC instruments. These aerosol layers were located in the 0.8-2.0km altitude range above the station, with extinction coefficient values of 0.04-0.12 km^{-1} (360 nm) and 0.05-0.25 km^{-1} (477 nm). Our recommendation for the future is to perform co-located multi-wavelengths profiling LIDAR observations to confirm both aerosol entrainment and elevated aerosol layers features and to firmly exclude possible artefacts in the MAX-DOAS retrievals. However, the installation and operation of such LIDAR instrument at PES is potentially very expensive.

4.2.4 Estimation of cloud condensation nuclei and of ice nuclei

The concentration of CCN (N_{CCN}) was derived from the CCN counter measurements (see setion 3.3.4). In order to derive the correct concentrations at the selected super-saturations (ss%) with respect to water, the particle number size distribution measured by the LAS was needed. A detailed analysis and description is given in the paper of Herenz et al. (2019). Table 2 gives the median concentrations and 10 % and 90 % percentiles of N_{CCN} at the selected ss%. At the lowest ss% of 0.1%, only few particles activated to cloud droplets (14 cm^{-3}). At higher ss%, distinctly more particles were activated. This was caused by the specific size distribution measured at PE station (see section 4.2.1). At low ss%, only larger particles activated usually, and at PE station, particles of such size were rare. Table 2 lists also the ratios of N_{CCN} to N_{TOTAL}. The ratio of N_{CCN} to N_{TOTAL} at ss% of 0.7 % was 0.64. Assuming a hygroscopicity parameter κ of 0.8 for the coastal area of East Antarctica, taken from Pringle et al. (2010), the critical diameter for ss% = 0.7 % was determined to be approximately 35 nm. On the basis of this assumption, 36 % of the particles detected at PE station were smaller than around 35 nm. That is indicative of a high amount of newly formed particles, which form from precursor gases emitted from the Southern Ocean and the coastal areas, such as ammonia and dimethylsulfid (DMS).

Table 2: Overview showing N_{TOTAL} and N_{CCN} at different ss%, given as median and 10 % and 90 % percentiles in column 1 for data covering the measurement periods when the CCNc was installed at PE station. Column 2 show the ratio of NCCN to NTOTAL

Parameter	Median concentration (cm^{-3}) (10% and 90% percentiles)	ration N_{CCN}/N_{TOTAL}
N_{TOTAL}	333 (206; 893)	---

N_{CCN} (0.1 %)	14 (10; 23)	0.04
N_{CCN} (0.2 %)	81 (56; 110)	0.24
N_{CCN} (0.3 %)	121 (90; 168)	0.36
N_{CCN} (0.5 %)	177 (125; 260)	0.53
N_{CCN} (0.7 %)	212 (138; 326)	0.64

From the set of CCN measurements, the hygroscopicity parameter κ could only be derived for ss = 0.1 %, for which the median critical activation diameter was determined to be 110 nm. For higher ss%, was above the total particle number larger than 90 nm, i.e., the critical activation diameter was below the lower size limit of the measured number size distribution of the LAS. Therefore, the hygroscopicity derived here is only valid for the low number of particles that were activated at ss = 0.1 % (see Table 2). All κ values from the three seasons had a median value of 1 (see Figure 35). These are generally high atmospheric κ values covering a broad range between 0.5 and 1.6. Large κ values such as those are typically found for particles consisting of inorganic substances (Petters and Kreidenweis, 2007). In particular, values of 1 or above are only known to occur for sea salt. The lower values for κ are too low to originate from pure sea salt particles. In addition to inorganic compounds, marine aerosol may also contain internally mixed organic substances which reduce their hygroscopicity. Secondarily formed aerosol particles of marine origin are a result of DMS oxidation and further reactions. They can be expected to contain sulphates, and Petters and Kreidenweis (2007) give a κ value of 0.61 for ammonium sulphate derived from CCN measurements.

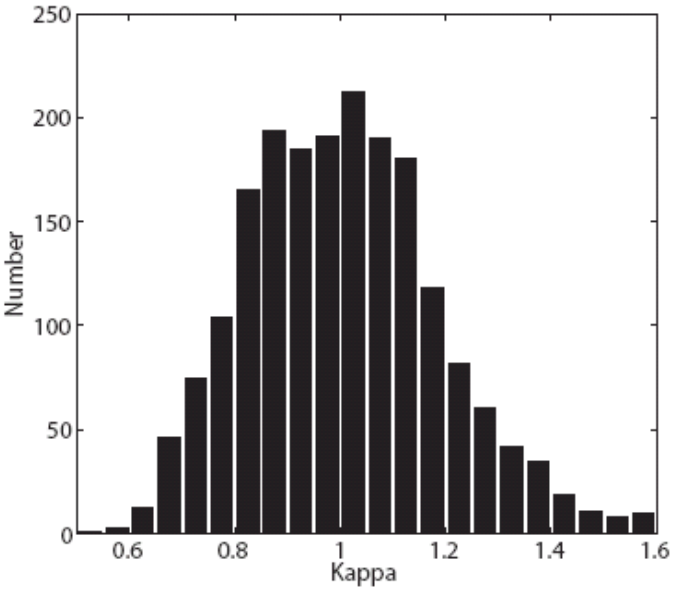

Figure 35: Histogram showing all κ values of the three seasons, derived for ss = 0.1 %, for which the median critical activation diameter was determined to be 110 nm.

Future measurements of CCN at PE should be continued in order to derive a wider coverage and improved statistics. Further, the particle number size distribution should also be measured for sizes smaller than 90 nm because from the CCN measurements it is obvious that the majority of particles at PE stations were smaller than 90 nm and activate only at higher ss than 0.1 %.

4.2.5 Assessment of the atmospheric aerosol variability at Utsteinen: composition by season, meteorological regime and altitude level

Results for aerosol properties and seasonality have been described in section 4.2.1. Results of the MAX-DOAS instrument (see section 4.2.3) revealed that it was possible to derive the vertical profile of the particle extinction coefficient, providing information whether the in situ aerosol measurements in the boundary layer could be linked to the cloud level. Cases when the MAX-DOAS measurements could be linked unambiguously to an aerosol signal and when that signal showed a connection between boundary layer and the upper layers were rare. Most often there was either no connection to be detected or clouds were present, blurring the potential aerosol signal.

An analysis on the dependency of aerosol properties on meteorology showed no significant correlations, neither with temperature, wind, relative humidity or radiation. The variability of the particle concentration is too large and in either case of, e.g., katabatic meteorological regimes, strong insolation, synoptic weather regimes, the particle properties showed the whole range of their respective characteristics. Only for temperature and stability, a weak correlation (still not significant) could be found what reflected mainly the seasonality between winter and summer, i.e., the seasonal cycles shown in section 4.2.1. This seasonality is the clearest for particle number and the particle light-absorbing properties. This indicates a strong link to the strength of the circumpolar circulation and the polar vortex. E.g., when this strength weakens in austral spring and the photooxidative reactions could start, more particles from the free troposphere could be entrained to the lower troposphere and into the boundary layer (e.g., Fiebig et al., 2014). This was reflected in the strong increase in particle number in Figure 19.

In order to derive relationships of aerosol properties and meteorological conditions, it was therefore more useful to define specific 'events' (like strong increase in particle number, change in AAE) and calculate the probability or risk ratio and its significance that this event is connected to another condition (like precipitation, low clouds, high clouds, strong wind, wind direction, atmospheric stability). Events when the particle number N_{TOTAL} increased abruptly (N_{TOTAL}-events) were often connected to changing wind and cloud conditions and sometimes to precipitation.

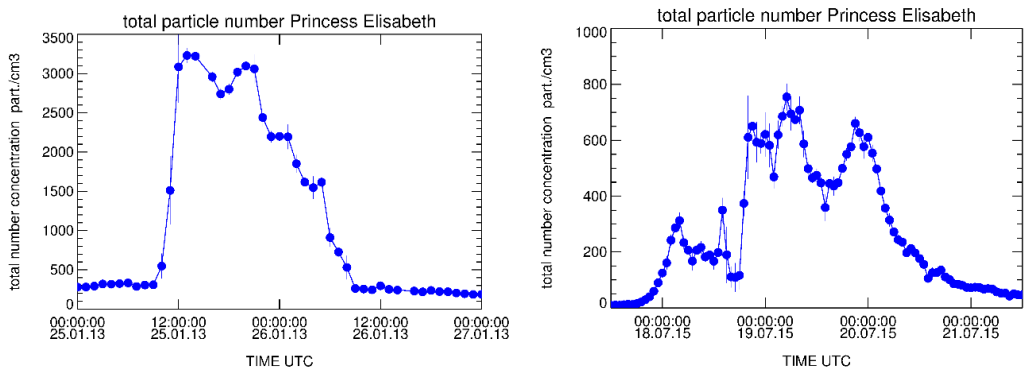

Figure 36: examples for so-called N_{TOTAL}-events; (left): 'Peak'-events and (right) 'Mountain'-events; for a description, see text

An analysis to characterise those N_{TOTAL}-events resulted in three types (see Figure 36) which could be distinguished due to their specific evolution of N_{TOTAL}. Each type could be linked to certain conditions which had significantly higher probability during these events. 'Spikes' (steep increase and also steep decrease in short time) occur at high wind speeds from NE to E with no distinct change of wind direction. They occur very often after precipitation connected with drifting snow conditions. These events have high probability to happen in summer, during turbulent conditions and when there are low liquid clouds. 'Peak events' (steep increase with gradual decrease thereafter) occur mostly during wind direction changes from NE over E to SE. These events have high probability to happen in summer, during turbulent conditions, drifting snow conditions, and when there are low ice-containing clouds. 'Mountain events' (several steep increases after each other, at least one peak higher than the first one) occur at high wind speeds from N to NE. They happen very often during precipitation with drifting snow conditions. These events have high probability to happen during turbulent conditions, and when there are low ice-containing clouds. These findings indicate that during N_{TOTAL}-events the boundary layer was not completely de-coupled from atmospheric layers above, although this was not seen in the MAX-DOAS signal, mostly due to the simultaneous presence of clouds.

This analysis shows that the unique combination of the AEROCLOUD observatory allows for many insights which would not be possible if only a part of the instrumentation was present. A continuation of the measurements of the whole observatory is thus very important. However, such a continuation is at the moment of writing this report not assured due to the end of the budgets for Antarctic research projects. Further, in order to better resolve the vertical aerosol profile, a strong lidar would be necessary, as discussed in section 4.2.3.5).

4.3 Evaluation and improvement of the regional climate model

4.3.1 Antarctic-wide climate model simulations with COSMO-CLM²

In order to evaluate the long-term hindcast simulation with COSMO-CLM² over Antarctica, observations from several sources are collected. Observations are retrieved from the SCAR database (Turner et al., 2004), the AMRC program (http://amrc.ssec.wisc.edu/), the Australian Antarctic AWS dataset (http://aws.acecrc.org.au/) and the Italian Antarctic Research Program (http://www.climantartide.it). From this record, in total 101 individual sites were retained, having monthly temperature and wind speed observations for a time period of at least 10 years (Figure 37). More than 50% of these locations have observations available for periods exceeding 20 years. Wind speed is generally not measured at the same height for each location. In the last decade, Automatic Weather Stations (AWSs) have been installed on several remote locations over the AIS. These devices do not only record temperature and wind speed, but also radiative fluxes and relative humidity. Relative humidity measurements are recorded with respect to water and are converted to humidity with respect to ice using the conversion of Anderson et al. (1994). Long-term information of these variables are available for 11 AWSs over the AIS, which are part of the IMAU Antarctic AWS Project (https://www.projects.science.uu.nl/iceclimate/aws/antarctica.php). These observations are

nevertheless mainly located in Dronning Maud Land and the ice shelves of the Antarctic Peninsula (Figure 37).

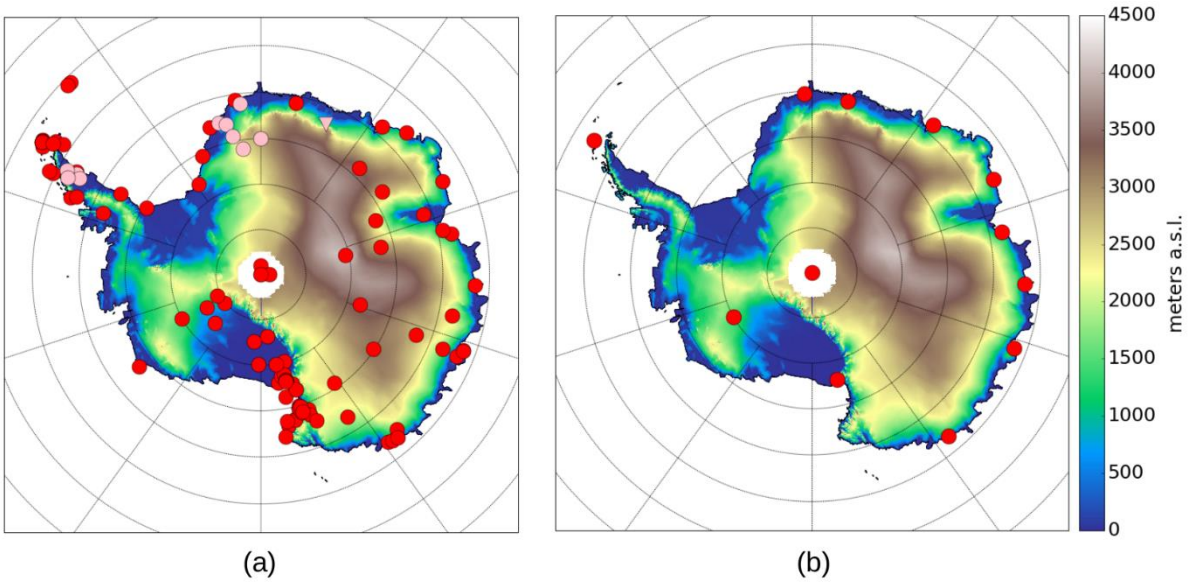

Figure 37: Observational network over Antarctica with data availability of minimally 10 years for (a) ground-based observations and (b) radiosoundings. Pink indicates the availability of measurements of relative humidity and radiative fluxes by Automatic Weather Stations.

Several scientific stations across the AIS launch radiosondes each day at 12-hourly intervals (00 and 12 UTC). Monthly average temperature, wind speed and humidity profiles are retrieved from the Integrated Global Radiosonde Archive (IGRA) Version 2, a collection of radiosounding data across several sources at specified pressure levels (300-500-700-850-925 hPa). A total of 12 locations have observations for a time period longer than 10 years (Figure 37).

Apart from meteorological observations of ground-based measurements and radiosoundings, satellite products can also be used to retrieve relevant climatological information over the AIS. The MODerate-resolution Imaging Spectroradiometer (MODIS) sensor on board of the Terra and Aqua satellites observe the albedo of the underlying surface in cloud-free conditions (Schaaf et al., 2002). To facilitate the comparison, the MODIS albedo product was aggregated to the COSMO-CLM² grid.

Generally, the COSMO-CLM² long-term simulation achieves an excellent average and temporal performance of the atmospheric temperature profile for all locations (MAE $< 1.5°C$; Figure 38). For wind speed, a typical S-shaped profile is correctly simulated, including the low-level inversion, which is katabatically forced near the surface. The model has a slight tendency to underestimate wind speed, mainly for heights between 700 hPa and 300 hPa. Relative humidity in the lower atmospheric layers is on average well represented at the coastal areas and the typical inversions are well simulated. For the inland stations nevertheless, there is a clear discrepancy between the radiosoundings and the COSMO-CLM² simulation, leading to an average overestimation larger than 20 %.

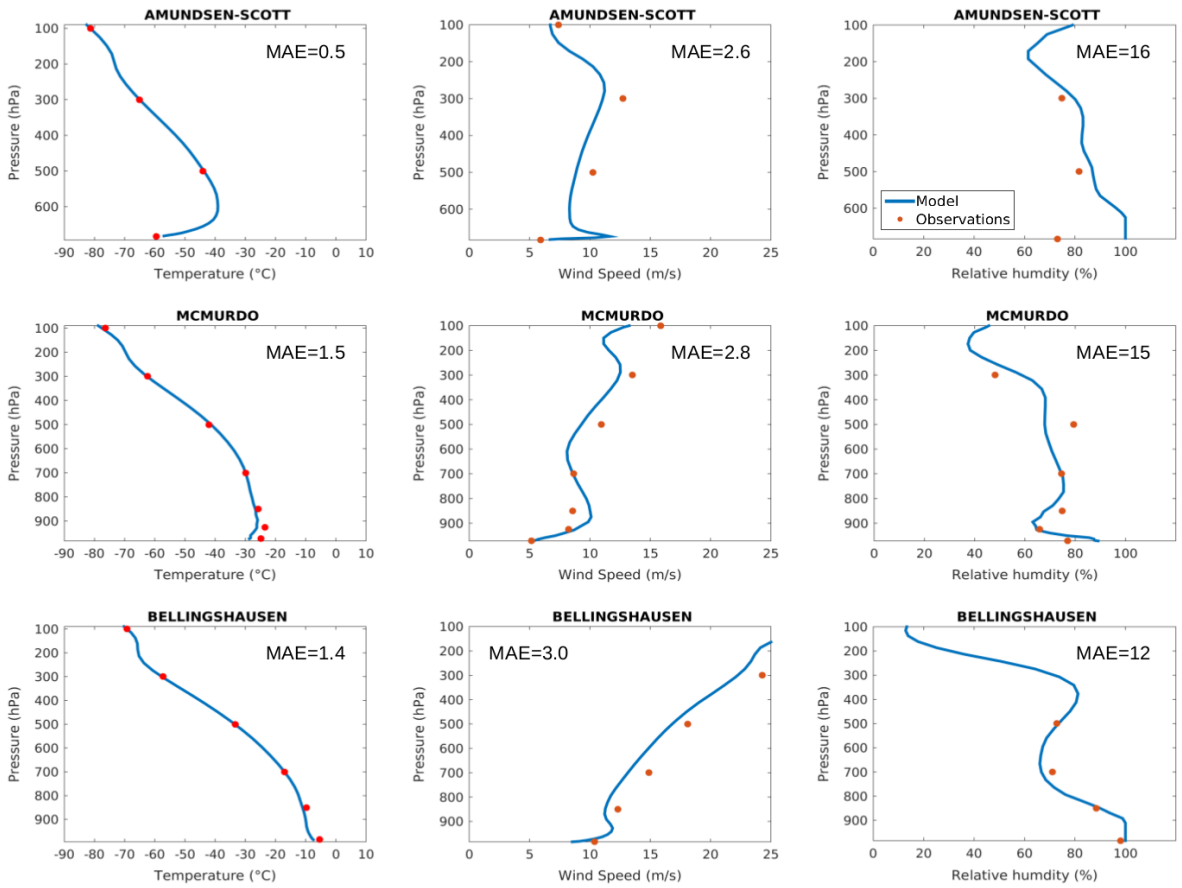

Figure 38: Average radiosounding at distinct pressure levels and vertical model profiles for the austral summer season (DJF) of temperature (column 1), wind speed (column 2) and relative humidity (column 3). Three stations are displayed: Amundsen Scott (inland), McMurdo (coastal) and Bellingshausen (Antarctic Peninsula). The blue line denotes the average field in the model, while the red dots indicate radiosounding average values. The top of the profile is always located at the 100 hPa level, while the lower boundary equals the average surface pressure. MAE denotes the Mean Absolute Error calculated based on each individual monthly observation and does not include the surface and the 100 hPa level.

Apart from the AWSs, MODIS provides a continent-wide albedo product. This can directly be compared to the albedo parameter in the COSMO-CLM² simulation for the austral summer months. Biases in COSMO-CLM² are observed at the coast of East-Antarctica (Figure 39). In this region, the long-term model simulation underestimates the albedo by a factor up to 0.1, which leads to an underestimation of the reflected shortwave radiation. The surface albedo on the plateau of the AIS is well simulated and no consistent biases are detected. Over the Transantarctic Mountains and the Antarctic Peninsula, the long-term simulation overestimates the albedo. In reality large parts of the mountains are snow-free, leading to very low albedo values. In the model, these mountains are smoothed, allowing the snow pack to persist.

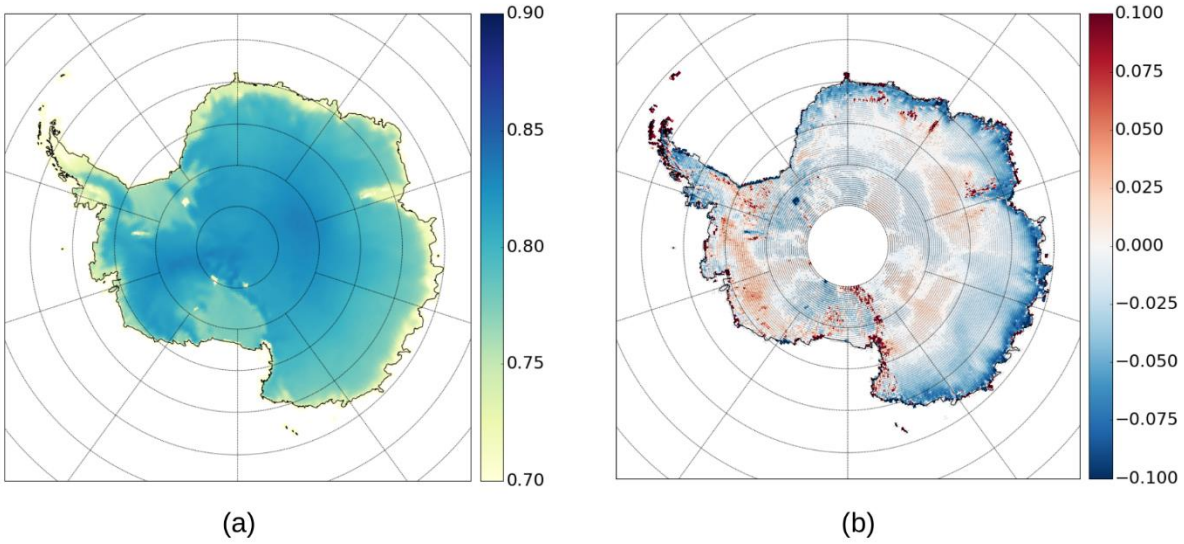

Figure 39: (a) Albedo climatology during austral summer (DJF) in COSMO-CLM² and (b) the absolute difference between the COSMO-CLM² simulation and the MODIS white sky albedo climatology. Dotted areas denote statistically significant differences, calculated using the two-sided Kolmogorov-Smirnov test on interannual differences in albedo values.

In general, near-surface temperatures have a MAE in the range of 2-4°C compared to observations and attain very high correlation coefficients, indicating good average and temporal performance. For coastal areas, temperatures are slightly underestimated by the COSMO-CLM² model. This feature is persistent throughout the year, apart from the austral summer, during which the temperature match is excellent (Figure 40).

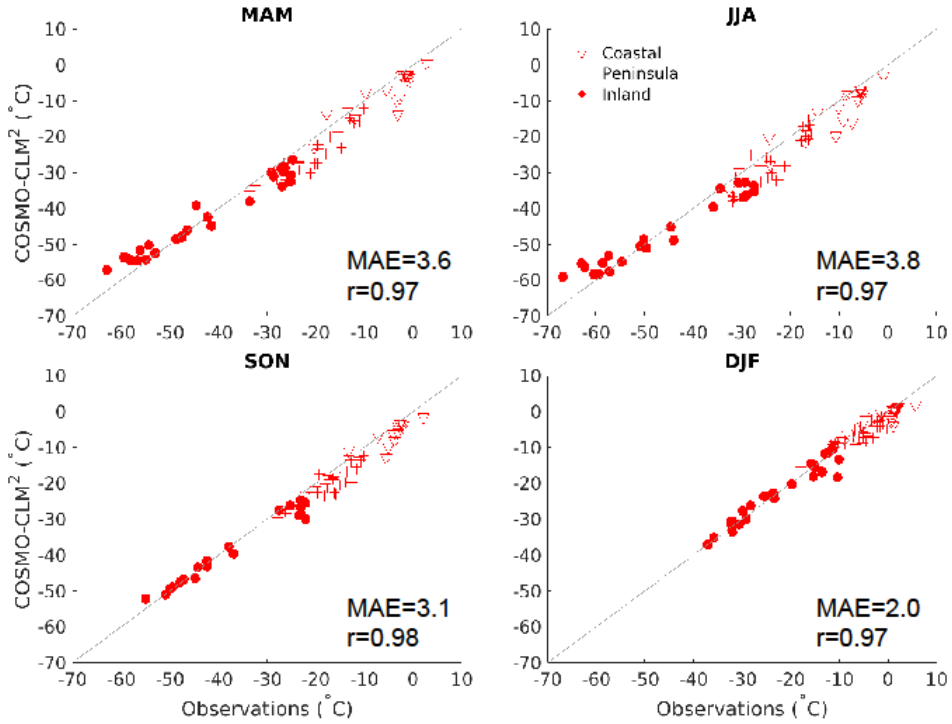

Figure 40: Seasonally averaged 2 m temperature observations (°C) compared to the corresponding pixel in COSMO-CLM². MAE denotes the Mean Absolute Error, while r is the Pearson correlation coefficient, both calculated based on individual monthly observations.

Near-surface wind speeds are generally overestimated by COSMO-CLM² in the AIS interior by 2-5 m s^{-1} (Figure 41). This might be related to the low roughness length coefficient, representative for glazed areas and leading to higher wind speeds. However, at the coastal margins, the performance improves, showing smaller biases (MAE $<$ 3 ms^{-1}) mainly in the austral summer period. A large variability in the performance of wind speed representation in COSMO-CLM² is present for the coastal stations and over the Antarctic Peninsula (Figure 41). These measurement areas are often located in highly variable topography near the ice sheet margins not representative for the ice sheet surface. On the local scale, stations might be shielded from katabatic flow or located in a wind confluence zone.

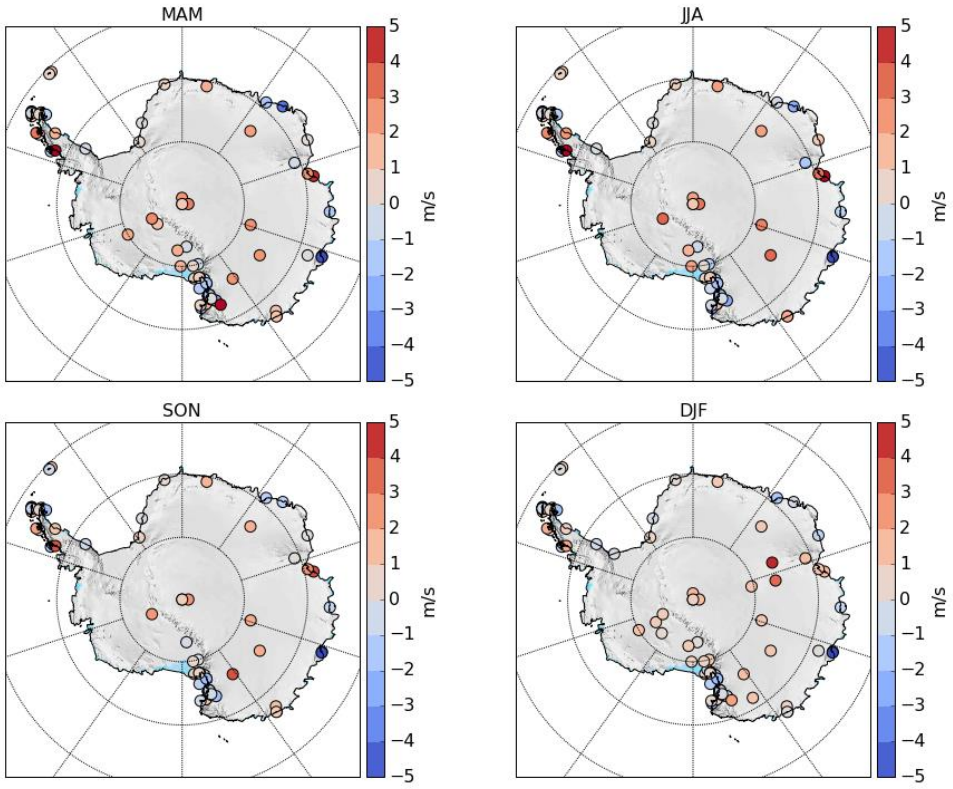

Figure 41: Wind speed bias between seasonally averaged near-surface observations and the corresponding pixel in COSMO-CLM².

Apart from simulating the climatology correctly, it is also important to simulate meteorological variability. This is illustrated for stations located on the coast, inland and the Antarctic Peninsula (Figure 42). The seasonal cycle present in temperature and wind speed is adequately simulated and is consistent with the results obtained above. A consistent underestimation of temperature is present for the coastal Mawson station, which is a common feature that is also detected in Figure 40. Regarding wind speed, the model has a tendency to overestimate wind speeds for most of the AIS, which can be observed for the Amundsen Scott station (2 m s^{-1} on average) and for the coastal station Mawson during austral winter. Furthermore, the yearly variability in monthly temperature and wind speed is adequately simulated by COSMO-CLM². This is nicely illustrated for near-surface temperature where in austral winter, the spread in observed and modelled values is much larger than in austral summer for all three stations. Wind speed values at the coastal Mawson station also are characterized by an interannual variability, which is also nicely captured by the model. For relative humidity, the model strongly underestimates observed values for all stations (Figure 42). Furthermore, for the coastal station and the station located on the Antarctic Peninsula, a reversed seasonal cycle is modelled and the interannual variability is not well simulated. This indicates that problems persist regarding the representation of humidity near the surface and that more work regarding this issue is necessary.

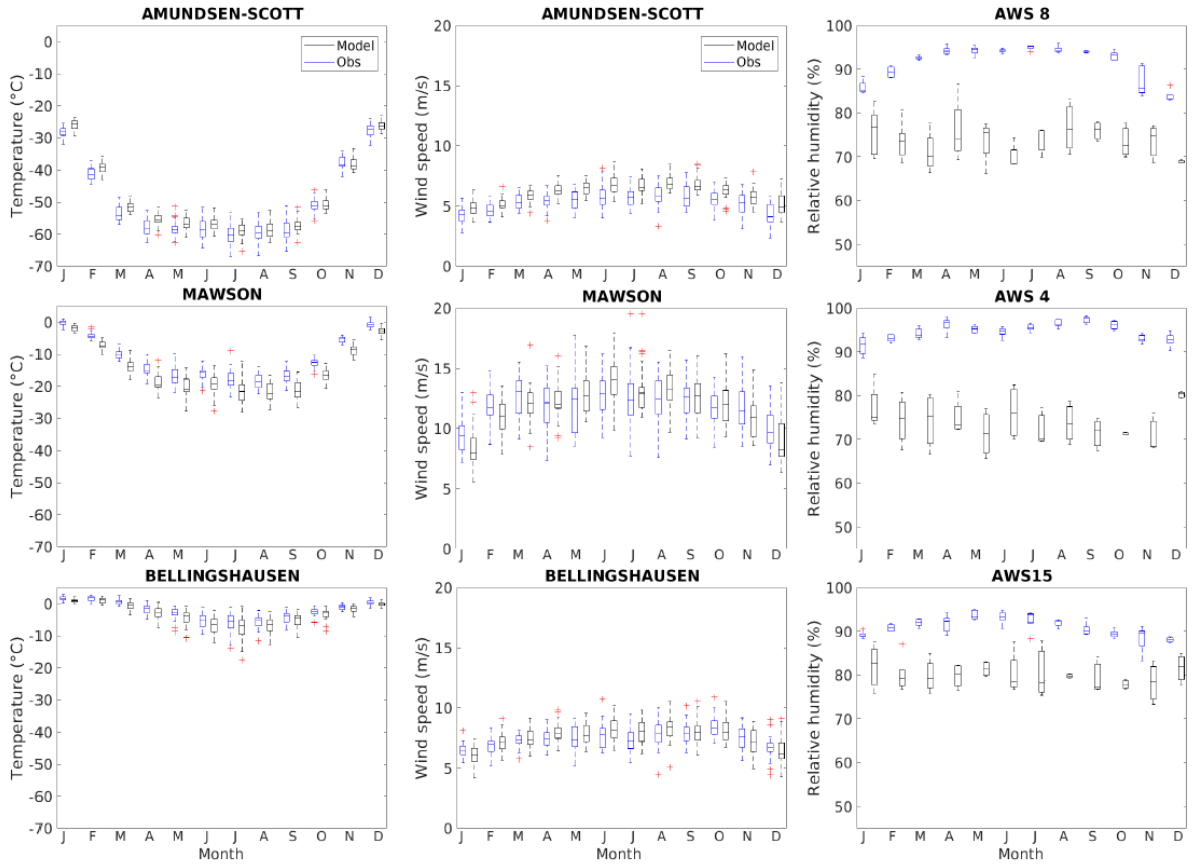

Figure 42: Seasonal cycle and monthly variability of near-surface temperature, wind speed and relative humidity for inland (first row), coastal (second row) and station located on the Antarctic Peninsula (third row). Different stations were chosen for relative humidity due to the unavailability of relative humidity measurements near the surface at Amundsen Scott, Mawson and Bellingshausen.

SMB is simplified in our COSMO-CLM² simulation to snowfall minus surface sublimation. Generally, a good agreement is found between the observational SMB based on Favier et al. (2013) and Medley and Thomas (2019) and the integrated mean SMB in the long-term COSMO-CLM² simulation for the 1987-2010 period for most of the locations higher than 500m a.s.l. (Figure 43). The SMB is however underestimated for the lowest elevation areas, i.e. the ice shelves and the coast. There, the displacement and sublimation of snow particles, not represented in the model, can explain most of the variations in the local SMB, visible in the observational database, and not captured in the model.

When investigating the spatial pattern of the COSMO-CLM² simulated SMB with the reconstruction based on ice cores and ERA-Interim (Medley and Thomas, 2019), a significant underestimation of the SMB is found for most of the coastal sites including the Antarctic Peninsula (Figure 44). This underrate of the SMB at coastal sites is attributed to both an underestimation of snowfall and the simplification of modelled SMB to snowfall minus sublimation. The underestimation of snowfall is larger for the Antarctic Peninsula, and affects the albedo and thereby the surface energy balance. The neglect of surface melt and snowdrift processes, especially active on the ice shelves and coastal areas, leads to local under- and overestimation of the modelled SMB.

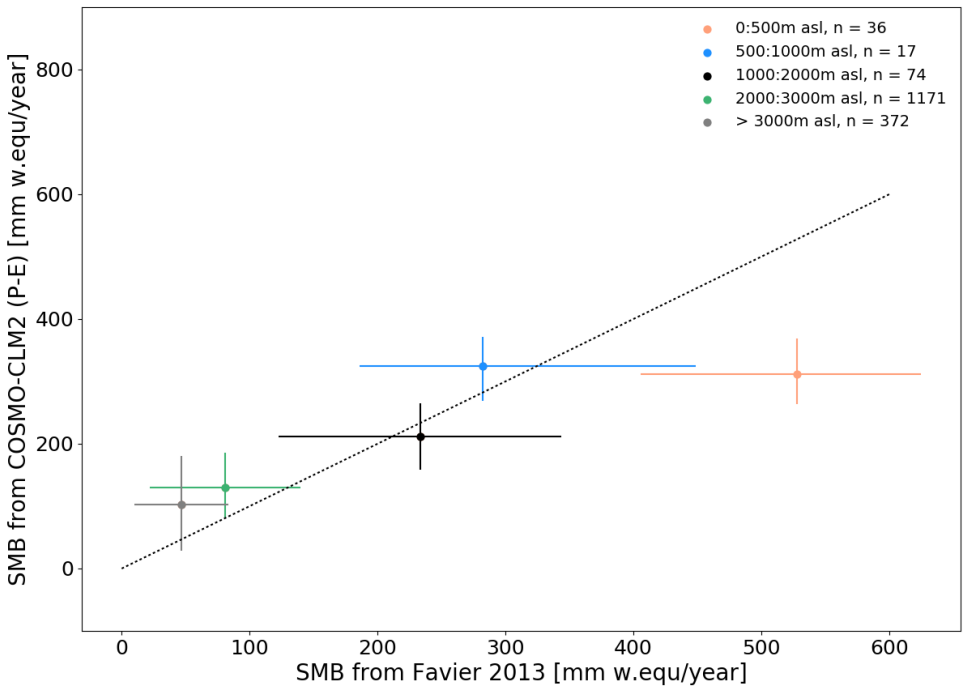

Figure 43: Surface mass balance estimates obtained by Favier et al. (2013) and Medley and Thomas (2019) for the period 1987-2010 compared to the surface mass balance reconstruction of COSMO-CLM². The observations are binned in different height classes. The dot denotes the mean value of the height bin, while the error bars denote the 10th and 90th percentile of the data points for each class (horizontal) and the corresponding model (vertical).

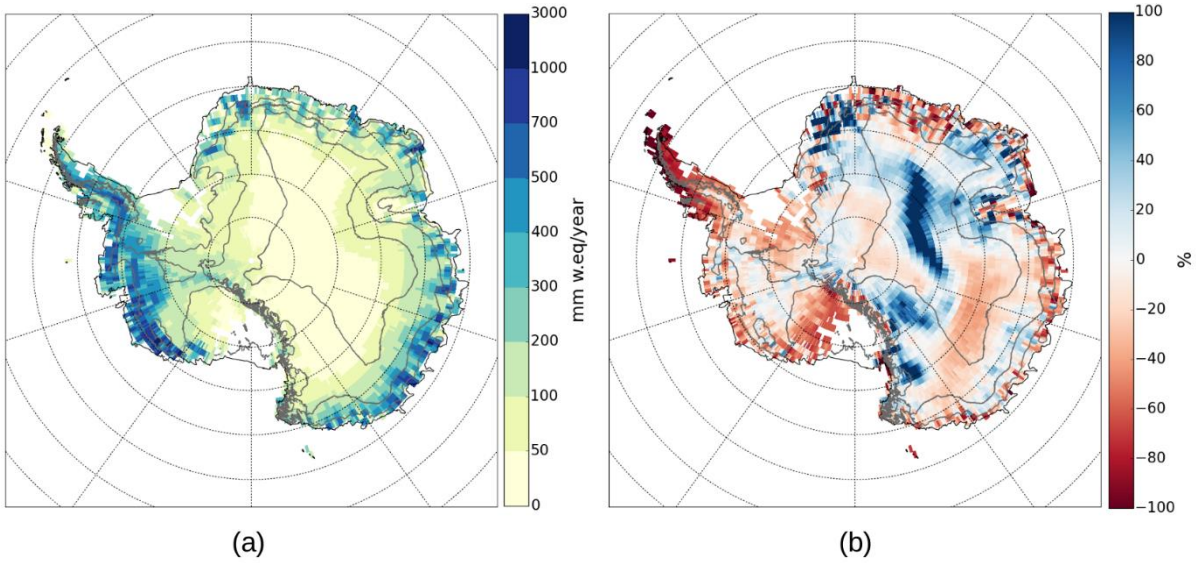

Figure 44: (a) Surface mass balance reconstruction in COSMO-CLM² based on the difference between snowfall and evaporation (sublimation) and (b) the relative difference compared to the reconstruction presented in Medley and Thomas (2019), for the model period. Contours denote elevation with an interval of 1000m.

The data compiled in the AEROCLOUD project have also been used to evaluate re-analyses products. The performance of the individual re-analyses regarding accumulation (precipitation

minus evaporation) vary according to the zones investigated. We compared re-analyses accumulation to the SAMBA dataset (Favier 2013), binned in different elevation classes. Despite a general similar pattern for all re-analyses, ERA-5 shows the smallest bias to the observations, but tends to underestimate SMB, while all other re-analyses overall overestimate accumulation over the AIS. Era-Interim and ERA-5 strongly underestimate accumulation at coastal areas an ice shelves, while MERRA-2 overestimates SMB at those locations. We also assessed the ability of re-analyses to represent the atmospheric rivers, visible in the cumulative mass change retrieved from the Grace satellite, in Dronning Maud land for the years 2009 and 2011. All re-analyses are able to simulate these atmospheric rivers to some extent, and ERA-5 and ERA-Interim show the smallest bias. SMB is very challenging to model accurately, and includes processes not accounted for in the re-analyses. Therefore, inclusion of blowing snow and melt processes, as well as a better representation of snowfall over the AIS are crucial to represent the observed SMB in an accurate way. Finally, even though the different re-analyses perform very differently and there is no best model for all variables (Figure 44), the analysis performed enables the users to choose the best performing reanalysis, depending on the area of investigation, the season and the variable to represent.

	T	WS	RH	SMB
ERA-5	2.0	2.8	13.5	48.1
ERA-Interim	2.6	2.7	11.9	54.2
CFSR	3.4	2.9	18.9	59.5
MERRA-2	3.1	2.4	13.6	58.5

Figure 45: Mean absolute error for each re-analysis for each of the studied variables: temperature (T, in degrees), wind speed (WS, in m s^{-1}), relative humidity (RH, in %) and surface mass balance (SMB) from both methods (validation against Favier et al. (2013) and Grace mass anomaly derived from altimetry. The colour denotes the relative performance compared to the other re-analysises.

Future work on the COSMO-CLM^2 model is necessary to further improve its performance regarding Antarctic climate representation. This is pursued in the Excellence of Science funded PARAMOUR project, which will couple the model to an ocean and ice sheet model in order to investigate potential interactions between the different components of the climate system.

4.3.2 High-resolution simulations with COSMO-CLM²

Blowing snow fluxes were measured during two years by FlowCaptsTM in Terre Adélie, Antarctica. The measurements were taken between 0-1 m and 1-2 m high, in 2010-2011 at D47 (located at 67.4°S, 138.7°E, 1565 m a.s.l.) and 2014-2015 at D17 (located at 66.7°S, 139.7°E, 465 m a.s.l.). We simulate blowing snow using the simple bulk blowing snow scheme developed by Déry and Yau (2001). This scheme is implemented in the Community Land model and runs in offline mode at the two locations, and is forced with observed wind speed

and air temperature. Simulated blowing snow agrees well with the on-site measurements (Figure 46). Both the temporal variation of blowing snow frequency and the general pattern and magnitude of the bowing snow transport rates is well matched by the bulk model. While modelled blowing snow fluxes are slightly over estimated at D47 and under-estimated at D17, the magnitude of the modelled transport is comparable to that observed (Figure 47). Overall, the exponential relation between the wind speed and the blowing snow flux is well captured by the model at both sites.

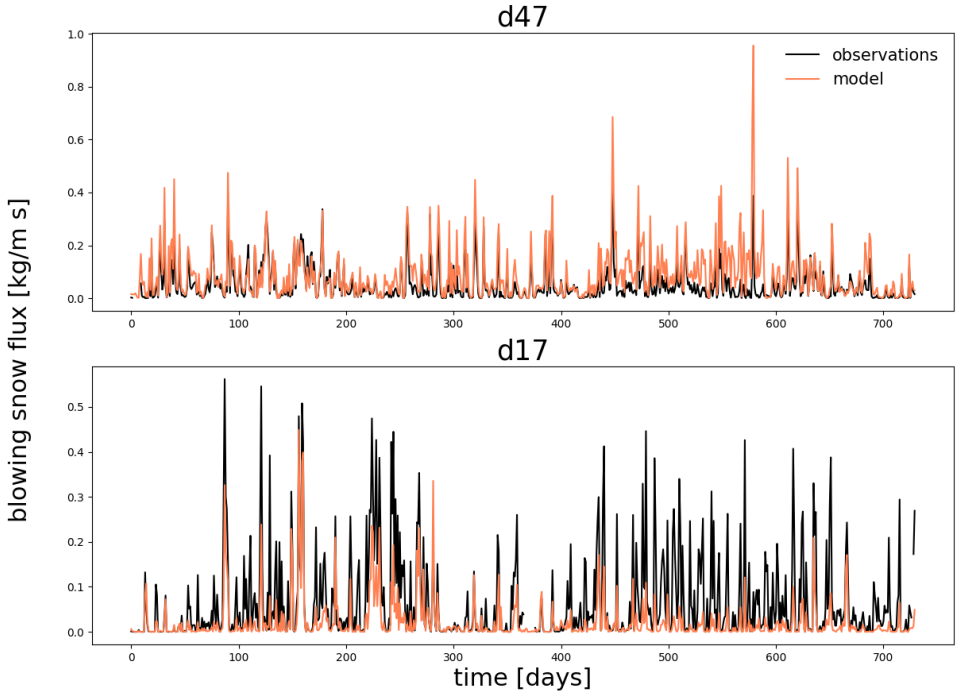

Figure 46: Comparison between observed and modelled blowing snow fluxes at D47 and D17

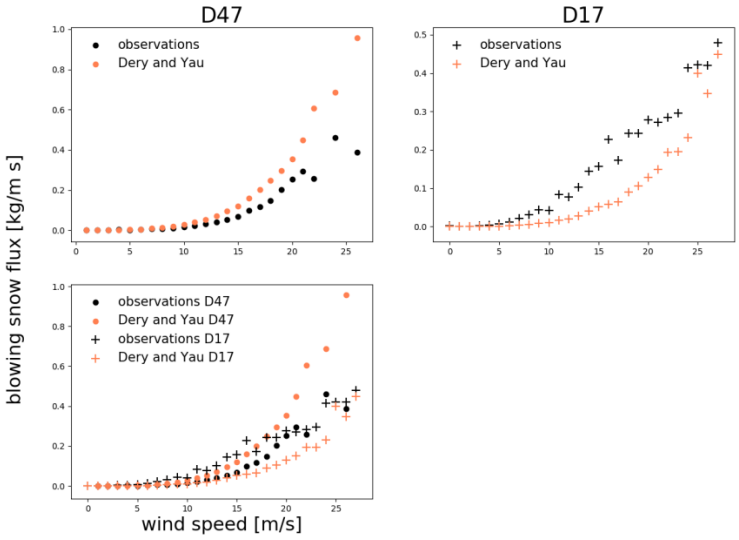

Figure 47: Statistical comparison between observed blowing snow flux and the parameterisation of Dery and Yau in relation to wind speed

4.4 Assessment of the indirect aerosol effect in Dronning Maud Land

4.4.1 Identification of the relationship between atmospheric composition, cloud and precipitation properties and air mass origin

4.4.1.1 Air mass origin and precipitation properties

Within the assessment of the individual components of the surface mass balance, also the relation between large precipitation events, the origin of the air mass and the amount of precipitation that was recorded at PE station was investigated. The origin of the air masses (five days prior to the precipitation event) were deduced from back trajectories arriving at PE station at altitudes below 3000 m asl. Back trajectories were calculated with the FLEXTRA model (see section 3.5.1). The most intense precipitation events (> 5 mm w.e. of precipitation per event) were associated with air masses typically originating from areas north of 50° S, taking up moisture close to the oceanic surface and were generally lifted upwards when reaching the Antarctic ice shelf continental margin. A significant relation between the transport capacity of the cyclone, the origin of the air mass and the amount of precipitation was observed (see Souverijns et al., 2018a). In case a cyclone was present, a tendency for higher precipitation amounts during larger pressure gradients was present. Furthermore, during such conditions, air masses originated from more northern areas. Thus, when the cyclone or trough was more developed and high pressure blocking was present NE of PE station, moisture from more northern areas was able to be transported, leading to higher precipitation rates at the station.

4.4.1.2 Air mass origin and particle and CCN properties

Figure 48 shows the Potential Source Contribution Function (PSCF; see section 3.5.1), calculated for N_{TOTAL}, N_{TOTAL}-$N_{CCN-0.7\%}$, $N_{CCN-0.7\%}$ and $N_{CCN-0.1\%}$. These four parameters represent concentrations of all particles, particles in the size range up to around 35 nm, particles with sizes above 35 nm and the largest particles above 110 nm, respectively. (The parameter N_{TOTAL}-$N_{CCN-0.7\%}$ denotes concentrations of all particles minus those that are CCN at ss = 0.7 %.) The analysis was done using the data of all three austral summer periods. High values in the maps in Figure 48 indicate which regions had a high potential to contribute to the 25% of the highest number concentrations measured at the receptor site.

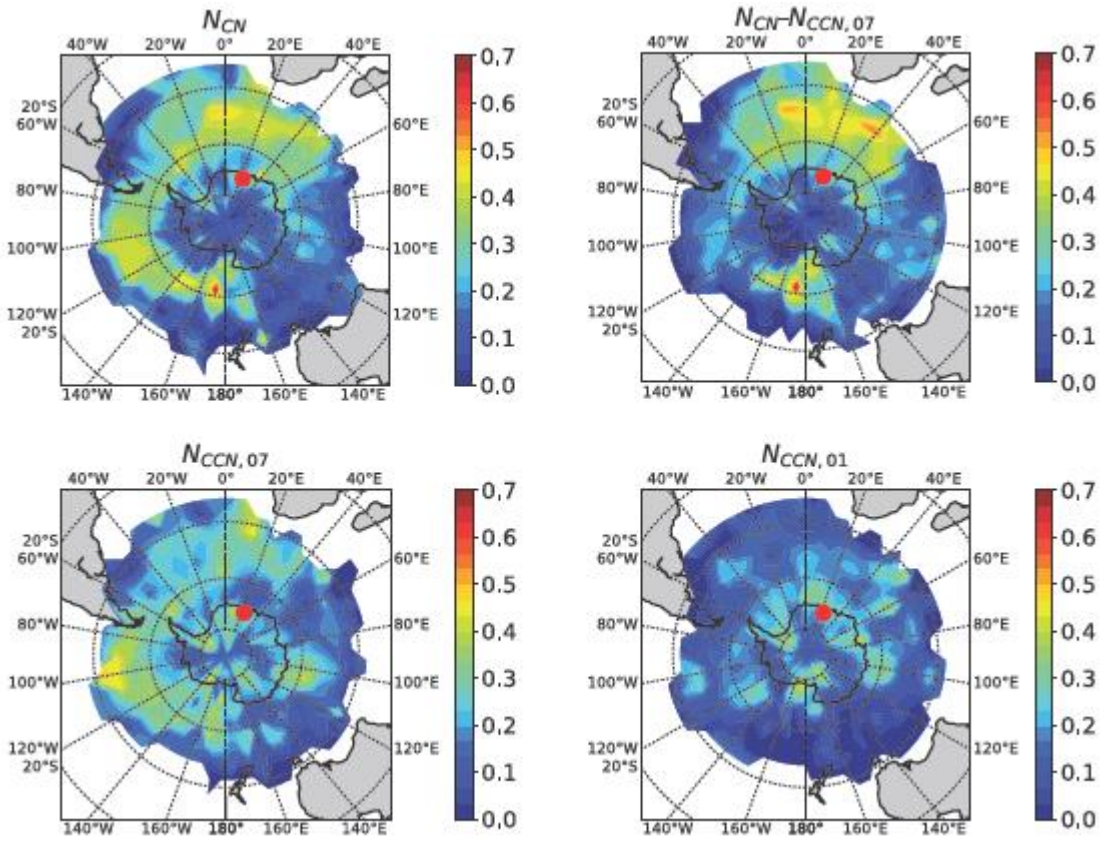

Figure 48: Potential Source Contribution Function (PSCF,) plotted over a map of Antarctica for N_{TOTAL}, N_{TOTAL}-$N_{CCN-0.7\%}$, $N_{CCN-0.7\%}$, *and* $N_{CCN-0.1\%}$. *The colour bar indicates the value of the PSCF.*

The PSCF of N_{TOTAL} shows enhanced values over the region of the Southern Ocean, mostly between 60° and 40° S, but not over the Antarctic continental region. Hence, the Southern Ocean was likely to be the dominant source region leading to an enhancement in N_{TOTAL} measured at PE, while the Antarctic continent itself was not likely to act as a particle source. N_{TOTAL}-$N_{CCN-0.7\%}$ and $N_{CCN-0.7\%}$ are two complementary parameters, adding up to N_{TOTAL} The PSCF maps of $N_{CCN-0.7\%}$ and N_{TOTAL}-$N_{CCN-0.7\%}$ show clearly distinct patterns, indicating that different source regions likely contributed to high concentrations of particles with sizes below and above 35 nm. However, both share that their highest signals were in the Southern Ocean between 60° and 40° S, though at different longitudes. The PSCF of N_{TOTAL}-$N_{CCN-0.7\%}$ (particles with sizes smaller than 35 nm) shows a large area of high signals between 40° W and 60° E. When calculating transport times based on air mass back trajectories, an average transport time of 5.1 days from this area to PE station was obtained. The PSCF of $N_{CCN-0.7\%}$ (particles with sizes above 35 nm) shows the largest area of high signals in a region between 140° and 80° W for which the average transport time to the PE station was 8.8 days. As already discussed in section 4.2.4, the aerosol observed at the PE station featured a dominant Aitken mode. This can be brought in line with the results discussed here. The aerosol particles that originated from the marine areas that show up dominantly in the PSCF were likely mainly secondary aerosol particles that grew during the transport to PE station. The size of the measured aerosol particles can be assumed to be a function of average transport time, corresponding to source regions for larger particles that

were further away (considering air mass traveling times). Our analysis clearly indicates that the Southern Ocean region was a region potentially acting as a source of the majority of particles observed at PES. The PSCF map for $N_{CCN-0.1\%}$ differs from the others. Overall, values were lower, pointing towards a more uniformly distributed origin of particles with sizes above 110 nm. But it should also be stressed that values for $N_{CCN-0.1\%}$ were generally low (see section 4.2.4). The PSCF map shows almost no areas of enhanced values over the Southern Ocean, but several spots of comparably enhanced values show up along the coast of Antarctica. Hence, the Antarctic shelf ice regions seemed to be potential source regions for enhanced values of $N_{CCN-0.1\%}$.

4.4.1.3 Recommendations

As already mentioned in the results and recommendations for the aerosol and CCN properties (sections 4.2.1 and 4.2.4), it is recommended to have in future also aerosol instrumentation which measures the size distribution below 90 nm. This would give more insights into the atmospheric aerosol processes and also into the transport pathways. Further, the air mass origin should be continued, e.g., with respect to the origin during different seasons, depending on atmospheric humidity fields, or carrying out cluster analyses. That the Southern Ocean seemed to be an important source region of atmospheric particles justifies more directed research on this region. This is of particular importance because with the changing climate, the coastal areas and sea ice zones of Antarctica are likely to be affected strongly what in return could change the emission sources of particles.

4.4.2 Identification of the model sensitivity to cloud condensation nuclei and ice nuclei

A set of high-resolution model simulations centred over the PE station were executed using the COSMO-CLM² expanded with an aerosol module and driven by aerosol concentration as stated in Table 1. The period of simulation is 7-13 January (excluding a few days of spin-up). During the period of simulation, Dronning Maud Land and the PE station were influenced by a weak low pressure system located in the northwest. The analysed period was characterised by cloudy conditions most of the time (Figure 49). A large part of the clouds show relatively low backscatter values, indicating a majority of ice particles. However, at the top of the cloud systems and at the end of 11 January 2016, high backscatter values were observed, indicating the presence of supercooled liquid water in the clouds. At the end of 9 January 2016, a few hours of precipitation were observed at the PE station reaching the surface (Figure 50). In the following days, virga was detected, i.e. precipitation sublimating before reaching the ground.

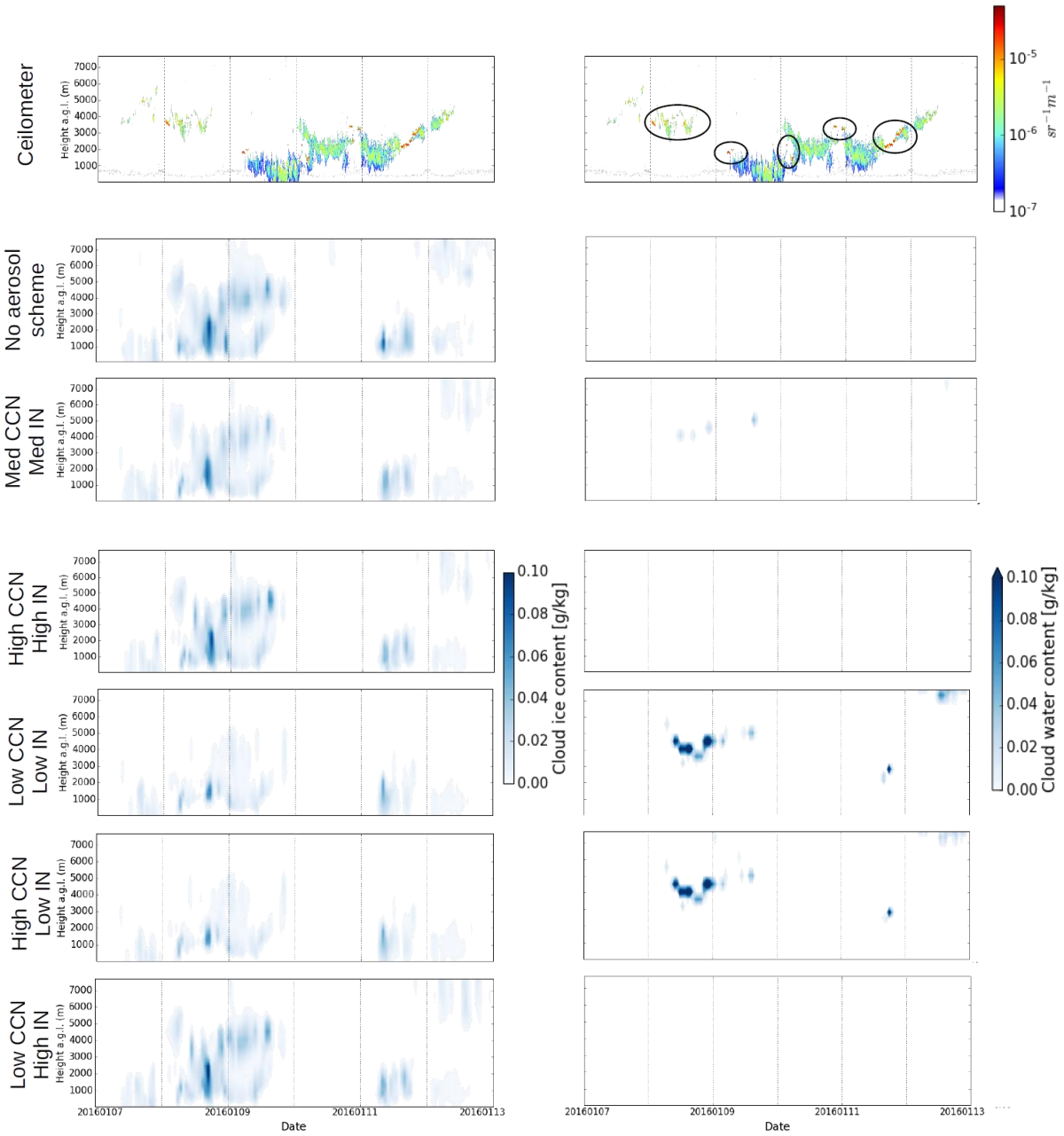

Figure 49: Comparison between cloud ice (left) and water content (right) in the different model simulations and the measurements of the ceilometer (top panel). Values above 10^{-5} denote the presence of liquid water.

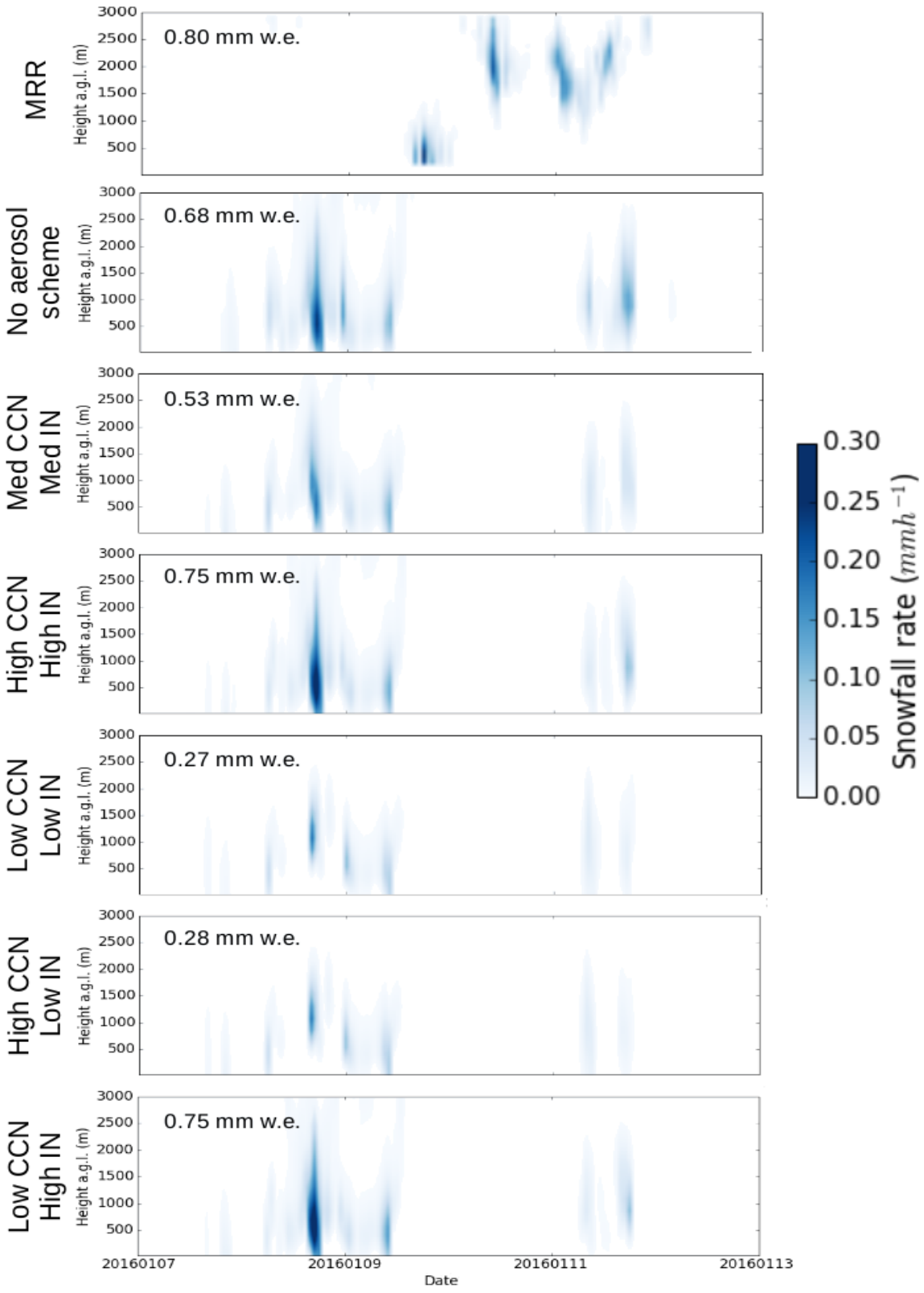

Figure 50: Comparison of precipitation in the different model simulation and the measurements of the Micro Rain Radar (top panel). The value in the top left corner denotes the total precipitation amount registered at 300 m a.g.l. (lowest measurement bin of the MRR).

Each of the different model setups lead to contrasting results regarding the representation of clouds and precipitation. However, the macrophysical characteristics are the same in all simulations. The cloud systems arrive too soon at the PE station (1 day too early) and has a vertical extent exceeding recordings by the ceilometer. Furthermore, its temporal extent is discontinuous, showing one day of cloud-free conditions, contrasting the observations (Figure 49). Regarding precipitation, the simulations are also ahead of MRR observations by approximately 1 day. The time span of the precipitation event is also shorter in reality. Furthermore, in some simulations, precipitation is simulated near the surface on 11 January 2016, while in reality, all has sublimated in more upper levels. Despite these features, the large-scale process driving clouds and precipitation towards the PE station are represented in all model simulations.

Varying the aerosol/CCN and IN content does not impact the large-scale structure of the cloud and precipitation system simulated by the model. However, a clear impact on the cloud microphysical structure is observed. In the simulation without the aerosol module, no liquid water is simulated in the clouds. In the simulations with low IN concentrations, patches of liquid water at the top of the clouds are simulated, and also the small liquid cloud at the end of 11 January is represented in the model. However, the frequency of liquid water occurrence is overestimated in these simulations compared to reality. In the simulations with high IN concentrations, no liquid water is simulated, while in case of medium concentrations of CCN and IN, the amount of liquid water is very limited. In this latter simulation, the presence of liquid water is limited to the top of the clouds, matching observations, but the liquid cloud at the end of 11 January is not simulated. These preliminary results for this limited case study seem to point out that the amount of IN determines the presence of liquid and mixed-phase clouds, while variations in CCN concentration do not impact cloud microphysics, corresponding the results of Solomon et al. (2018) for Arctic mixed-phase stratocumulus clouds.

Too high concentrations of IN limit the formation of liquid or mixed-phase clouds. Once IN are activated, water vapour is diffused more easily to ice crystals compared to liquid cloud drops, as supersaturation over ice is lower compared to liquid water. Since most vapour is used to diffuse on the ice crystals, the clouds will consist of ice particles only. This is called the Wegener-Bergeron-Findeisen process (Korolev, 2007). It is therefore postulated, based on the preliminary results for this case study, that in certain air masses at the PE station, a limited number of IN is available, allowing the formation of liquid and mixed-phase clouds, reducing ice formation and limiting the Wegener-Bergeron-Findeisen process. The sensitivity of the model results on IN concentrations generates a need for more accurate observations of IN concentrations over Antarctica. Only when the models can be driven by accurate concentrations, correct responses on clouds can be simulated.

Different aerosol concentrations also affect precipitation. Our simulations show a substantial variability in near-surface precipitation ranging from 0.27-0.75 mm w.e. (Figure 50). In this case, the simulations with ice clouds attain the best performance compared to the observations, while the simulations with higher liquid concentrations attain for much less precipitation. It is

suggested that the higher abundance of IN allows for faster nucleation, formation and growth of ice particles, depleting the amount of moisture in the clouds. These larger particles have a lower cloud residence time, precipitate faster and lead to higher precipitation amounts. Liquid clouds have a much longer cloud residence time, delaying precipitation.

Changes in cloud properties also affects the surface radiation balance. Generally, clouds limit shortwave radiation reaching the surface, while increasing the longwave downward radiation. The CRE is calculated as the net radiation difference at the surface between cloudy conditions and the same situation without clouds and can also be calculated for shortwave and longwave radiation separately. Over snow surfaces, the net longwave CRE is generally larger than the net shortwave CRE, leading to a net positive CRE and a warming at the surface. This is the case in all our simulations (Figure 51). The larger well-developed cloud structure of 9 January 2016 has a large CRE, while during clear-sky moments, the CRE equals zero. Apart from the cloud macrophysical appearance, the microphysical properties of the clouds influence the CRE. For this we calculated the difference in CRE between our simulations and the standard simulation without the aerosol module (Figure 51). It is shown that the simulation with a high concentration of IN only has limited differences compared to the simulation without the aerosol module in both shortwave and longwave radiation. Both of these simulations also had very similar cloud microphysical and macrophysical structures (Figure 49). Simulations with a lower concentration of IN generally have a larger CRE. The liquid clouds, which are present here, reflect more incoming shortwave radiation, lowering the amount reaching the surface (Figure 51). However, they are also increasing the amount of net surface longwave radiation. This latter effect is dominating, leading to a larger positive impact of liquid clouds on the radiation balance.

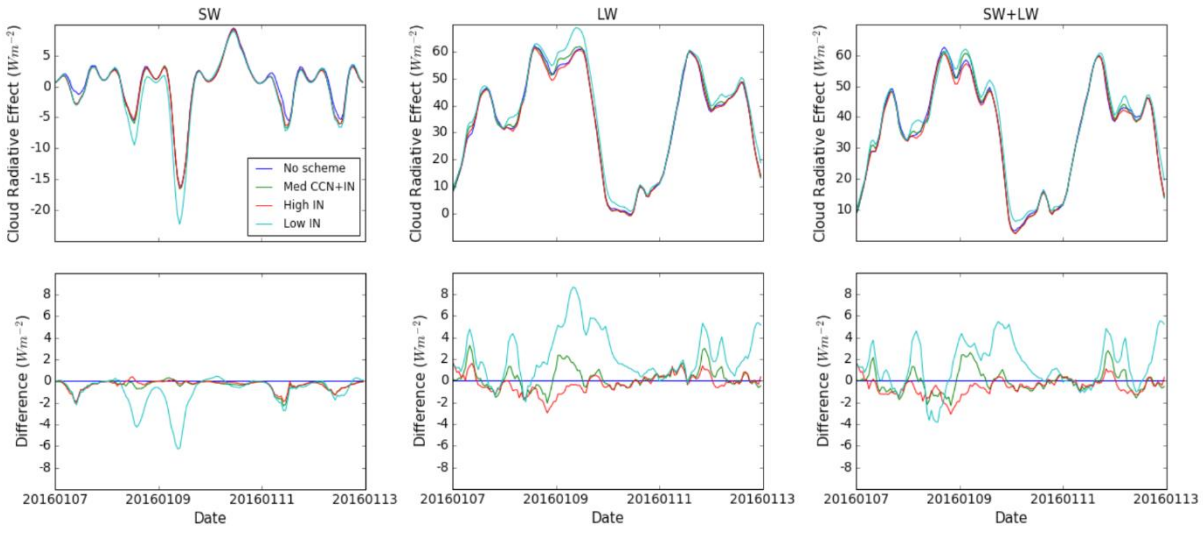

Figure 51: (first row) Shortwave (SW), longwave (LW) and combined (SW+LW) cloud radiative effect at the PE station. (second row) Difference in cloud radiative effect compared to the model simulation without the aerosol module. The low and high IN simulation are both with a low concentration of CCN.

Despite these promising results, it must be noted that the impact on clouds, the radiative balance and precipitation were derived for a single case study only. A set of long-term simulations are needed to confirm these findings and to draw conclusions.

5. DISSEMINATION AND VALORISATION

5.1 Network management

5.1.1 Internal

Throughout the course of the project, bi-annual meetings were organised bringing together all partners of the AEROCLOUD project alternating the location of the meeting at KU Leuven, RMI and BIRA. During these meetings, the scientific progress and collaboration between the partners were discussed. Furthermore, plans for the Antarctic campaigns and the instrumentation of the different partners were considered. Apart from this, ad-hoc meetings took place to discuss scientific matters or campaign planning.

Several of the publications listed in section 6 (Publications) are based on collaboration between the different partners of the AEROCLOUD project and have partners from the different institutes as co-author.

5.1.2 Follow-up committee

Annual meetings with members of the follow-up committee have been organised each year during the EGU General Assembly. During these meetings, progress regarding the project was discussed. Furthermore, possible future steps were postulated, offering the opportunity for collaboration and future projects.

5.2 Contribution to other projects

5.2.1. Contribution to the scientific community

During the AEROCLOUD project, there has been a lot of outreach to the scientific community. This led to several collaborations regarding data distribution and exchanging expertise among different research groups. As such, the AEROCLOUD team got involved in the APRES3 project (Antarctic Precipitation, Remote Sensing for Surface and Space). This led to three publications (of which one with an AEROCLOUD member as first author) and good relations with the Antarctic climate community (see also section 6).

5.2.2 Contribution to POLAR-CORDEX

Apart from observations, also the COSMO-CLM² model has drawn the attention of the international community. During meetings of the POLAR-CORDEX group, the importance of Antarctic RCMs was highlighted several times for ensemble studies of important climate variables. As a result, the COSMO-CLM² model developed during the AEROCLOUD project will now contribute to a model intercomparison study regarding the surface mass balance over Antarctica, together with five other models. The addition of our model will allow a more reliable estimation (including an assessment of the uncertainty) of the SMB over Antarctica. A publication on this topic is under preparation.

5.3 Instrument maintenance and calibration

The instruments of the AEROCLOUD observatory were regularly maintained and calibrated, following the respective guidelines of the individual instruments. The pyrometer and the sunphotometer were shipped back yearly for calibration at the manufacturer or the Aeronet network, respectively. The pyrometer had a double, so continuous whole-year measurements were assured. The sunphotometer is a summer-only instrument and was shipped back and forth yearly. The data of the automatic weather station (AWS) of IMAU, University of Utrecht (NL) is quality-checked by IMAU and then sent to the AEROCLOUD partners. Each austral summer season, staff of the AEROCLOUD project was present at PES and carried out the necessary maintenance and calibration procedures per instrument.

The following gives a brief description of further important points to mention per austral summer season at PES:

Season 2014/2015: 2 Pax present November-December 2014 (Alexander Mangold, Quentin Laffineur, both RMI); cloud condensation nuclei counter (TROPOS) present; station had power during whole winter 2015 period;

Season 2015/2016: 2 Pax present November-December 2015 (Quentin Laffineur, RMI, Christian Hermans, BIRA); cloud condensation nuclei counter (TROPOS) present; installation of Snowflake Video Imager (SVI-PIP) and of Maxdoas instruments; installation of updated AWS in parallel with existing one; general power-outage in May 2016 (i.e. data stop);

Season 2016/2017: no scientific Belgian research expedition (Enserink, 2017); as consequence no re-start-up of instruments and continuation of data gap; no maintenance;

Season 2017/2018: 1 Pax present November-December 2017 (Alexander Mangold, RMI); restart of many instruments since power outage in May 2016; installation of a second micro-rain radar (borrowed from University of Bonn, Germany) for comparison during summer season; reorganisation by the station operator of the general IT set up and of the data storage and transfer; station had power during whole winter 2018 period; however, due to the new storage and transfer policy some data have been lost;

Season 2018/2019: no AEROCLOUD-Pax, but support from 2 Pax of Brain-be project CHASE present at the station during November-December 2018; de-installation and return of many instruments because they needed severe repair (sunphotometer, Maxdoas; Aethalometer; Optical Particle Counter LAS).

5.4 Management of the PE database and data dissemination

A general AEROCLOUD website (aerocloud.be), on which the project is described and via which the AEROCLOUD data can be accessed, has been set up. The data of the aerosol, cloud and precipitation instruments are available (on demand) via this website. Data of the AWS are available via the Global Telecommunication System (GTS) of WMO, as are the radio sounding

data. Data of the sunphotometer are available via the Aeronet website (aeronet.gsfc.nasa.gov). Data of the Maxdoas instrument can be found on the NDACC website (www.ndacc.org). Quicklooks per day of the data of most of the instruments are available on the website. AEROCLOUD data have been requested by several research institutes (e.g., British Antarctic Survey, Brain-be project Microbian, Antarctic GNSS research of the Royal Observatory of Belgium, EPFL Switzerland and CNRS-LMD/IPSL France) and led to several collaborations and international publications (see also section 6).

It is further envisaged to submit AEROCLOUD data to doi.org-referenced data bases PANGAEA (www.pangaea.de) or data set publishing journals (e.g., Polar Data Journal; https://pdr.repo.nii.ac.jp/).

5.5 Organization of symposia

5.5.1. EGU General assembly splinter meetings

The European Geoscience Union General Assembly is an annual meeting bringing together scientist of all nations working on geosciences. From 2015-2019 members of the AEROCLOUD project were present at this meeting to present the results of the AEROCLOUD project (see section 6.5). Within the framework of the AEROCLOUD project (and its predecessor HYDRANT), every year, a 'Splinter meeting' was organised entitled 'Clouds and precipitation in polar regions and beyond: bridging observations and modelling'. This meeting brought together researchers involved and interested in cloud and precipitation measurements and modelling in the Arctic and/or Antarctic regions for an open discussion on using observations to improve cloud/precipitation representation in the regional models. This meeting also was frequently visited by members of the AEROCLOUD supervisory committee.

Furthermore, every year, a session on 'Clouds and precipitation in polar regions' was organised and convened by Dr. Irina Gorodetskaya (previously working as a postdoctoral researcher on the HYDRANT and AEROCLOUD projects; now at the University of Aveiro in Portugal) and co-convened by members of the AEROCLOUD project. This session was initiated from the HYDRANT project and has grown ever since.

5.5.2 Antarctic climate symposium

On the 10th of May 2019, members of the AEROCLOUD team together with team members of other BELSPO (BRAIN-be) funded projects such as CHASE, PARAMOUR and Mass2Ant organised a symposium devoted to climate research on the Princess Elisabeth station and more generally Queen Maud Land (ees.kuleuven.be/aerocloud-event/). The organizing committee consisted of Nicole van Lipzig (KU Leuven), Alexandra Gossart (KU Leuven), Alexander Mangold (RMI), Francois Hendrick (BIRA), Hugues Goosse (UCL), Frank Pattyn (ULB) and Maaike Vancauwenberghe (BELSPO), and was supported by BELSPO and BNCAR. This symposium brought researcher working with both observations and climate models in the region together to exchange experiences. The symposium took place in the new BELSPO premises (WTC III) and offered 14 oral presentations and 7 posters (Figure 52). In total 55

researchers (Figure 53) attended the event originating from several national (Université Liège, Université Catholique de Louvain-La-Neuve, Université Libre de Brussel, KU Leuven, UGent, Vrije Universiteit Brussel, RMI, BIRA) and international institutes (TU Delft, British Antarctic Survey, Tropos, ETH Zürich, IMAU, AWI, Norwegian Polar Insitute). This was also the end symposium of the AEROCLOUD project.

Figure 52: Impression of the Antarctic Climate Symposium, BELSPO 10 May 2019.

Figure 53: Participants of the Antarctic Climate Symposium, BELSPO 10 May 2019.

6. PUBLICATIONS

6.1 Scientific publication in international journals

- Herenz, P., Wex, H., Mangold, A., Laffineur, Q., Gorodetskaya, I.V., Fleming, Z., Panagi, M., Stratmann, F. (2019). CCN measurements at the Princess Elisabeth Antarctica Research station during three austral summers, Atmospheric Chemistry and Physics 19, 275-294.
- Souverijns, N., Gossart, A., Demuzere, M., Lenaerts, J.T.M., Gorodetskaya, I.V., Vanden Broeke, S., van Lipzig, N.P.M. (2019). A new regional Climate Model for POLAR-CORDEX: Evaluation of a 30-years hindcast with COSMO-CLM^2 over Antarctica, Journal of Geophysical Research Atmospheres 124, 1405-1427.
- Durán-Alarcón, C., Boudevillain, B., Genthon, C., Grazioli, J., Souverijns, N., van Lipzig, N. P. M., Gorodetskaya, I. V., and Berne, A. (2019). The vertical structure of precipitation at two stations in East Antarctica derived from micro rain radars, The Cryosphere, 13, 247-264.
- Lemonnier, F., Madeleine, J. B., Claud, C., Genthon, C., Durán-Alarcón, C., Palerme, C., Berne, A., Souverijns, N., van Lipzig, N. P. M., Gorodetskaya, I. V., L'Ecuyer, T., and Wood, N. (2019). Evaluation of CloudSat snowfall rate profiles by a comparison with in-situ micro rain radars observations in East Antarctica, The Cryosphere, 13, 943-954.
- Vignon, E., O. Traullé and A. Berne, On the fine vertical structure of the low troposphere over the coastal margins of East Antarctica, Atmos. Chem. Phys., 19, 4659-4683, 2019, https://doi.org/10.5194/acp-19-4659-2019 (having used PES radio sounding data). .
- Souverijns, N., Gossart, A., Lhermitte, S., Gorodetskaya, I.V., Grazioli, J., Berne, A., Duran-Alarcon, C., Boudevillain, B., Genthon, C., Scarchili, C., van Lipzig, N.P.M. (2018), Evaluation of the CloudSat surface snowfall product over Antarctica using ground-based precipitation radars, The Cryosphere 12,3775-2018.
- Souverijns, N., Gossart, A., Gorodetskaya, I.V., Lhermitte, S., Mangold, A., Laffineur, Q., Delcloo, A., van Lipzig, N.P.M. (2018). How does the ice sheet surface mass balance relate to snowfall? Insights from a ground-based precipitation radar in East Antarctica. The Cryosphere 12, 1987-2003.
- Helmert, J., Lange, M., Dong, J., de Rosnay, P., Gustafsson, C., Churulin, E., Kurzeneva, E., Müller, R., Trentmann, J., Souverijns, N., Koch, R., Böhm, U., Bartik, M., Osuch, M., Rozinkina, I., Bettems, J. M., Samuelsson, P., Marcucci, F., Milelli, M. (2018). Workshop Report: 1st Snow Data Assimilation Workshop in the framework of COST HarmoSnow ESSEM 1404, Meteorologische Zeitschrift, 27, 325-333.
- Gossart, A., Souverijns, N., Gorodetskaya, I.V., Lhermitte, S.m Lenaerts, J.T.M., Schzeen, J.H., Mangold, A., Laffineur, Q. and van Lipzig, N.P.M. (2017). Blowing snow detection from ground-based remote sensing ceilometers: application to East Antarctica, The Cryosphere 11, 2755-2772.

- Souverijns, N., Gossart, A., Lhermitte, S., Gorodetskaya, I.V., Kneifel, S., Maahn, M., Bliven, F., van Lipzig, N.P.M. (2017). Estimating radar reflectivity - Snowfall rate relationships and their uncertainties over Antarctica by combining disdrometer and radar observations, Atmospheric Research, 196,211-223.
- Haeffelin, M., Laffineur, Q., Bravo-Aranda, J.-A., Drouin, M.-A., Casquero-Vera,J.-A., Dupont, J.-D., De Backer, H. (2016). Radiation fog formation alerts using attenuated backscatter power from automatic lidars and ceilometers, Atmospheric Measurement Techniques 9,5347-5365.
- Van Tricht, K., Lhermitte, S., Gorodetskaya, I.V and van Lipzig, N.P.M. (2016). Improving satellite-retrieved surface radiative fluxes in polar regions using a smart sampling approach. The Cryosphere 10, 2379-2397.
- Gorodetskaya, I.V., Kneifel,S., Maahn, M., Van Tricht, K., Thiery, W., Schween, J.H., Mangold, A., Crewell, S. and van Lipzig, N.P.M. (2015). Cloud and precipitation properties from ground-based remote sensing instruments in East Antarctica. The Cryosphere 9, 285-304.

6.2 Contributions to conference proceedings & national publications

Please refer to section 6.5 (Posters and presentations) for details.

6.3 Outreach to the scientific community

Please refer to section 5 (Valorisation and Dissemination) for details.

6.4 Outreach articles for the general public

- van Lipzig, N.P.M. (2016). Wolken over Antarctica. Koninklijke Vlaamse Academie van België, 11 February 2016.
- Mangold, A., Measurements of atmospheric particles in Antarctica: what even a low number of particles can tell us about the Antarctic atmosphere, Nanoparticles and air quality (talk in French), Seminar of TSI, JJBos for aerosol measurement stakeholders, 21 May 2019, Ottignies-Louvain-La-Neuve, Belgium
- Mangold, A., L'Antarctique, le pôle Sud et la Belgique, explaining to school children (8-9 and 10-11 years) of the Ecole Communale de Linkebeek (BE) what Antarctica is, why research is done there and what are the conditions for work and life, 26 June 2018, Linkebeek, Belgium
- Mangold, A., Antarctica and Climate – what it is about, Asgard IX, European Space Education Resource Office, weather balloon launch competition for schools, talk and discussion with students from international secondary schools, 25 April 2019 Uccle, Belgium.

6.5 Posters & presentations

6.5.1 Oral Presentations

- Hendrick, F., M. Friedrich, A. Mangold, A. Gossart, C. Hermans, C. Fayt, Q. Laffineur, H. De Backer, N. Souverijns, N. Van Lipzig, and M. Van Roozendael, MAX-DOAS measurements of aerosol vertical distribution at PES as part of the AEROCLOUD project, Antarctic Climate Symposium, Brussels, Belgium, 10 May 2019.
- Gossart, A., Souverijns, N., van Kampenhout, L., Amory, C., van Lipzig, N.P.M. and Lenaerts, J.T.M. (2019), Towards blue ice representation in COSMO-CLM^2, European Geophysics Union Assembly 2019, Vienna, 08-12 April 2019.
- Gossart, A., Souverijns, N., Demuzere, M., Lenaerts, J.T.M., Medley, B., Vanden Broucke, S. and van Lipzig, N.P.M. (2018) , A Long-term Hindcast Simulation with COSMO-CLM² over Antarctica, Polar 2018, Warsaw, Poland, 17-19 October 2018.
- Gossart, A., Souverijns, N., Gorodetskaya, I.V., Lhermitte, S., Lenaerts, J.T.M., Palm, S.P., and van Lipzig, N.P.M. (2018), An New Algorithm to Detect Blowing Snow from Ceilometers in East Antarctica, SCAR/IASC Open Science Conference, Davos, Switzerland, 19-23 June 2018.
- Gossart, A., Souverijns, N., Gorodetskaya, I.V., Demuzere, M., Lenaerts, J.T.M., and van Lipzig, N.P.M (2018), A Long-term Hindcast Simulation with COSMO-CLM² over Antarctica, Polar 2018, SCAR/IASC Open Science Conference, Davos, Switzerland, 19-23 June 2018.
- Mangold, A., Laffineur, Q., Delcloo, A., Heremans, C., Hendrick, F., Gossart, A., Souverijns, N., Herenz, P., Wex, H., van Lipzig, N.P.M., De Backer, H. (2018), Aerosol variability linked to clouds and precipitation in the Sor Rondane area, Polar 2018, SCAR/IASC Open Science Conference, Davos, Switzerland, 19-23 June 2018.
- Souverijns, N., Gossart, A., Lhermitte, S., Gorodetskaya, I.V., Crewell, S., Mech, M., Grazioli, J., Berne, A., Duran-Alarcon, C., Boudevillain, B., Genthon, C., Scarchilli, C., and van Lipzig, N.P.M. (2018), A High-resolution Climatological Snowfall Map for Antarctica, Polar 2018, SCAR/IASC Open Science Conference, Davos, Switzerland, 19-23 June 2018.
- P. Herenz, H. Wex, A. Mangold, Q. Laffineur, I. V. Gorodestkaya, Z. L. Fleming, M. Panagi and F. Stratmann, Aerosol and CCN Properties and Sources in East Antarctica during Austral Summer, POLAR2018, SCAR/IASC Open Science Conference, Davos, Switzerland, 19-23 June 2018.
- Souverijns, N., Gossart, A., Lhermitte, S., Gorodetskaya, I., Kneifel, S., Maahn, M., Bliven, F., Mangold, A., Laffineur, Q., Delcloo, A., Van Lipzig, N. (2018). Snowfall retrieval and its relation with the Antarctic Surface Mass Balance. European Geosciences Union General Assembly, Vienna, Austria, 9-13 April 2018.
- Gossart, A., Souverijns, N., Gorodetskaya, I.V., Demuzere, M., Lenaerts, J.T.M., and van Lipzig, N.P.M. (2018). A long-term hindcast simulation with COSMO-CLM² over Antarctica, CESM winter meetings, Boulder, Colorado, USA, 10-12 January 01/2018.

- Gossart, A., Souverijns, N., Gorodetskaya, I.V., Demuzere, M., Lenaerts, J.T.M., and van Lipzig, N.P.M. (2017). A long-term hindcast simulation with COSMO-CLM² over Antarctica, Belgian Geography Days, Liege, Belgium, 17 November 2017.
- Souverijns, N., Gossart, A., Lhermitte, S., Demuzere, M., Lenaerts, J., Van Lipzig, N. (2017). A Long-term Hindcast simulation with COSMO-CLM2 over Antarctica. POLAR CORDEX Meeting, Cambridge, United Kingdom, 18-20 October 2017.
- Gossart, A., Souverijns, N., Lhermitte, S., Gorodetskaya, I.V., Demuzere, M., van Lipzig, N.P.M. (2017) A long-term hindcast simulation with COSMO-CLM^2 over Antarctica, COSMO Assembly, Graz, 19-22 September 2017.
- Gossart, A., Souverijns, N., Gorodetskaya, I., Lhermitte, S., Lenaerts, J.T.M., Schween, J.H., van Lipzig, N.P.M. (2017) A new algorithm to detect blowing snow from ground-based remote sensing ceilometer observations in Dronning Maud Land, East Antarctica, 74th Eastern Snow Conference, Ottawa, 6-8 June 2017.
- Souverijns, N., Gossart, A., Lhermitte, S., Gorodetskaya, I.V., Grazioli, J., Berne, A., Duran-Alarcon, C., Genthon, C., van Lipzig, N.P.M. (2017) Precipitatiom over Antarctica: First evaluation of Cloudsat snowfall rates and properties by ground-based remote sensing (Micro-Rain-Radar), 74th Eastern Snow Conference, Ottawa, 06-08 June 2017.
- Mangold, A., Laffineur, Q., De Backer, H., Delcloo, A., Herenz, P., Wex, H., Gossart, A., Souverijns, N., Gorodetskaya, I.V., van Lipzig, N.P.M. (2017). CCN and aerosol properties at Princess Elisabeth station, East Antarctica, combined with cloud and precipitation observations and air mass origin, EGU, Vienna, Austria, 23-28 April 2017.
- Mangold, A., Aerosol-cloud-precipitation interaction at Princess Elisabeth station in the perspective of climate research, Conference of the Belgian National Committee for Geodesy and Geophysics, 12 May 2017, Brussels, Belgium.
- van Lipzig, N.P.M. (2016). Long-term evaluation of regional models. Workshop on applications of satellite climate data records in numerical modeling. European Centre for Medium-Range Weather Forecasts (ECMWF), Reading, 15 – 17 November 2016. (invited)
- van Lipzig, N.P.M., Thiery, W. (2016). Remote sensing from space for climate research. Space Expo, Brussels, 19 October 2016.
- van Lipzig, N.P.M. (2016). Why climate science needs high-performance computing: Demonstrations, prospects and challenges. HPC Tier-1 inauguration, KU Leuven, 17 October 2016.
- Souverijns, N., Gossart, A., Demuzere, M., Lhermitte, S., Gorodetskaya, I., van Lipzig, N.P.M., Evaluation of a default COSMO-CLM² simulation over Antarctica with a focus on accumulation and the surface mass balance. Cosmo Assembly, Lüneberg, 20-23 September 2016.
- Mangold, A., De Bock, V., De Backer, H., Gielen, C., Hermans, C., Ozone, UV and aerosol optical depth derived from Brewer spectrophotometer observations at Princess Elisabeth Station, East Antarctica. Brewer Ozone Spectrophotometer and Metrology

Open Workshop, 15th Biennal WMO-GAW Brewer Users Group Meeting, Sao Miguel, Portugal, 17 – 20 May 2016.

- Gossart, A., Souverijns, N., Lhermitte, S., Gorodetskaya, I.V., Lenaerts, J.T.M., Mangold, A., Laffineur, Q., Palm, S.P., van Lipzig, N.P.M. , Remote sensing retrieval of drifting/blowing snow events: a comparison between satellite and ground-based observations at Princess Elisabeth station, East Antarctica, BNCAR/BNCGG symposium, Unlocking a continent: scientific research at the Belgian Princess Elisabeth station, Antarctica, Brussels, 29 April 2016.
- van Lipzig, N.P.M., De Backer, H., Van Roozendael, M., Souverijns, N., Gossart, A., Gorodetskaya, I.V., Lhermitte, S., Mangold, A., Laffineur, Q., Gielen, C., Hendrick, F., Hermans, C. (2016). The AEROCLOUD project: How do aerosols and clouds affect the East Antarctic climate? BNCGG-BNCAR Antarctica Symposium: Unlocking a continent: scientific research at the Belgian Princess Elisabeth Station, Antarctica, Brussels, 29 April 2016.
- Gorodetskaya, I.V., Gallée, H., Lenaerts, J.T.M., Maahn, M., Kneifel, S., Van Tricht, K., Schween, J.H., van den Broeke, M.R., Crewell, S. And N.P.M. Van Lipzig (2015) Cloud and precipitation properties in East Antarctica: ground-based remote sensing and regional climate models, International Union of Geodesy and Geophysics 26th General Assembly (22/06– 02/07/2015), Prague, Czech Republic.

6.5.2 Posters

- Souverijns, N., A. Gossart, A. Mangold, Q. Laffineur, P. Herenz, H. Wex, I.V. Gorodetskaya, G. Eirund, A. Possner and N.P.M. Van Lipzig, The impact of aerosols on clouds in the pristine environment of East Antarctica, European Geosciences Union General Assembly 2019, Geophysical Research Abstracts, Vol. 21, EGU2019-9838, 7-12 April 2019, Vienna, Austria, 2019.
- Mangold, A., Laffineur, Q., Van Malderen, R. Heremans, C., Nys, K., Verbruggen, M., De Backer, H. (2018) UV and radio sounding measurements in the Sor Rondane mountains, Polar 2018, SCAR/IASC Open Science Conference, Davos, Switzerland, 19-23 June 2018.
- Souverijns, S., Gossart, A., Lhermitte, S., Gorodetskaya, I.V., Kneifel, S., Maahn, M., Bliven, F.L., Mangold, A., Laffineur, Q., Delcloo, A., and van Lipzig, N.P.M. (2018) Snowfall Rate Retrieval and its Relation with the Antarctic Surface Mass Balance, Polar 2018, SCAR/IASC Open Science Conference, Davos, Switzerland, 19-23 June 2018.
- Gossart, A., Souverijns, N., Demuzere, M., Vanden Broeke, S., van Lipzig, N.P.M. (2018) HPC for climate modelling over Antarctica, VSC User day, Brussels, 22 April 2018.
- Souverijns, N., Gossart, A., Lhermitte, S., Gorodetskaya, I., Crewell, S., Mech, M., Grazioli, J., Berne, A., Duran-Alarcon, C., Boudevillain, B., Genthon, C., Scarchilli, C., Van Lipzig, N. (2018). An evaluation of the CloudSat snowfall climatology over Antarctica. European Geosciences Union General Assembly, Vienna, Austria, 09-13 April 2018.

- Souverijns, N., Gossart, A., Gorodetskaya, I., Demuzere, M., Lenaerts, J., Van Lipzig, N. (2018). Evaluation of a long-term hindcast simulation with COSMO-CLM^2 over Antarctica. ICCARUS. Offenbach, Germany, 26-28/02/2018.
- Gossart, A., Souverijns, N., Gorodetskaya, I.V., Lhermitte, S., Demuzere, M., van Lipzig, N.P.M. (2017) A long-term hindcast simulation with COSLO-CLM2 over Antarctica, Swiss Climate Summer School, Ascona, 03-08 September 2017.
- Mangold, A., Laffineur, Q., De Backer, H., De Bock, V., Delcloo, A., Hermans, C., Gielen, C., Herenz, P., Wex, H., Atmospheric aerosol and CCN properties in Dronning Maud Land, East Antarctica, European Aerosol Conference 2017, Zurich, Switzerland, 27 August - 01 September 2017. Abstract T205N2a2.
- Herenz, P., Wex, H., Mangold, A., Stratmann, F. (2017) CCN measurements at the Princess Elisabeth Antarctica Research station, 20th International Conference on Nucleation and Atmosphere Aerosold, Helsinki, Finland, 25-30 June 2017.
- Gossart, A., Souverijns, N., Demuzere, M., van Lipzig, N.P.M. (2017) Assessing the surface mass balance of the Antarctic Ice Sheet using a regional climate model, VSC User day, Brussels, 03 June 2017.
- Souverijns, N., Gossart, A., Lhermitte, S., Gorodetskaya, I., Kneifel, S., Maahn, M., Bliven, F., Van Lipzig, N. (2017). Estimating radar reflectivity - snowfall rate relationships and their uncertainties over Antarctica by combining disdrometer and radar observations. EGU, Vienna, Austria, 23-28 April 2017.
- Souverijns, N., Gossart, A., Gorodetskaya, I., Lhermitte, S., Demuzere, M., Wouters, H., Van Lipzig, N. (2017). Adapting COSMO-CLM^2 for Antarctic climate representation. COSMO User Seminar, Offenbach, Germany, 6-8 March 2017.
- Herenz,P., Mangold, A., Wex, H., Stratmann, F. (2016) CCN measurements at the Princess Elisabeth Antarctica Research Station, 17th international Conference on clouds and precipitations, Manchester, 25-29 July 2016.
- Gossart, A., Lhermitte, S., Gorodetskaya, I.V., Lenaerts, J.T.M. and van Lipzig, N.P.M, 2016. The importance of wind on East Antarctic ice shelf stability. Meltwater retention workshop, Copenhagen, June 2016.
- Gossart, A., Souverijns, N., Lhermitte, S., Gorodetskaya, I.V., Lenaerts, J.T.M., Mangold, A., Laffineur, Q., Palm, S.P., van Lipzig, N.P.M. (2016) Snowdrift events detection : a comparison of satellite imagery with ground-based remote sensing observations at Princess Elisabeth station, East Antarctica, European Geosciences Union General Assembly, Vienna, 17-22 April 2016.
- Mangold, A., Laffineur, Q., De Backer, H., Herenz, P., Wex, H., Gossart, A., Souverijns, N., Gorodetskaya, I., van Lipzig, N.P.M. (2016). Aerosol and CCN properties at Princess Elisabeth station, East Antarctica: seasonality, new particle formation events and properties around precipitation events, European Geosciences Union General Assembly, Vienna 17-22 April 2016.
- Souverijns, N., Gossart, A., Gorodetskaya, I., Lhermitte, S., Mangold, A., Laffineur, Q., van Lipzig, N. (2016). Climatology of clouds and precipitation over East Antarctica using

ground-based remote sensing at the Princess Elizabeth station. European Geosciences Union General Assembly, Vienna, 17-22 April 2016.

- Mangold, A., Laffineur, Q., De Bock, V., Hermans, C., Gielen, C., Gorodetskaya, I.V., Herenz, P., Wex, H., Verhasselt, K., Oosterbos, S., Kuppens, S., De Backer, H. (2016). Atmospheric aerosol characterisation at Princess Elisabeth station, East Antarctica. BNCGG-BNCAR Symposium, Unlocking a continent: scientific research at the Belgian Princess Elisabeth Station, Antarctica, Brussels, 29 April 2016.
- Gielen, C., M. Van Roozendael, C. Hermans, F. Hendrick, C. Fayt, H. De Backer, A. Mangold, V. De Bock, Q. Laffineur, N. Van Lipzig, N. Souverijns, I. Gorodetskaya, S. Lhermitte, and A. Gossart, Poster presentation at Aerosol and ozone measurements from the recently installed MAX-DOAS instrument at the Princess Elisabeth station in the framework of the AEROCLOUD project, BNCAR/BNCGG symposium, Unlocking a continent: scientific research at the Belgian Princess Elisabeth station, Antarctica, Brussels, 29 April 2016.
- Gossart, A.,Souverijns, N., Lhermitte, S., Gorodetskaya, I.V., Lenaerts, J.T.M., Mangold, A., Laffineur, Q. and van Lipzig, N.P.M. (2016) - Snowdrift and blowing snow in East Antarctica; Preliminary observations towards modelisation in COSMO-CLM, Cosmo Users Seminar, Offenbach, 7-8 March 2016.
- Souverijns, N., Gossart, A., Gorodetskaya, I., Lhermitte, S., Mangold, A., Laffineur, Q., van Lipzig, N. (2016). Radiation, clouds and precipitation at Princess Elisabeth, Antarctica. COSMO User Seminar, Offenbach, 7-9 March 2016.
- Gorodetskaya, I.V., Souverijns, N., Ferrone, A., Trusilova, K., Van Lipzig, N. (2015). Atmospheric rivers and anomalous snow accumulation in East Antarctica: case study using regional climate model COSMO-CLM². COSMO Assembly , Esch-Sur-Alzette, Luxemburg, 29 September - 02 November 2015.
- Mangold, A., De Backer, H., De Bock, V., Delcloo, A., Hermans, C., Gorodetskaya, I., Herenz, P., Henning, S. and H. Wex, Atmospheric aerosol properties at Princess Elisabeth station, East Antarctica,: seasonality and indication of new particle formation, European Aerosol Conference 2015, Milan, Italy, 06-11 September 2015.

7. ACKNOWLEDGEMENTS

We would like to acknowledge very much the support of the Belgian Science Policy Office (BELSPO) which funded this research under several grants: BR/143/A2/AEROCLOUD, EA/34/1A, EA/34/1B, EA/01/04A, EA/01/04B. In particular we thank very much Maaike Vancauwenberghe for her steady support of Antarctic research. We thank Research Foundation – Flanders (FWO) for supporting a parallel project (G.0C22.15). We thank Clio Gielen for her exploratory work on MAXDOAS aerosol retrieval at PES. We thank Wim Boot, Carleen Reijmer, and Michiel van den Broeke (Utrecht University, Institute for Marine and Atmospheric Research Utrecht) for the development of the automatic weather station, technical support and raw data processing. Jan Lenaerts is acknowledged for sharing the data from the RACMO2.3 high-resolution simulation. We thank Susanne Crewell, Irina Gorodetskaya and Stef Lhermitte for their collaboration and their input in designing the project. The supervisory committee (Michiel van den Broeke, Dr. Jan Lenaerts, Susanne Crewell, Murray Hamilton, Carine Bruyninx, Eric Pottiaux, Frank Pattyn, Tom Lachlan-Cope, Annick Wilmotte, Willy Maenhaut, Rolf Weller, Hubert Gallée, Xavier Fettweis) are warmly thanked for their continuous advise. The CCN data analyses were supported by BACCHUS, an EU FP7 research project. In this respect we are grateful for our colleagues of the Leibniz Institute for Tropospheric Research, TROPOS, Leipzig, Germany, for providing their CCNc and the respective expertise, namely Heike Wex, Paul Herenz, Silvia Henning and Frank Stratmann. We acknowledge very much the support of the respective operators of Princess Elisabeth station: the International Polar Foundation during seasons 2014/15, 2017/18, 2018/19) and AntarctiQ (season 2015/16). We thank especially the respective science liasion officers Johnny Gaelens, Koen Verschraegen and Benoit Verdin. The implementation of the radio soundings were also supported by the Swiss Institute for Forest, Snow and Landscape research (WSL). Further we thank all the logistic support we received from our colleagues at the institutes.

8. REFERENCES

- Agosta, C., Favier, V., Genthon, C., Gallée, H. Krinner, G., Lenaerts, J.T.M., van den Broeke, M.R. (2012). A 40-year accumulation dataset for Adelie Land, Antarctica and its application for model validation. Climate Dynamics 38, 75-86.
- Agosta, C. et al. (2019). Estimation of the Antarctic surface mass balance using the regional climate model MAR (1979-2015) and identification of dominant processes. The Cryopshere 13, 281-296.
- Amory, C., Trouviliez, A., Gallée, H., Favier, V., Naaim-Bouvet, F., Genthon, C., Agosta, C., Picard, L., Bellot, H. (2015). Comparison between observed and simulatied aeolian snow mass fluxes in Adélie Land, East Antarctica. The Cryosphere 9, 1373-1383.
- Anderson, P.S. (1994). A method for rescaling humidity sensors at temperatures well below freezing. Journal of Atmospheric and Oceanic Technology 11, 1388-1391.
- Asmi, E. et al., Hygroscopicity and chemical composition of Antarctic sub-micrometre aerosol particles and observations of new particle formation, Atmos. Chem. Phys., 10, 4253-4271, https:/doi.org/10.5194/acp-10-4253-2010, 2010.
- Bagnold, R.A. (1954). The Physics of Blown Sand and Desert Dunes. Mathuen. London, 256 pp.
- Barral, H., Genthon, C., Trouviliez, A., Brun, C., Amory, C. (2014). Blowing snow in coastal Adélie Land, Antarctica: three atmospheric-moisture issues. The Cryosphere 8, 1905-1919.
- Bennartz, R., Shupe, M.D., Turner, D.D., Walden, V.P., Steffen, K., Cox, C.J., Kulie, K.S., Miller, N.B., Pettersen, C. (2013). July 2012 Greenland melt extent enhanced by low-level liquid clouds. Nature 496, 83-86.
- Bintanja R., van den Broucke, M.R. (1995). The Surface Energy Balance of Antarctic Snow and Blue Ice. Jouranl of Applied Meteorology 34, 902-926.
- Brandes, E.A., Ikeda, K., Zhang, G., Schönhuber, M., Rasmussen, R.M. (2007). A statistical and physical description of hydrometeor distributions in Colorado snowstorms using a video disdrometer. Journal of Applied Meteorology and Climatology 46, 634-650.
- Bromwich, D.H. (1988). Snowfall in high lsouthern latitudes. Review of Geophysics 26, 149-168.
- Bromwich, D.H., Nicolas, J.P., Hines, K.M., Kay, J.E., Key, E.L., Lazzara, M.A., Libn, D., McFarquhar, G.M., Gorodetskaya, I.V., Grosvenor, D.P., Lachlan-Cope, T., van Lipzig, N.P.M. (2012). Tropospheric clouds in Antarctica. Reviews of Geophysics 50, RG1004.
- Bromwich, D.H., Nicolas, J.P., Monaghan, A.J., Lazzara, M.A., Keller, L.M., Weidner, G.A., Wilson, A.B. (2013). Central West Antarctica among the most rapidly warming regions on Earth. Nature Geoscience 6, 139-145.
- Budd, W.F., Dingle, W.R.J., Radok, U. (1966) The Byrd snow drift project : outline and basic results. In: Studies in Antarctic Meteorology. Antarctic Research Services 9. Edited by: Rubin, M.J. AGU, Washington, D.C., 71-134.
- Carslaw, K.S., et al., Large contribution of natural aerosol to uncertainty in indirect forcing, Nature, 503, 67-71, 2013.

- Cesana, G., Kay, J.E., Chepfer, H., English, J.M., de Boer, G. (2012). Ubiquitous low-level liquid-containing Arctic clouds: new observations and climate model constraints from CALIPSO-GOCCP. Geophysical Research Letters 39, L20804.
- Dai, X., Huang, N. (2014). Numerical simulation of drifting snow sublimation in the saltation layer. Science Reports UK 4, 1-5.
- Dall'Osto,M. et al., Antarctic sea ice region as a source of biogenic organic nitrogen in aerosols, Sci. Rep. 7, 6047, https://doi.org/10.1038/s41598-017-06188-x, 2017.
- DeFelice, T., V. Saxena and S. Yu, On the measurements of cloud condensation nuclei at Palmer station, Antarctica, Atmos. Environ., 31, 4039-4044, 1997.
- Déry, S.J., Tremblay, L.B. (2004). Modelling the effects of wind redistribution on the snow mass budget of polar sea ice. Jouranl of Physical Oceanography 34, 258-271.
- Déry, S.J., Yau, M.K. (2002). Large-scale mass balance effects of blowing snow and surface sublimation. Journal of Geophysical Research 107, D23, 4679.
- Dong, X., Xi, B., Minnis, P. (2006). A Climatology of midlatitude continental clouds from the ARM SGP central facility, Part II: Cloud fraction and surface radiative forcing. Journal of Climate 19, 1765-1783.
- Enserink, M., Science suffers in cold war over polar base, Science, 2017, https:/doi.org/10.1126/science.aal0623.
- Favier, V., Agosta, C., Parouty, S., Durand, G., Delaygue, G., Gallée, H., Drouet, A.-S., Trouvilliez, A., Krinner, G. (2013). An updated and quality controlled surface mass balance dataset for Antarctica. The Cryosphere 7, 583-597.
- Fiebig, M., D. Hirdman, C.R. Lunder, J.A. Ogren, S. Solberg, A. Stohl and R.L. Thompson, Annual cycle of Antarctic baseline aerosol: controlled by photooxidation-limited aerosol formation, Atmos. Chem. Phys., 14, 3083-3093, https://doi.org/10.5194/acp-14-3083-2014, 2014.
- Fleming, Z.L., P.S. Monks and A.J. Manning, Review: Untangling the influence of air-mass history in interpreting observed atmospheric composition, Atmos. Res., 104-105, 1-39, https://doi.org/10.1016/j.atmosres.2011.09.009, 2012.
- Frezzotti, M., Pourchet, M., Flora, O., Gandolfi, S., Gay, M., Urbini, S., Vincent, C., Becagli, S., Gragnani, R., Proposito, M., Severi, M., Traversi, R., Udisti, R., Fily, M. (2004). New estimations of precipitation and surface sublimation in East Antarctica from snow accumulation measurements. Climate Dynamics 23, 803-813.
- Friedrich, M. M., Rivera, C., Stremme, W., Ojeda, Z., Arellano, J., Bezanilla, A., García-Reynoso, J. A., and Grutter, M.: NO_2 vertical profiles and column densities from MAX-DOAS measurements in Mexico City, Atmos. Meas. Tech., 12, 2545-2565, https://doi.org/10.5194/amt-12-2545-2019, 2019.
- Frieß, U., Beirle, S., Alvarado Bonilla, L., Bösch, T., Friedrich, M. M., Hendrick, F., Piters, A., Richter, A., van Roozendael, M., Rozanov, V. V., Spinei, E., Tirpitz, J.-L., Vlemmix, T., Wagner, T., and Wang, Y.: Intercomparison of MAX-DOAS vertical profile retrieval algorithms: studies using synthetic data, Atmos. Meas. Tech., 12, 2155-2181, https://doi.org/10.5194/amt-12-2155-2019, 2019.

- Gallée, H., et al. (2015). Characterisation of the boundary layer at Dome C (East Antarctica) during the OPALE summer campaign. Atmospheric Chemistry and Physics 15, 6225-6236.
- Gallée, H., Guyomarc'h G., an Brun, E. (2001). Impact of snow drift on the Antarctic ice sheet surface mass balance: possible sensitivity to snow-surface properties. Boundary Layer Meteorology 99, 1-19.
- Giles, D. M., Sinyuk, A., Sorokin, M. G., Schafer, J. S., Smirnov, A., Slutsker, I., Eck, T. F., Holben, B. N., Lewis, J. R., Campbell, J. R., Welton, E. J., Korkin, S. V., and Lyapustin, A. I.: Advancements in the Aerosol Robotic Network (AERONET) Version 3 database – automated near-real-time quality control algorithm with improved cloud screening for Sun photometer aerosol optical depth (AOD) measurements, Atmos. Meas. Tech., 12, 169-209, https://doi.org/10.5194/amt-12-169-2019, 2019.
- Giorgi, F., Gutowski, W.J. (2015). Regional dynamical downscaling and the CORDEX initiative. Annual Review of Environment and Resources 40, 467-490.
- Giorgi, F., Gutowski, W.J. (2016). Coordinated Experiments for Projections of Regional Climate Change. Current Climate Change Reports 2, 202-210.
- Girard, E., Blanchet, J.P. (2001). Simulation of Arctic diamond dust, ice fog, and thin stratus using an explicit aerosol-cloud-radiation model. Journal of the Atmospheric Sciences 58, 1199-1221.
- Gonzales-Toril, E.R. et al., Bacterial diversity of autotrophic enriched cultures from remote, glacial Antarctica, Alpine and Andean aerosol, snow and soil samples, Biogeosciences, 6, 33-44, 2009.
- Gorodetskaya, I.V., van Lipzig, N.P.M., Boot, W., Reijmer, C., van den Broeke, M.R. (2011). AWS measurements at the Belgian Antarctic station Princess Elisabeth, in Dronning Maud Land, for precipitation and surface mass balance studies. Workshop on Automatic weather stations on glaciers 40-44.
- Gorodetskaya, I.V., van Lipzig, N.P.M., van den Broeke, M.R., Mangold, A., Boot, W., Reijmer, C.H. (2013). Meteorological regimes and accumulation patterns at Utsteinen, Dronning Maud Land, East Antarctica: analysis of two contrasting years. Journal of Geophysical Research: Atmospheres 118, 1700-1715.
- Gorodetskaya, I.V., Tsukernik, M., Claes, K., Ralph, M.F., Neff, W.D., van Lipzig, N.P.M. (2014). The role of atmospheric rivers in anomalous snow accumulation in East Antarctica. Geophysical Research Letters 16, 6199-6206.
- Gorodetskaya, I.V., Kneifel, S., Maahn, M. Van Tricht, K., Thiery, W., Schween, J.H., Mangold, A., Crewell, S., and van Lipzig, N.P.M. (2015). Cloud and precipitation properties from ground-based remote sensing instruments in East Antarctica. The Cryosphere, 9, 285-304.
- Gossart, A., Souverijns, N., Gorodetskaya, I.V., Lhermitte, S., Lenaerts, J.T.M., Schween J.H., Mangold, A., Laffineur, Q., van Lipzig, N.P.M. (2017). A new algorithm to detect blowing snow from ground-based remote sensing ceilometer observations in Dronning Maud Land, East Antarctica. The Cryosphere 11, 2755-2772.

- Grenier, P., Blanchet, J.P., Munoz-Alpizar, R. (2009). Study of polar thin ice clouds and aerosols seen by CloudSat and CALIPSO during midwinter 2007. Journal of Geophysical Research, 114, D09201.
- Groot-Zwaaftink, C.D., Cagnati, A., Crepaz, A., Fierz, C., Macelloni, G., Valt, M., Lehning, M. (2013). Event-driven deposition of snow on the Antarctic plateau: analyzing field measurements with SNOWPACK. The Cryosphere 7, 333-347.
- Gysel, M. and F. Stratmann, WP3-NA3: In-situ chemical, physical and optical properties of aerosols, Deliverable D3.11: Standardized protocol for CCN measurement, Tech. Rep., http://www. actris.net, 2013.
- Hamilton, D.S., L.A. Lee, K.J. Pringle, C.L. Reddington, D.V. Spracklen and K.S. Carslaw, Occurrence of pristine aerosol environment on a polluted planet, Procced. Natl. Acad. Sci. USA, 111, 18466-18471, https://doi.org/10.1073/pnas.1415440111, 2014.
- Herenz, P., Wex, H., Mangold, A., Laffineur, Q., Gorodetskaya, I.V., Fleming, Z.L., Panagi, M., Stratmann, F. (2019). CCN measurements at the Princess Elisabeth Antarctica Research station during three austral summers, Atmospheric Chemistry and Physics 19, 275-294.
- Hoose, C. and O. Möhler, Heterogeneous ice nucleation on atmospheric aerosols: a review of results from laboratory experiments, Atmos. Chem. Phys., 12, 9817-9854, https://doi.org/10.5194/acp-12-9817-2012, 2012.
- Jones, A. D. Thompson, M. Hort and B. Devenish, The U.K. Met Office's Next Generation Atmospheric Dispersion Model, NAME III, Springer US, Boston, MA, 580-589, https://doi.org/10.1007/978-0-387-68854-1_62, 2007.
- Kajikawa, M. (1972). Measurement of falling velocity of individual snow crystals. Journal of the Meteorological Society of Japan, Series II 50, 577-584.
- Kim, J., Y.I. Yoon, Y. Gim, H.J. Kang, J.H. Choi, K.-T. Park and B.Y. Lee, Seasonal variations in physical characteristics of aerosol particles at the King Sejong Station, Antarctic Peninsula, Atmos. Chem. Phys., 17, 12985-12999, https://doi.org/10.5194/acp-17-12985-2017, 2017.
- Kneifel, S., von Lerber, A., Tiira, J., Moisseev, D., Kollias, P., Leinonen, J. (2015). Observed relations between snowfall microphysics and triple-frequency radar measurements. Journal of Geophysical Research: Atmospheres 120, 6034-6055.
- Kneifel, S., Kollias, P., Barraglia, A., Leinonen, J., Maahn, M., Kalesse, H., Tridon, F. (2016). First observations of triple frequency radar droppler spectra in snowfall: interpreation and applications. Geophysical Research Letters 43, 2225-2233.
- Kodama, Y., Wendlern G., Gowink, J. (1985). The effect of blowing snow on katabatic winds in Antarctica. Annals of Glaciology 6, 59-62.
- Koponen, I.K., A. Virkkula, R. Hillamo, V.M. Kerminen and M. Kulmala, Number size distribution and concentrations of the continental summer aerosol in Queen Maud Land, Antarctica, J. Geeophys: Res., 108, 4587, https:/doi.org/10.1029/2003jd003614, 2003.
- Korolev, A. (2007). Limitations of the Wegener-Bergeron-Findeisen mechanism in the evolution of mixed-phase clouds. Journal of Atmospheric Sciences 64, 3372-3375.

- Kuipers Munneke, P., Reijmer, C.H., van den Broeke, M.R. (2011). Assessing the retrieval of cloud properties from radiation measurements over snow and ice. International Journal of Climatology 31, 756-769.
- Kyrö, E. et al., Antarctic new particle formation from continental biogenic precursors, Atmos. Chem. Phys., 13, 3527-3546, https:/doi.org/10.5194/acp-13-3527-2013, 2013.
- Li, L., Pomeroy, J.W. (1988). estimates of threshold wind speeds for snow transport using meteorological data. Jouranle of Applied Meteorology 36, 205-213.
- Lachlan-Cope, T. (2010). Antarctic clouds. Polar Research 29, 150-158.
- Lachlan-Cope, T., Listowski, C., O'Shea, S. (2016). The microphysics of clouds over the Antarctic Peninsula – part 1: observations. Atmospheric Chemistry and Physics 16, 15605-15617.
- Lenaerts, J.T.M., van den Broeke, M.R., Déry, S.J., König-Langlo, G., Ettema, J., Kuipers Munneke, P. (2010). Modelling snowdrift sublimation on an Antarctic ice shelf. The Cryosphere 4, 179-190.
- Lenearts, J.T.M., van den Broeke, M.R. (2012). Modeling drifting snow in Antarctica with a regional climate model: 2. Results. Journal of Geophysical Research 117, D05109.
- Lenaerts, J.T.M. et al. (2017). Meltwater produced by wind-albedo interaction stored in an East Antarctic ice shelf. Nature Climate Change 7, 58-62.
- Lenaerts, J.T.M. et al. (2018). Climate and surface mass balance of coastal West Antarctica resolved by regional climate modelling. Annals of Glaciology 59, 29-41.
- Leonard, K.C., Tremblay, L.B., Thorn, J.E., and MacAyeal, D.R. (2014). Drifting snow measurements near McMurdo station, Antarctica: a sensor comparison study. Cold Regions Sciences and Technology 70, 71-80.
- Ligtenberg, S.R.M., van de Berg, W.J., van den Broeke, M.R., Rai, J.G.L., van Meijgaard, E. (2013). Future surface mass balance of the Antarctic ice sheet and its influence on sea level change, simulated by a regional atmospheric climate model. Climate Dynamic 41, 867-884.
- Listowski, C., Lachlan-Cope, T. (2017). The microphysics of clouds over the Antarctic Peninsula – Part 2: modelling aspects within Polar WRF. Atmospheric Chemistry and Physics 17, 10195-10221.
- Maahn, M., Burgard, C., Crewell, S., Gorodetskaya, I.V., Kneifel, S., Lhermitte, S., Van Tricht, K., van Lipzig, N.P.M. (2014). How does the spaceborne radar blind zone affect derived surface snowfall statistics in polar regions? Journal of Geophysical Research: Atmospheres 119, 13604-13620.
- Mahesh, A., Walden , V.P., Warren, S.P. (2001). Ground-based infrared remote sensing of cloud properties over the Antarctic Plateau. Part I: cloud-base heights. Journal of Applied Meteorology 40, 1265-1278.
- Mahesh, A., Walden , V.P., Warren, S.P. (2001). Ground-based infrared remote sensing of cloud properties over the Antarctic Plateau. Part II: cloud optical depths and particle sizes. Journal of Applied Meteorology 40, 1279-1294.
- Mahesh, A., Campbell, J.R., Spinhirne, J.D. (2005). Multi-year measurements of cloud base heights at South Pole by lidar. Geophysical Research Letters 32, L09812.

- Matus, A.V., L'Ecuyer, T.S. (2017). The role of cloud phase in Earth's radiation budget. Journal of Geophysical Research: Atmospheres 122, 2559-2578.
- Medley, B., Thomas, E.R. (2019). Increased snowfall over the Antarctic Ice Sheet mitigated twentieth-centry sea level rise. Nature Climate Change 9,34-39.
- Mellor, M. (1965). Blowing Snow, Cold Regions Science and Engineering Part II. Cold Regions Research and Enigineering lab. Hanover nh. Section A3c, 78pp.
- O'Shea, S.J. et al., In situ measurements of cloud microphysics and aerosol over coastal Antarctica during the MAC campaign, Atmos. Chem. Phys., 17, 13049-13070, https://doi.org/acp-17-13049-2017, 2017.
- Palerme, C., Kay, J.E., Genthon, C., L'Ecuyer, T.L., Wood, N.B., Claud, C. (2014). How much snow falls on the Antarctic ice sheet? The Cryosphere 8, 1577-1587.
- Palm, S.P., Kayetha, V., Yang, Y., Pauly, R. (2017). Blowing snow sublimation and transport over Antarctica drom 11 years of CALIPSO observations. The Cryosphere 11, 2555-2569.
- Palm, S.P., Yang, Y., Spirnhirne, J.D., Marshak, A. (2011) Satellite remote sensing of blowing snow properties over Antarctica. Journal of Geophysical Research 116, D16123.
- Pattyn, F., et al. (2018). The Greenland and Antarctic ice sheets under 1.5°C global warming. Nature Climate Change 8, 1053-1061.
- Petters, M.D. and S.M. Kreidenweis, A single parameter representation of hygroscopic growth and cloud condensation nucleus activity, Atmos. Chem. Phys., 7, 1961-1971, https:/doi.org/10.5194/acp-7-1961-2007, 2007.
- Pringle, K.J., H. Tost, A. Pozzer, U. Pöschl and J. Lelieveld, Global distribution of the effective aerosol hygroscopicity parameter for CCN activation, Atmos. Chem. Phys., 10, 5241-5255, https://doi.org/10.5194/acp-10-5241-2010, 2010.
- Possner, A., Ekman, A.M.L., Lohmann, U., 2017. Cloud response and feedback processes in stratiform mixed-phase clouds perturbed by ship exhaust. Geophysical Research Letters 44, 1964-1972.
- Roberts, G.C. and A. Nenes, A continuous-flow streamwise thermal-gradient CCN chamber for atmospheric measurements, Aerosol Sci. Tech., 39, 206-221, https://doi.org/10.1080/027868290913988, 2005.
- Rodgers, C. D.: Inverse Methods for Atmospheric Sounding, Theory and Practice. World Scientific Publishing, Singapore-NewJersey-London-Hong Kong, 2000.
- Rosenfeld, D., Lohmann, U., Raga, G.B., O'Dowd, C.D., Kulmala, M., Fuzzi, S., Reissell, A., Andreae, M.O. (2008). Science 321, 1309-1313.
- Rosenfeld, D., Sherwood, S., Wood, R., Donner, L. (2014). Climate effects of aerosol-cloud interactions. Science 343, 379-380.
- Scarchili, C., Frezzotti, M., Grigioni, P., De Silvestri, L., Agnoletto, L., Dolci, S. (2010). extraoridnary blowing snow transport events in East Antarctica. Climate Dynamics 34, 1195-1206.
- Schaaf, C.B. et al. (2002). First operational BRDF, albedo nadir reflectance products from MODIS. Remote Sensing of Environment 83, 135-148.
- Schmale, J., J. Schneider, E. Nemitz, Y.S. TangU. Dragosits, T.D. Blackall, P.N. Trathan, G.J. Phillips, M. Sutton and C.F. Braban, Sub-Antarctic marin aerosol: dominant contributions

from biogenic sources, Atmos. Chem. Phys., 13, 8669-8694, https://doi.org/acp-13-8669-2013, 2013.

- Sheperd, A., et al. (2018). Mass balance of the Antarctic Ice Sheet from 1992 to 2017. Nature 558, 219-222.
- Scott, R.C., Lubin, D., Vogelmann, A.M., Kato, S. (2017). West Antarctic ice sheet cloud cover and surface radiation budget from NASA A-train satellites. Journal of Climate 30, 6151-6170.
- Seifert, A., Beheng, K.D. (2006). A two-moment cloud microphysics parameterization for mixed-phase clouds. Part 1: model description. Meteorology and Atmospheric Physics 92, 45-66.
- Shupe, M.D., Intrieri, J.M. (2004). Cloud radiative forcing of the Arctic surface: the influence of cloud properties, surface albedo, and solar zenith angle. Journal of Climate 17, 616-628.
- Silber, I., Verlinde, J., Cadeddu, M., Flynn, C.J., Vogelmann, A.M., Eloranta, E.W. (2019). Antarctic cloud macrophysical, themodynamic phase, and atmospheric inversion coupling properties at McMurdo station, Part II: Radiative impact during different synoptic regimes. Journal of Geophysical Research: Atmospheres 124, 1697-1719.
- Schmidt, R.A. (1980). Threshold wind speeds and elastic impact in snow transport. Jouranl of Glaciology 26, 453-467.
- Schmidt, R.A. (1980). Properties of blowing snow. Reviews of Geophysics 20, 39-44.
- Solomon, A., de Boer, G., Creamean, J.M., McComiskey, A., Shupe, M.D., Maahn, M., Cox, C. (2018). The relative impact of cloud condensation nuclei and ice nucleating particle concentrations on phase partitioning in Arctic mixed-phase stratocumulus clouds. Atmospheric Chemistry and Physics 18, 17047-17059.
- Souverijns, N., Gossart, A., Lhermitte, S., Gorodetskaya, I.V., Kneifel, S., Maahn, M., Bliven, F.L., van Lipzig, N.P.M. (2017). Estimating radar reflectivity - snowfall rate relationships and their uncertainties over Antarctica by combining disdrometer and radar observations. Atmospheric Research, 196, 211-223.
- Souverijns, N., Gossart, A., Gorodetskaya, I.V., Lhermitte, S., Mangold, A., Laffineur, Q., Delcloo, A., van Lipzig, N.P.M. (2018a). How does the ice sheet surface mass balance relate to snowfall? Insights from a ground-based precipitation radar in East Antarctica. The Cryosphere 12,1987-2003.
- Souverijns, N., et al. (2018b). Evaluation of the CloudSat surface snowfall product over Antarctica using ground-based precipitation radars. The Cryosphere 12, 3775-3789.
- Souverijns, N., Gossart, A., Demuzere, M., Lenaerts, J.T.M., Gorodetskaya, I.V., Vanden Broucke, S., van Lipzig, N.P.M. (2019). A new regional climate model for POLAR-CORDEX: evaluation of a 30-year hindcast with COSMO-CLM² over Antarctica. Journal of Geophysical Research: Atmospheres 124, 1405-1427.
- Stein A.F., et al., NOAA's HYSPLIT Atmospheric Transport and Dispersion Modelling system, B. Am. Meteorol. Soc., 96, 2059-2077, https://doi.org/10.1175/BAMS-D-14-00110.1, 2015.
- Stevens, B., Feingold, G. (2009). Untangling aerosol effects on clouds and precipitation in a buffered system. Nature 461, 607-613.

- Stohl, A. and G. Wotawa, A method for computing single trajectories representing boundary layer transport, Atmos. Environ., 29, 3235-3239, 1995.
- Stohl, A., L. Heimberger, M.P. Scheele and H. Wernli, An intercomparison of results from three trajectory models, Meteorol. Appl., 8, 127-135, 2001.
- Takahashi S., Endoh, T., Azuma, N., Meshida, S. (1992). Bare ice fields developed in the inland part of Antarctica. Processings NIPR symposium Polar Meteorological Galcaiology 5, 128-139.
- Teinilä, K., V.M. Kerminen and R. Hillamo, A study of size-segregated aerosol chemistry in the Antarctic atmosphere, J. Geophys. Res., 105, 3893-3904, https://doi.org/10.1029/1999jd901033, 2000.
- Thiery, W., Gorodetskaya, I.V., Bintanja, R., van Lipzig, N.P.M., Van den Broeke, M.R., Reijmer, C.H., Kuipers Munneke, P. (2012). Surface and snowdrift sublimation at Princess Elisabeth station, East Antarctica. The Cryosphere, 6, 841-857.
- Town, M.S., Walden, V.P., Warren, S.G. (2007). Cloud cover over the south pole from visual observations, satellite retrievals, and surface-based infrared radiation measurements. Journal of Climate 20, 544-559.
- Trouviliez, A., Naaim-Bouvet, F., Ghenthon, C., Picard, L., Favier, C., Bellot, H., Agosat, C., Palerme, C, Amory, C., Gallée, H. (2014). A novel experimantal study of aeolian snow transport in Adelie Land (Antractica). Cold Regions Sciences and Technology 108, 125-138.
- Turner, J. et al. (2004). The SCAR READER project: towards a high-quality database of mean Antarctic meteorological observations. Journal of Climate 17, 2890-2898.
- Turner, J., Pendlebury, S. (2004). The international Antarctic weather forecasting handbook. British Antarctic Survey, Cambridge, 685pp.
- Turner, J., Lachlan-Cope, T.A., Colwell, S., Marshall, G.J., Connolley, W.M. (2006). Significant warming of the Antarctic winter troposphere. Science 311, 1914-1917.
- Uotila, P., Vihma, T., Pezza, A.B., Simmonds, I., Keay, K. Lynch, A.H. (2011). Relationships between Antarctic cyclones and surface conditions as derived from high-resolution numerical weather prediction data. Journal of Geophysical Research 116, D07109.
- Van de Berg, W., van den Broucke, M.R., Reijmer, C.H., van Meijgaard, E. (2005). Characteristics of the Antarctic surface mass balance, 1958-2002, using a regional atmospheric climate model. Annals of Galciology 41, 97-104.
- van den Broucke, M.R. (1997). Spatial and temporal variation for sublimation on Antarctica: results of a high-resolution general circulation model. Jouranl of Geophysical Research 102, 765-777.
- van den Broeke, M., Reijmer, C., van As, D., Boot, W. (2006). Daily cycle of the surface energy balance in Antarctica and the influence of clouds. International Journal of Climatology 26, 1587-1605.
- van den Broucke, M.R., Reijmer, C.H., van de Wal, R.S.W. (2004). A study of the surface mass balance in Dronning Maud Land, Antarctica, using weather automatic stations. Journal of Galciology 50, 565-581.
- van den Broucke, M.R., van den Berg, W.J., Van Meijgaard, E. (2008). Firn depth correction along the Antarctic grounding line. Antarctic Science 20, 513-517.

- van Kampenhout L., Lenaerts, J.T.M., Lipscomb, W.H., Sacks, W.J., Lawrence, D.M., Slater, A.G., van den Broeke, M.R. (2017). Improving the Representation of Polar Snow and Firn in the Community Earth System Model, Journal of Advances in Modeling Earth Systems, 9, 2583-2600.
- van Lipzig, N.P.M., van Meijgaard, E., Oerlemans, J. (1999). Evaluation of a regional atmospheric model using measurements of surface heat exchange processes from a site in Antarctica. Monthly Weather Review 127, 1994-2011.
- Van Tricht, K., Lhermitte, S., Lenaerts, J.T.M., Gorodetskaya, I.V., L'Ecuyer, T.S., Noël, B., van den Broeke, M.R., Turner, D.D., van Lipzig, N.P.M. (2016). Clouds enhance Greenland ice sheet meltwater runoff. Nature Communications 7, 10266.
- Van Wessem, J.M. et al. (2018). Modelling the climate and surface mass balance of polar ice sheets using RACMO2 – Part 2: Antarctica (1979-2016). The Cryosphere 12, 1479-1498.
- Vaughan, D.G., Bamber, J.L., Giovinetto, M., Russel, J., Cooper, A.P.R. (1999). Reassessment of net surface mass balance in Antarctica.. Journal of Climate 12, 933-946.
- Vaughan, D.G. et al. (2013). Observations: Cryosphere, in: climate change 2013: The physical science basis. Contribution of Working Group I to the fifth assessment report of the IPCC. Cambridge University Press, Cambridge, United Kingdom and New York, USA.
- Virkkula, A. et al., Review of aerosol research at the Finnish Antarctic research station Aboa and its surroundings in Queen Maud Land, Antarctica, Geophysica, 45, 163-181, 2009.
- Wagenbach, D. U. Görlach, K. Moser and K.O. Münnich, Coastal Antarctic aerosol: The seasonal pattern of its chemical composition and radionuclide content, Tellus B, 40, 426-436, https://doi.org/10.3402/tellusb.v40i5.16010, 1988.
- Weller, R. and A. Lampert, Optical properties and sulphate scattering efficiency of boundary layer aerosol at coastal Neumayer station, Antarctica, J. Geophys. Res., 113, D16208, https://doi.org/10.1029/2008JD009962, 2008.
- Weller, R., K. Schmidt, K. Teinilä and R. Hillamo, Natural new particle formation at the coastal Antarctic site Neumayer, Atmos. Chem. Phys., 15, 11399-11410, https://doi.org/10.5194/acp-15-11399-2015, 2015.
- Wood, N.B., L'Ecuyer, T.S., Bliven, F.L., Stephens, G.L. (2013). Characterisation of video disdrometer uncertainties and impacts on estimates of snowfall rate and radar reflectivity. Atmospheric Measurement Techniques 6, 3635-3648.
- Yang, D., Elomaa, E., Tuominen, A., Aaltonen, A., Goodison, B., Gunther, T., Golubev, V., Sevruk B., Madsen, H., Milkovic, J. (1999). Wind-induced precipitation undercatch of the Hellman gauges. Nordic Hydrology 30, 57-80.